Exploring the structure and dynamics of proteins in non-native states using fluorescence spectroscopy

A thesis submitted to the Department of Biotechnology
in partial fulfillment of the requirements for the degree of
Doctor of Philosophy

by

Satish Kumar
Department of Biotechnology
Indian Institute of Technology Guwahati
Assam, India.

August 2008

INDIAN INSTITUTE OF TECHNOLOGY GUWAHATI

Department of Biotechnology

STATEMENT

I do hereby declare that the matter embodied in this thesis is the result of investigations carried out by me in the Department of Biotechnology, Indian Institute of Technology Guwahati, India, under the guidance of Dr. Rajaram Swaminathan.

In keeping with the general practice of reporting scientific observations, due acknowledgements have been made wherever the work described is based on the findings of other investigators.

IIT Guwahati,
August, 2008. Satish Kumar

INDIAN INSTITUTE OF TECHNOLOGY GUWAHATI

Department of Biotechnology

CERTIFICATE

It is certified that the work described in this thesis, entitled "*Exploring the structure and dynamics of proteins in non-native states using fluorescence spectroscopy*" done by Mr. Satish Kumar for the award of degree of Doctor of Philosophy is an authentic record of the results obtained from the research work carried out under my supervision in the Department of Biotechnology, Indian Institute of Technology Guwahati, India, and this work has not been submitted elsewhere for a degree.

IIT Guwahati,
August 2008.

Dr. R. Swaminathan,
Associate Professor,
Department of Biotechnology,
IIT Guwahati

Dedicated to……

Bade pitaji, Late Sri Ram avatar singh

Acknowledgements

I am quite fortunate to begin my research life at IIT Guwahati, which was full of challenges which led to the new heights of learning. I wish to acknowledge some of the brightest people who influenced and helped me in shaping my life in a new dimension.

I feel privileged to have been able to complete my Ph.D. with Dr. R. Swaminathan as supervisor. His support, interest, and criticism have been very valuable.

I owe special gratitude to my doctoral committee, chairperson Dr. S. Ghosh; members, Dr. P. K. Iyer and Dr. A. Ramesh for their constant support and encouragement.

I wish to thank Head, department of chemistry and staff members for allowing me to use the necessary tools.

The financial support and excellent instrumentation facilities provided by Indian Institute of Technology, Guwahati, is greatfully acknowledded.

I would also like to thank Prof. N. Periasamy, TIFR, Mumbai for the anisotropy decay analysis software and Dr Suresh Kumar at IICB, Kolkata for CD measurements.

I gratefully acknowledge all the faculty and staff members of my department for their affection and support.

I express my heartiest thanks to my senior Dr. Lopamudra Homchaudhuri and my current lab members Vijay, Venkat satish and Nividh for their support.

I will always cherish my invaluable friendship with Gopi, Atul, Sandeep, Siva and all my friends for their consistent love and support.

I have reserved my final thanks for my families. My parents have given me all their love over the years. My parents-in-law have loved me like their own son. My seven months old son, Krishna, has given me a lot of joy being a parent. Finally, my deepest thanks go to my wife, Smita, for being supportive to me, especially the last several months when I was not around.

Finally, I am thankful to The Almighty for divine grace and guidance on this arduous journey and also for placing everyone and everything in the exact position to carry out your plan for my life.

ABSTRACT

In the present thesis, structure and dynamics of non-native states in proteins are discussed under different experimental conditions. Owing to their conformation heterogeneity their involvement in protein folding pathway including their role in different protein misfolding diseases, non-native forms of protein are important both for basic and applied areas of biological science.

Local structures in protein under extreme denaturing conditions are known as residual structures and are believed to act as nucleation site for protein folding events. Locating these structures are important to reveal protein folding/unfolding events. I used fluorescence from trp(s) as a simple and sensitive tool to hunt for these structures in different proteins, namely, barstar, subtilisin carlsberg (SC), human serum albumin (HSA), melittin, myelin basic protein (MBP), glucagon, Ribonuclease T_1 (RNase T_1), Trp-Met-Asp-Phe, bovine serum albumin (BSA) and hen egg white lysozyme (HEWL) after nightlong (~12 hours) incubation in 6 M GdnCl at room temperature. Except BSA and HEWL all other proteins used here contain single trp per polypeptide chain.

Two different biophysical parameters namely, bimolecular fluorescence quenching rate constant (k_q) and steady-state anisotropy (r_{ss}) which reflect surface accessibility of fluorophore to the external quencher and rotational freedom of fluorophore respectively, indicated local structures in five proteins RNase T_1, BSA, melittin, barstar and HEWL as compared to model compound N-Acetyl-L-tryptophanamide (NATA) after overnight incubation in 6 M GdnCl. On the contrary trp(s) emission maximum (λ_{max}) from all protein (except tetrapeptide) was not conclusive in locating these structures as there was little change in λ_{max} arising from residual structures.

Aggregated protein is another form of non-native protein, which is the causative agent of different protein misfolding diseases like Alzheimer's and Parkinson's. With the known fact that soluble oligomers are real pathogenic species in these diseases, halting the growth of diffusible protein oligomers in solution phase is necessary for an effective therapeutic approach against pathogenic protein aggregates.

In next part of my thesis, I tried to elucidate the molecular mechanism underlying the HEWL oligomerization at alkaline condition and also tried to inhibit the *in vitro* growth of HEWL aggregates using sodium dodecyl sulfate (SDS), cetyl

trimethyl ammonium bromide (CTAB) and disulphide breaking agent, 1,4 dithioerythritol (DTT).

Gradual increase in steady-sate anisotropy of dansyl labeled HEWL at pH 12.2 upto 360 minutes and saturation thereafter till ~1500 minutes indicated the growth of lysozyme aggregates which was not observed in presence of SDS, CTAB or DTT for the same time period of incubation. This observation was further supported by time-resolved anisotropy decay data of labeled protein where tight molecular packing inside large aggregates of HEWL at pH 12.2 without additives [which contributed to slow (~5 ns) and restricted segmental motion of dansyl probe with global motion of ~60 ns] was clearly loosened up in presence of additives, enabling fast (1-2 ns) and free motion after ~1500 minutes of incubation. We observed that surfactants and DTT inhibited the growth of lysozyme aggregates however, inhibitory effect was more emphatic with DTT. Employing ANS fluorescence we observed the gradual increase in exposure of hydrophobic regions of lysozyme at pH 12.2 but not in presence of DTT. By employing thioflavin T (ThT) fluorescence we observed the kinetics of amyloid fibril formation at pH 12.2 but not in presence of either CTAB or DTT at alkaline condition. Circular dichroism of lysozyme at pH 12.2 in different experimental condition show reduced helical content compared to native lysozyme except in presence of SDS. Estimation of free thiol groups indicated that intermolecular disulfide bonds stabilize the lysozyme aggregates in later phase of incubation. Once the aggregates are stabilized, they are tightly packed preventing DTT, DTNP [2,2'-Dithiobis(5-nitropyridine)] or hydroxyl ion from gaining any access to inner core of aggregates. Gradual decrease in HEWL catalytic activity at pH 12.2 clearly reflects the formation of soluble aggregates through a slow but irreversible process. However, inhibiting the growth of HEWL aggregates does not necessary result in recovery of native and functional protein as we did not recovered HEWL catalytic activity at pH 12.2 soaked protein in presence of SDS/CTAB or DTT.

I also observed that pre-incubation of HEWL with its competitive inhibitor, N,N′,N″-Triacetylchitotriose (chitotriose) at neutral pH imparts it significant stability to misfolding and aggregation at pH 12.2 whereas pre-incubation with single sugar, N-Acetyl-D-glucosamine (NAG) has no such inhibitory effect. Reduced ANS and ThT fluorescence coupled with absence of large aggregates as in SDS PAGE suggested that chitotriose substantially stabilizes HEWL against misfolding and

aggregation. Recovery of >70% catalytic activity in chitotriose incubated HEWL at pH 12.2 after 24 hours of incubation followed by ~16% activity after seven days of incubation suggests that strong binding in HEWL-chitotriose complex in contrast to weakly bound HEWL-NAG complex, raises the activation energy barrier for protein misfolding and aggregation, thereby retarding the aggregation kinetics substantially.

While monitoring the HEWL amyloid formation in different experimental conditions, we observed that ThT fluorescence is not an exclusive feature of amyloid but anionic surfactant like SDS also exhibits enhanced fluorescence upon binding with this dye. We showed for the first time that the anionic micellar microenvironment of SDS has a profound impact on the absorption and fluorescence spectra of ThT in sharp contrast to cationic (CTAB) and neutral micelles (Triton X-100 and Tween 20). Unlike CTAB or Triton X-100 or Tween 20 micelles, formation of SDS micelles shifts the λ_{max} for ThT absorption from 412 nm in buffer to 428 nm inside the micelle, with a 28% increase in the peak molar absorptivity and a ~13 fold increase in ThT fluorescence (λ_{max} = 489 nm). Extending these observations to cell plasma membranes, we show that ThT can quickly enter and appear selectively fluorescent inside mammalian cells like BHK21 and HT29, against a dark background owing to negligible fluorescence from free ThT in aqueous medium. These findings suggest that ThT can be a useful probe for live cell imaging and for selectively labeling micelles on the basis of the charge in the polar headgroup.

TABLE OF CONTENTS

Chapter 1

Introduction and literature review

Ever Since 1958 when John Kendrew proposed the three dimensional model of myoglobin, understanding of protein native structure grew immensely and achieved a new dimension. However, non-native structures of proteins are poorly understood and characterized due to their conformational heterogeneity. In past few decades denatured or non-native conformation of protein has attracted diverse pool of scientist owing to their active role in folding and stability, different biochemical reactions and their involvement in many neurodegenerative diseases like Alzheimer's, Parkinson's and Huntington's.

Local structures in protein under extreme denaturing conditions are known as residual structures. In contrast to native and denatured states of protein which are separated by energetically unfavorable transition state, native-like structure in denatured protein have significant biophysical and biochemical importance. Residual structures are believed to act as nucleation site for protein folding events. Thus by initiating the folding process at these sites the Levinthal search is reduced, allowing energetically favorable interactions that help protein to attain their native conformation. Apart from their involvement in folding process recent evidence suggests that residual structures also promote protein aggregation.

Misfolding and aggregation of proteins under certain physiological condition culminates into many neuropathic and nonneuropathic diseases which are either sporadic or familial. Identifying the lethal protein aggregates and their subsequent prevention is one of the biggest challenges of 21st century. Early soluble protein oligomers have been found to be the toxic species rather than mature fibrils in various aggregation related disorders.

Understanding the importance of residual structure and their implication we tried to locate these structures in different denatured proteins using fluorescence techniques. With the fact that NMR has extensively been used to obtain averaged structure of denatured protein, we employed fluorescence techniques, a sensitive and simple tool to search for native like structures in different non-native proteins with different size.

Knowing the consequences of protein aggregation and their socioeconomic

impact we targeted early soluble aggregates and attempted different maneuvers to inhibit their growth.

Here, non-native states of protein have been reviewed with their potential involvement in folding pathway and diverse range of diseases. Some recent advancement in protein pathogenesis is also reviewed with the challenges that we taken into the account.

1.1 Proteins

Proteins are the workhorses that are required to maintain housekeeping activities inside the cells. They contain information encoded in the gene through transcription, translation and post translational modifications (Kapp and Lorsch 2004). The characteristic feature of proteins to perform diverse cellular functions is entrusted in their structural specificity and ability to bind with other molecules. A distinctive three dimension structure and overall dynamics of protein is essentially required for their specific activity and stability (Daniel et al., 2003).

Structure

Protein structure has been illustrated in terms of four levels (Creighton 2nd Eds). The primary structure is the linear sequence of amino acids and the position of covalent disulfide bonds between cysteine residues. The secondary structure refers to regular folding regions of polypeptide chains, e.g., the α-helix and the β-sheet. These regular structures are cooperative in nature. In globular proteins, α-helix is consists of 10-15 residues held together by hydrogen bonds. These hydrogen bonds are formed between backbone carbonyl oxygen of each peptide bond to the hydrogen on the amino group of the every fourth amino acid. In the β-pleated sheet, hydrogen bonds exists between adjacent sections of polypeptides that are either running in the same direction or in the opposite direction.

The secondary structure elements fold into structural units, called domains, which comprise the tertiary structure. The folding of the secondary structure elements into the tertiary structure is cooperative in nature. The tertiary structure is maintained by four types of interaction between side chain groups of amino acid residue. (1) hydrogen bonding, (2) ionic interactions between oppositely charged groups (salt bridges), (3) hydrophobic interactions, and (4) disulfide cross-linkages. Covalent bonding stabilizes protein structure much stronger than non-covalent interactions

(Weber and Osborn 1969). Proteins containing more than one polypeptide chain exhibit quaternary structure. Each polypeptide chain in such a protein is called as a subunit (or monomer). Quarternary structure refers to the spatial arrangement of the subunits. The functional aspect of proteins can be attributed by the movement and interaction between different subunits leading to wide range of cellular events like enzyme activity, cellular transport, signal transductions and immune response (Daniel et al., 2003; di Prisco et al., 1991; Weyden et al., 2007; Silverton et al., 1977).

Function

Varied cellular activities like enzymatic catalysis, cellular transport, signal transduction, immunological responses are controlled either directly or indirectly by proteins.

Enzymes are biocatalysts which increase the rate of chemical reaction without being used up. Enzymatic activities are usually specific and coherent about the reactions they catalyze and about the substrate that are involved in these reactions. Enzyme catalyzed reactions are governed by interaction between enzyme and substrate, leading to the formation of enzyme and product. Excellent degree of steriospecificity, regioselectivity, and chemoslectivity is required for enzymatic activity (Jaeger and Eggert 2004). Emil Fischer's "Lock and Key" model suggested that both the enzyme and the substrate have specific complimentary geometric shape that fits exactly into one another and leads to catalysis, but this hypothesis fails to explain the stabilization of transition states during reaction. However, structural flexibility in active sites of enzymes was convincing explanation about enzyme catalyzed reactions (Koshland 1958). Development in molecular biology have added the new dimension about our understanding about structural and functional specificity of proteins with highest fidelity, where DNA polymerase catalyses DNA to RNA in a first step followed by proof reading in the second step (Shevelev and Hubscher 2002; Goodman 2002).

The reversible binding of oxygen with hemoglobin is a primitive but excellent example of cellular transport and protein ligand interaction. Atmospheric oxygen is carried to the different tissues through cooperative binding of oxygen with hemoglobin in the form of oxyhemoglobin. Structural change in hemoglobin leads to severe diseases like sickle-cell anemia and thalassemia (Huehns 1970).

Complex cellular immune system is nicely structured by different classes and types of proteins. Two complimentary immune systems namely, humoral immune

system and cellular immune system provide overall immunity in higher organism. The humoral immunity which relies on soluble proteins called as *antibody* or immunoglobulin (Ig), constitutes about 20% of blood protein whereas cellular immunity is mediated by T-Lymphocyte or T-cells like Cytotoxic T cells (T_c) and helper T-cells (T_H) (Kuby 5^{th} Edn). Transmembrane proteins like Major histocompatibility complex (MHC I and MHC II) helps to distinguish between self and non-self during development of immune system (Boehm and Zufal 2006; Bech et al., 1999).

Dynamics

Knowing the protein structure itself is not sufficient to fully unfold its behavior; rather, dynamic behavior that occurs within proteins is vital to elucidate their function at microscopic level. Protein dynamics which range from picosecond to millisecond is essential for diverse biological functions like cellular transport, signal transduction, immune system, and numerous enzymatic activities (Cavanagh and Venters 2001). Local motions in proteins, such as side chain and backbone fluctuations occur at pico and nanosecond (Kungl et al., 1998) whereas enzymatic catalysis, protein folding and allosteric modulation take place at microsecond (μs) to millisecond (ms) time scale (Daniel et al., 2003; Roder and Shastry 1999; Eisenmesser et al., 2002). Comprehensive biological mechanism of a protein can be explained with synchronous understanding of its structure and dynamics. Eisenmesser and co-workers using NMR relaxation method has shown that during catalysis of human cyclophilin A, internal dynamics of enzyme occur on a time scale of hundred of microsecond. It has also been observed that conformational dynamics of this enzyme correlates with microscopic rate of substrate turnover (Eisenmesser 2002). Involvement of global movement of enzyme along with segmental movement of active site clearly indicates that overall dynamics of enzymes are highly coordinated during catalysis (Eisenmesser 2005). Residual fluctuation in HIV-1 protease using Gaussian network model correlates the slow mode of motion in protein with its functional identity whereas fast motion underlies stability of protein (Bahar et al., 1998). Erman and co-workers also confirmed that "kinetically hot" sequences, 22-32 and 84-91 of HIV-1 protease show faster fluctuation, create the folding core and this core retains native like structure even in unfolded state (Bahar et al., 1998). These findings thus indicate the interdependence of structural and functional aspect of proteins.

Structural dynamics of immunoglobulin is an intriguing phenomenon of nature

about its functional specificity against antigens. Measuring the rotational motion of dansyl labeled antibody subsequent to nanosecond excitation, Stryer and co-workers observed two type of motion in antibody (Yguerabide et al., 1970). Segmental motion of 33 ns time scale was observed due to movement in F_{ab} whereas global movement of 168 ns was monitored due to rotational motion of whole antibody. Upon binding with specific antigen, structural fluctuation and relative motion among different segment of antibody is crucial to evoke many effector molecules which ultimately clear the pathogens (Burton 1990). Structural modifications during signal transduction are crucial phenomenon in different proteins (G-protein, Insulin). Dissociation of Gα subunit of G-protein coupled receptors (GPCRs) from its heterotrimeric form Gα,Gβ,Gγ subsequent to binding with ligands causes change in structure and dynamics of G protein leading to its interaction with other molecules to continue the downstream signal transduction processes (Pitcher et al., 1998). Receptor tyrosine kinases (RTK), Toll-like receptors and Integrins are the other different classes of transmembrane receptor which elicits cascade of signal transduction by their structure flexibility and dynamics subsequent to their binding with different extracellular signaling molecules (Li and Hristova 2006; Imler and Hoffmann 2001; Hirata et al., 2005).

Dynamic nature of nascent polypeptide or denatured protein is very important phenomenon by which a protein attains the native conformation. During folding process most of the secondary structures are found to populate at nanosecond to sub microsecond time scale whereas formation of tertiary structure starts as early as microsecond and can last for minutes or even hours (Callender et al., 1998; Kleinschmidt and Tamm 1996).

Techniques to study protein structure and dynamics

Unison of structure and dynamics makes any protein functional and it is thus imperative to understand these properties at highest resolution. The application of many biophysical tools has enriched our understanding about protein structure and dynamics. However, each of these techniques has their own limitations. X–ray crystallography is one of the most commonly used technique to determine protein three dimensional structure with highest accuracy with <2.0 Å (Lundstrom 2006). Apart from three dimentional structure, details of subunit arrangement, ligand binding site, molecular weight and topology can be predicted with highest precision. However, crystalline form and radiational damage of the sample are intrinsic

constraint associated with this technique (Saibil et al., 2002). Since 1958 when the first protein structure was revealed, there are about 42000 solved protein structures in protein data bank out of which about 36000 structures were contributed by X-ray crystallography (RCSB statistics). Atomic resolution of x-ray crystallography have given a wealth of information about ribosome, cytoskeletal filament, viruses, and other biological assemblies to understand biological function accurately (Saibil et al., 2002). X-ray structure of sensory rhodopsin II from Natronobacterium pharaonis (pSRII) at 2.1-Å resolution elucidated the mechanisms of phototransduction and color tuning (Royant et al., 2001). In a popularly called "post genomic era" macromolecular crystallography became a preferred technique used by pharmaceutical and biotechnology companies, where details of protein-ligand interactions can be monitored at highest levels of resolution. This approach holds the promise of novel, more effective, safer and cheaper drugs (Scapin 2006).

Nuclear Magnetic Resonance (NMR) relaxation, particularly ^{13}C is powerful method to study protein structure and dynamics at atomic level. In the last decades NMR has been successfully used for the determination of 3D structures of a large number of macromolecules, including receptors and ligand/receptor complexes. In 1985 Kurt Wüthrich proposed first NMR structure of bull seminal protease inhibitor (Williamson et al., 1985) whose structure shows excellent agreement with homologous protein porcine pancreatic secretory trypsin inhibitor, whose structure was extracted using x-ray crystallography. Since then, NMR has been widely used to reveal native and non-native structure of proteins (Bai et al., 1995; McDermott 2004; Kamatari et al., 2004; Mittag and Forman-Kay 2007). Over the course of years NMR experiments have been used to monitor complex biological phenomenon like protein folding, protein–protein and protein–ligand interaction which occurs at µs–ms time scale (Eisenmesser 2002; McDermott 2004; Eichmuller et al., 2007).

Cryo-electron microscopy has recently been used to determine protein structures at subnanometer resolution. In spite of the limitation of sample damage by radiation, high resolution image of SH3 amyloid fibril and yeast prion protein has been obtained using this technique (Glover et al., 1997; Jimenez et al., 1999).

Other optical tool like circular dichroism (CD) is very informative about overall secondary structure of protein in solution. Apart from secondary structure prediction, CD is popularly been used to monitor protein-ligand interaction and determining the thermodynamics and kinetics of protein folding (Greenfield 1999).

Absorption from peptide bond in the "far-UV" region indicates the relative propensity of α helix and β sheet in protein, whereas absorption in the "near-UV" is sensitive to certain aspect of tertiary structure in different environmental conditions (McAllister et al., 2005).

Fluorescence from protein is a sensitive parameter for their structural and dynamic elucidation. The advantages of using fluorescence techniques are intrinsic sensitivity, suitable time scale, non-invasive nature, and minimum perturbation (Lakowicz 3rd Edn). Fluorescence from of aromatic side chains of protein particularly tryptophan fluorescence is sensitive to environmental factors and it is a valuable tool in studies of protein structure and dynamics. Fluorescence quantum yield, absorption and emission spectra, fluorescence and anisotropy decay of tryptophan are the important parameters which provides conformational and rotational fluctuation in protein (Gensch et al., 2004; Robillard et al., 1996; Beechem and Brand 1985; Swaminathan et al., 1994). Tryptophan emission maximum at 310-340 nm in folded form, compared to 350 nm in denatured state of protein is a simple and sensitive indicator of its exposure toward solvent. However, interpreting the fluorescence from indole become complex in multi tryptophan proteins. Close proximity of two different chromophores (donor and acceptor) with overlapping donor emission and acceptor excitation spectra with a favorable orientation and distance, leads to efficient non-radiative energy transfer between them by Resonance Energy Transfer (RET). This type of energy transfer is used to monitor *in vitro* and *in vivo* protein–protein interactions with high spatial and temporal specificity (Chen and Erickson 2005; Truong and Ikura 2001). Fluorescence quenching of fluorophore at their excited states by small molecule like O_2, acrylamide, I^- has been extensively used to monitor the solvent accessibility of fluorophore (Eftink 1991; Lakshmikanth and Krishnamoorthy 1999; Maity and Jarori 2002). Depolarization of light by intrinsic or extrinsic fluorophore during their life time subsequent to excitation by polarized light (fluorescence anisotropy) reveals lot about shape and dynamics of protein (Steiner 1991). Fluorescence anisotropy of dansyl chloride conjugated egg hen white lysozyme has been used to monitor nanosecond dynamics of protein aggregation at alkaline condition (Homchaudhuri et al., 2006). Auer and co-workers has shown the conformational characterization of HIV protease 1 with different inhibitors using time-resloved fluorescence obtained from tryptophan which had good agreement with the structures obtained with X-ray and NMR study (Kungl et al., 1998).

Apart from above mentioned techniques, Electron Paramagnetic Resonance (EPR), Raman scattering, Fourier Transform infrared (FTIR) are also in use to glean conformational detail of proteins (Chen et al., 2007; Thomas 1999; Smith et al., 2005). Hydrogen exchange mass spectroscopy is upcoming tool to provide detailed structure and dynamics of individual conformational states of proteins that may co-exist in solution (Eylesa and Kaltashovb 2004).

1.2 Non-native protein

To be biologically active, proteins retains specific folded three-dimensional tertiary structures called as *native structure*. The amino acids sequence in polypeptide chain along with the energy landscape help to attend native conformation of protein (Anfinson 1973; Onuchic and Wolynes 2004). Energy landscape theory suggests that the protein finds most stable configuration not by a random search, but through an organized process somehow encoded in the amino acid sequence.

Under extreme conditions proteins lose their native conformation and become denatured. Mirsky and Pauling described denatured protein molecule characterized by the absence of a uniquely defined configuration (Mirsky and Pauling 1936), whereas Tanford described this state as ". . . a major change from the original native structure..." that is noncovalent, cooperative, and reversible, in principle if not in practice (Dill and Shortle 1991). Loss of biological function is a major consequence of protein denaturation.

Denaturation of protein can be achieved by different physical agents like, temperature, pressure, or chemical agents like Guanidine hydrochloride (GdnCl), urea and different organic solvents (Mirsky and Pauling 1936; Sasahara and Nitta 2006). Increased temperature breaks the hydrogen bonds, where as extreme pH changes the protein structure by electrostatic repulsion between ionized groups which are normally nonionized and buried in native form. UV light irreversibly changes the protein structure by breaking the main peptide chain subsequent to their absorption by tyrosine or other phenolic residue. Although the denaturation mechanism by GdnCl and urea is poorly understood (Bennion and Dagget 2003) it is however a popular belief that preferential interaction of these denaturants at protein water interface changes the solvent property of water and makes them better solvent for the non-polar amino acids (Dill and shortle 1991; Bennion and Dagget 2003).

1.2.1 Residual structures

Even at high concentration of denaturant, some proteins are not fully unstructured but retain some local structures. Presence these local, non-random structures in protein even under strongly denatured condition are termed as *residual structures*. Residual structures are believed to act as nucleation site from where protein folding is likely to originate (Shortle 1993; Miranker and Dobson 1996). During the folding process these initiation sites facilitate polypeptide chain to form the first elements of secondary structures through short range interaction. These secondary elements then acts as structural scaffold around which protein attains their final three dimensional structure. Over the years, denatured conformation of protein posed a big challenge for structural biologist. Owing to conformational heterogeneity detail characterization of denatured state of protein and residual structures therefore, is quite formidable. Distribution of different molecular conformations with varied dynamics along with limited experimental techniques provides semi-quantitative information about these structural ensembles. High resolution NMR (Neri et al., 1992; Kazmirski et al., 2001; Seetharaman et al., 2002) along with other experimental tools like small angle scattering (Kohn et al., 2004) and fluorescence spectroscopy (Garcia et al., 1995; 1998) are widely used techniques to elucidate the structure of proteins in non-native form.

Hunting of residual structures in denatured environment was initiated by Robertson and Baldwin (Robertson and Baldwin 1991). Using NMR they observed totally disordered structure in thermally denatured ribonuclease A, whereas CD spectroscopy under same conditions indicated the persistence of about half of the secondary structures. Wuthrich and co-workers first time reported the existence of residual structure in bacteriophage 434 repressor in presence of 7 M urea (Neri et al., 1992). A well defined cluster of hydrophobic side chains involving residues 54-59 was identified in 7 M urea. Although these six residues were not identical to their structure in native state but only simple rearrangement of three residues was enough for interconversion of these two structures. The important aspect of these residual structures is the presence of hydrophobic clusters (Neri et al., 1992; Schwarzinger et al., 2002; Tafer et al., 2004). Employing ^{15}N relaxation experiments and comparing with molecular dynamics data Daggett and co-workers reported that GdnCl unfolded state of CI2 “includes a partially populated portion of the native helix” (Kazmirski et al., 2001) while majority of structures were found to be random coil.

Presence of tryptophan and histidine residues has also been observed in hydrophobic clusters in residual structures (Seetharaman et al., 2002; Saab-Rincon et al., 1996). It has been postulated that hydrophobic clusters in denatured form of proteins are stabilized by long range interaction. Evidence of this hypothesis has been proved by Seetharaman et al., where Trp^{62} has been observed to stabilize non-native structure of reduced lysozyme by long range interaction which is abolished by replacement of Trp^{62} to Glycine (Gly). Similar type of hydrophobic clustering has also been observed in urea unfolded rat intestinal fatty acid binding protein by Hodson and Frieden.

Since NMR is widely used technique to reveal native structural propensity in denatured protein, residual dipolar coupling (RDC) is commonly used method to analyze the structural asymmetry that persists on the NMR time scale. RDC observation for the chemically denatured states of large number of proteins (Shortle and Ackerman 2001; Louhivuori et al., 2003; Ohnishi et al., 2004) supported the fact that apparently highly unfolded proteins may retain some long range structure. Although the precise nature of this structures are still controversial (Mohana-Borges et al., 2004). Applying RDC Shortle and co-worker observed the presence of native topology in staphylococcal nuclease under 8 M urea (Ohnishi et al., 2004). Comparing the RDC of urea denatured staphylococcal nuclease with mutant verity Δ131 (which is known to be unfolded in absence of denaturant and still retain native-like structure) Shortle and Ackerman suggested that urea denatured nuclease also adopt native-like structure, however these structures cannot be correlated with native structure of protein (Shortle and Ackerman 2001).

It is however a matter of debate that whether unfolded state of protein is effectively random coil ensembles or they still retains some defined structure (McCarney et al., 2005). It is however a long standing view that unfolded state of protein is a random coil ensemble (Tanford et al., 1966; Wilkins et al., 1999; Tcherkasskaya and Uversky 2001; Kohn et al., 2004). Random coil nature of protein has been explained on the basis of torsion angle about the C_α-N bond (*phi,* ϕ) and C_α-C bond (*psi*, ψ). Even in most expanded form some structure at local level can be attributed by the sterically allowed value of ϕ/ψ around peptide bond (McCarney et al., 2005). However, persistence of local native like structures even in 8 M urea and 6 M GdnCl in many proteins (Neri 1992; Kazmirski et al., 2001; Seetharaman et al.,

2002; Hodson and Frieden 2001; Kumar et al., 2006) indicates that these conformations are not random coil in nature but have preferential structures depending upon amino acid sequence and solvent property (Dill and Shortle 1991; Shortle 1993; Kumar et al., 2006).

Apart from their probable role in reducing the conformational search during folding, residual structures in the unfolded protein play a role in the onset of aggregation of unfolded polypeptides. Presence of non-native short range and long range interaction, particularly cluster of hydrophobic residues is evident in amyloidogenic proteins. Although the effect of these hydrophobic clusters on amyloid formation is not fully understood, changes in the residual structure of the unfolded state can modulate the rate of fibril formation (Mishima et al., 2006).

1.2.2 Protein aggregation

Natively folded structure of protein is essentially required for different cellular activities. Under certain physiological circumstances correctly folded soluble proteins loose their native conformations, often leading to aggregation and subsequent deposition in different tissues. Deposition of these insoluble protein aggregates has been observed in many organs, including the central nervous system (CNS), kidney, liver, heart, bones, and joints, causing several diseases collectively known as protein misfolding diseases such as Alzheimer's disease (AD), Parkinson's disease (PD), type II diabetes, spongiform encephalopathies and Prion disease (Caughey and Lansbury 2003; Stefani 2004; Chiti and Dobson 2006; Rochet 2007). Protein misfolding diseases (PMDs) are characterized by the accumulation of highly organized fibrillar aggregates described as amyloid fibril when deposited extracellularly or intracellular inclusion when resides inside the cell (Chiti and Dobson 2006). Diseases associated with the accumulation of amyloid in different tissues and organs are referred as amyloidoses (Stefani 2004, Chiti and Dobson 2006). There are three category of amyloidoses (1) neurodegenerative condition where aggregation occur in brain or CNS (2) nonneuropathic localized amyloidose where aggregation occurs in tissue other than brain and (3) nonneuropathic systemic amyloidoses if aggregation occurs in multiple tissues. Neuronal cell death in different tissues due to protein deposition exhibit different morphology as dementia or memory loss in Alzheimer's disease (AD), uncontrolled movement in Parkinson's disease (PD). Deposition of nonneuropathic amyloids human islet amyloid polypeptide (IAPP) into pancreatic

amyloid is strongly associated with the pathogenesis of type II diabetes (Yan et al., 2005) where as aggregation of human lysozyme leads to hereditary systemic amyloidoses (Pepys et al., 1993).

In biotechnology industries, formation of protease-resistant misfolded protein or inclusion bodies (IBs) poses a major obstacle for efficient production of recombinant proteins. Concentration dependent aggregation of recombinant proteins in bacterial overexpression system poses a major challenge for *in vitro* recovery after their high yield (Carrio and Villaverde 2002). Reduced activity and solubility, altered immunogenicity are other potential limitations associated with the aggregation of recombinant proteins. Even after their successful recovery, most troubling and challenging tasks in the liquid protein pharmaceuticals are to deal with their physical and chemical instabilities during storage (Wang 1999). Interleukin-1 receptor antagonist (IL-1ra) in solution irreversibly form dimer during storage and its activity reduces three fold as compared to native monomer species (Chang et al., 1996). Owing to their instability in liquid form, protein drugs are stored frozen or freeze dried and administered traditionally through injection rather than taken orally like most small chemical drugs.

Although the mechanism of protein aggregation is not fully revealed, it is a general belief that globular protein needs to be unfolded at least partially for oligomerization. After partial unfolding the non-native population of protein interacts with each other forming different intermediate which ultimately end up in mature fibrils. Destabilization of native conformation can be achieved either by high temperature, high pressure, extreme pH, organic solvents or mutation. Apart from the conformational changes, the inability of molecular chaperones to correct the misfolded protein or the impairment in ubiquitine-proteasome complex to eliminate unwanted proteins promotes accumulation of toxic aggregates in different tissue (Benc et al., 2001, Muchowski and.Wacker 2005).

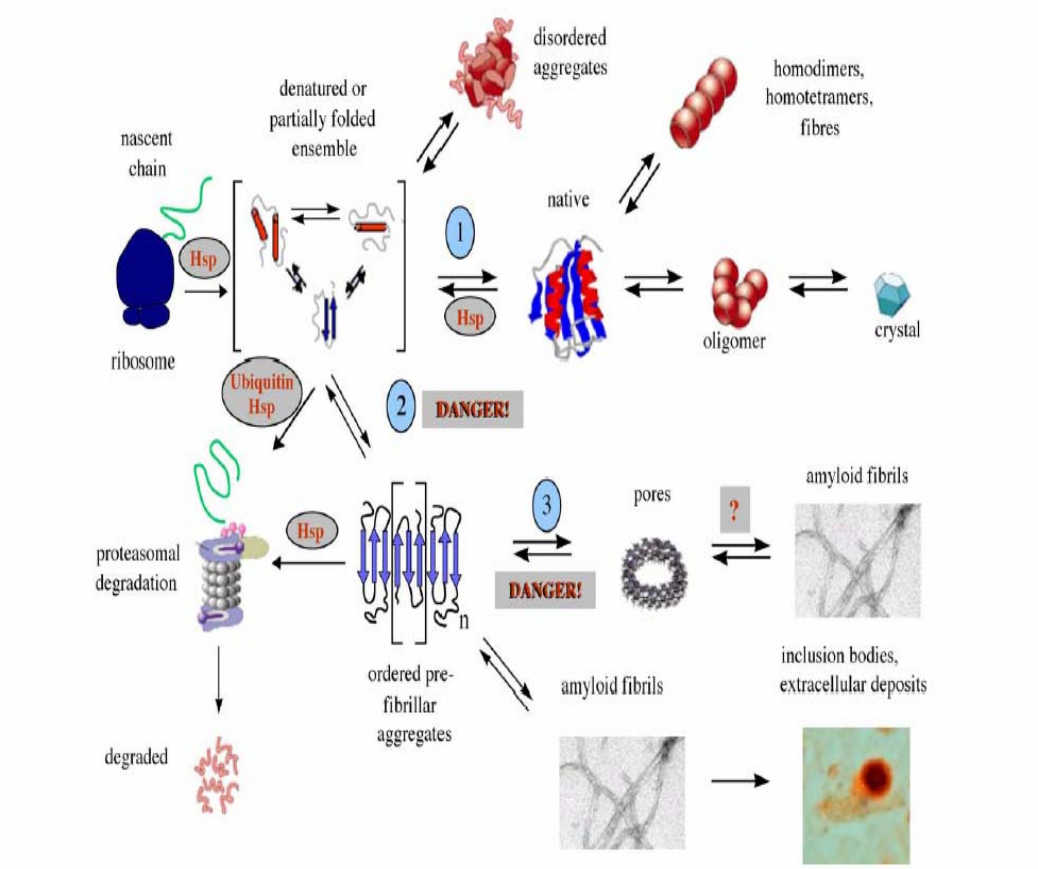

Figure 1.1 The possible model of protein aggregation and cytotoxicity. Partially unfolded ensembles of nascent polypeptide chains are assisted by molecular chaperones to attain their native conformation. If protein misfolds, normal cellular mechanism repairs it by chaperones or clears it by ubiquitine-proteosome machinery. Alteration in any of these two surveillance mechanism promotes ordered or disordered protein aggregation. Ordered prefibrillar aggregates may directly or indirectly related to the cytotoxic effect of amyloids. (Adapted from Stefani, M. Biochimica et Biophysica Acta, 2004, 1739:5-24)

Deposition of insoluble amyloids is hallmark in many neurodegenerative diseases. It is characterized by typical cross β sheet structure which is formed by the intermolecular hydrogen bonding of extended polypeptide strand (Kirschner et al., 1986; 1987). Despite the fact that primitive definition of amyloid having cross β sheet structure was proposed about 40 years ago (Eanes and Glenner 1968), till recently it was formidable task to obtain high resolution structure of amyloid fibril due to their insolubility and non-crystalline nature. Recent advances in solid state NMR (SSNMR), cryo-electron microscopy (cryoEM), Atomic force microscopy (AFM) and X–ray crystallography are providing detail informations about amyloid architecture (Tycko 2000, Glover et al., 1997, McAllister et al., 2005, Makin et al., 2005).

Amyloid fibrils in different amyloidoses share common structural feature irrespective of large difference in structure of the proteins and peptides contributing to the aggregates. Typically, amyloid fibril are straight, unbranched, consist of number (~2-6) of elementary fibril (protofilaments) each about 2-5 nm in diameter. These protofilaments twist around each other to form rope like fibrils that are usually 7-13 nm wide or associated laterally to form long ribbons that are 2-5 nm thick and up to 30 nm wide (Stefani 2004; Chiti and Dobson 2006). Specific binding of aromatic dyes such as thioflavin T (ThT) and congo red (CR) with amyloid fibrils is popularly being used for the detection of fibrils (Nilsson 2004). Recently, specific binding of CR with amyloid fibril and resulting green birefringence under cross polarized light has been questioned (Khurana et al., 2001) however, fluorescence from thioflavin T or their derivatives are widely used probe to detect *in vitro* and *in vivo* amyloid fibril formation (LeVine III 1993; Maezawa et al., 2007).

Mechanism of fibril formation

Deposition of ordered and amorphous aggregates in different diseases is a multi-step process that is governed by thermodynamics and kinetics of different intermediate species populated during the process. Amorphous aggregates rapidly forms when protein concentration exceeds the solubility whereas ordered aggregate formation needs time owing to overcome kinetic barrier required for 'nucleus' formation (Jarrett and Lansbury 1993).

Nucleated growth mechanism of amyloid formation suggests that protein monomers are converted to fibrillar structure via transiently populated aggregation nucleus. This mechanism is characterized with two phases, the thermodynamically unfavorable *lag phase* where oligomeric nuclei are formed in a slow process followed by highly favorable *elongation phase* where fibril are formed rapidly along or around nucleus (Chotia and Janin 1975). On the contrary, the assembly of spherical oligomers and other prefibrillar forms occurs with nucleation-independent kinetics, where formation of spherical particles or worm-like fibrils (Modler et al., 2003; Jahn and Radford 2007) are formed in absence of lag-phase.

Nucleus dependent fibril formation also exhibits "seeding behavior" where pre formed nucleus or seed accelerates the amyloid fibril formation and reduce lag phase considerably. Incubation of hen lysozyme peptide (49-64) wt in pH 2.0 with seeded nuclei has been found to reduced the lag phase to eight days as compared to 56 days

in unseeded lysozyme (Krebs et al., 2000) where as fibrillization kinetics of three different variant of α-synuclein, WT, A53T, and A30P indicates the significant reduction in the lag time if pre formed aggregates (1–2% by moles) of each proteins was added to their respected fresh samples (Conway et al., 2000). The effective *in vitro* seeding in hen lysozyme, α-synuclein and many other proteins suggests that this phenomenon could be a general feature of amyloid formation. Absence of lag phase in some cases does not always imply that nucleated growth mechanism is not operating but may reflects the notion that rate of fibril formation is very slow compare to the nucleation process and it is not the rate limiting step in the conversion of soluble protein into amyloid fibrils (Chiti and Dobson 2006).

Factors influencing protein aggregation

Regardless of opulent information about structural and functional feature, complete mechanism of fibril formation is still elusive. Mutational changes, environmental changes or a chemical modification which reduce the conformational stability of the protein has been found to trigger aggregation. Different physiochemical features of proteins such as mean hydrophobicity, net charge, and secondary structural propensities strongly influences the amyloid formation (Stefani 2004; Chiti and Dobson 2006).

Hydrophobicity of side chain in unfolded polypeptide critically affects their aggregation propensity. Likelyhood of protein misfolding changes with the hydrophobicity of protein (Otzen et al., 2000). Residual structures in reduced lysozyme, which contains six hydrophobic clusters, significantly affects amyloid fibril formation (Mishima et al., 2007). It was observed that the reduced W62G lysozyme, in which most of the hydrophobic clusters except for cluster 5 are disrupted, formed amyloid fibrils less efficiently in comparison with the reduced wild-type. However substitution of Trp 111 to Gly disrupts cluster 5 and considerable amyloid fibril formation was monitored.

High net charge on protein either locally or globally does not favour self-association (Chiti et al., 2002) whereas oligomerization of protein near their isoelectric point (where protein does not have any net charge) is evident in lysozyme and BSA (Homchaudhuri et al., 2006; Shweitzer et al., 2004). Comparative data between natively unfolded and natively folded protein has revealed that unfolded species contains lower content of hydrophobic residues and higher net charge than

folded ones (Uversky 2002). Higher propensity of β-sheet and lower α helical structure is also an important factor facilitating polypeptide self-association (Chiti and Dobson 2006).

Specific mutation in physiological condition may enhance protein aggregation either by destabilizing the native state of a globular protein or accelerating the conversion of partially folded conformations into oligomeric structures. Dominant mutations in three different genes (APP gene on chromosome 2, ApoE on chromosome 19 and mutation in the preseniline 1 and preseniline 2 gene) have been identified that account for the small number of familial, early-onset Alzheimer's disease (Parihar and Hemnani 2004). Rate of fibril formation in amyloid beta ($A\beta_{1-42}$) has found to be faster than truncated $A\beta_{1-40}$, whose two hydrophobic residue at C-terminal region was removed (Thirumalai et al., 2003). These observation indicates that presence of two hydrophobic residue at C-terminal critically affect protein self-association by lowering the free energy barrier for aggregation in amyloid beta protein. With a series of mutation in AcP, Dobson and co-workers reveal that presence of zero net charge but not the hydrophobicity and secondary structure of polypeptide, accelerate their oligomerization (Chiti et al., 2002). Different aggregation rate of wild type transthyretin than its mutant under similar conditions (Hammarstrom et al., 2002) indicate that mutation strongly influences kinetics and thermodynamic behavior of proteins. Huntington's disease (HD) is the outcome of mutation in Huntingtin gene which produces protein with the expansion of CAG trinucleotide. Expanded polyglutamine (poly Q) tract in protein makes it unstable and pathogenic under physiological condition (Perutz 1999).

It is interesting to mention that protein misfolding does not always arises due to mutation. In case of prion disease (transmissible spongiform encephalopathies, Creutzfeldt-Jakob disease) normal isoform of prion, PrP^{c}, misfold and aggregates after interacting with infectious isoform, known as PrP^{Sc}. Infectious nature of PrP^{Sc} support the "protein-only hypothesis" that a protein structure can replicate without the use of nucleic acid (Laurent 1996; Soto and Castilla 2004).

Pathogenesis of misfolded proteins

Understanding the pathogenicity in protein deposition diseases has changed radically in past few years. Highly organized fibrils as a culprit for neuronal cell death was supported with the observation that amyloid fibrils derived from Aβ peptide were

toxic to cultured neuronal cells. However there was some pitfall with this hypothesis. Amyloid plaques were found in individuals who lack any clinical symptoms of AD (Katzman et al., 2004)) and plaque density was not well correlated with the severity of dementia (Terry et al., 1988). Moreover, neuropathological observation in Parkinson's disease indicates that neurons which contain fibrillar protein deposits were healthier than surrounding cells (Tompkins and Hill 1997). Using cell culture model of HD, Finkbeiner and co-workers shown that inclusion body formation supports neuronal survival whereas small oligomers of Huntington cause significant cell death (Arrasate et al., 2004). All these evidences argues that mature amyloid fibrils may act as neuroprotective rather than cytopathic.

Incessant evidence from recent finding suggests that prefibrillar aggregates or soluble oligomers, rather than mature amyloid fibrils might trigger neuronal dysfunction in various PMDs (Bucchiantini et al., 2002; Kayed et al., 2003; Ross and Poirier 2004; Chiti and Dobson 2006). These soluble aggregates consist of spherical particle with a diameter of 2.5 to 5 nm or curvilinear structure called "protofibrils" (Kayed et al., 2003; Stefani 2004). Administration of soluble Aβ oligomers into rat hippocampus has been found to inhibit the late phase of Long Term Potential (LTP), indicating that soluble Aβ oligomers are potent neurotoxins *in vivo* (Walsh et al., 2002). Using highly infective mammalian prion protein Caughey and co-workers demonstrated that oligomers of about 20 molecules were more pathogenic than larger fibrils (Silveira et al., 2005). It is moreover interesting to know that pathogenicity of soluble oligomers are not only associated with disease related protein. Prefibriller aggregates from non-disease related protein like HypF-N from E coli, SH3 domain from bovine phosphatidylinositol 3' kinase (PI3-SH3), and apomyoglobin from sperm whale has also been found toxic towards cultural fibroblast and neurons, while, mature fibril were not cytopathic in nature (Bucchiantini et al., 2002; Sirangelo et al., 2004).

Exact mechanism by which soluble aggregates exhibit their cytotoxicity is not fully revealed, however, their common structural similarity among different amyloid forming protein predicts that they may impart their pathogenic behavior through same primary mechanism (Keyed et al., 2003, Glabe 2006). In a groundbreaking experiment Glabe and co-workers observed that oligomer specific antibody against Aβ not only recognize similar epitope on different unrelated protein aggregates but

pre-incubation of this antibody with unrelated soluble oligomers significantly abolished their cytotoxicity (Keyed et al., 2003).

The wealth of information advocates that cellular death in protein misfolding disease may be attributed primarily by the surface of disordered aggregates which expose the array of group that are generally buried in globular protein or dispersed in highly unfolded protein and peptide (Bucchiantini et al., 2002, Chiti and Dobson 2006). Soluble oligomers harbor higher proportion of such residue on their surface compared to large aggregates and mature fibrils. In the crowded and highly organized cellular environment, inappropriate interaction between exposed groups with cellular membrane, small metabolites, proteins or other macromolecules is inevitable. These interactions leads to dysfunction in cellular activities like membrane permeabilization (Hartley et al., 1999), alteration in cellular Ca^{++} ion balance, oxidative stress, sequestration of essential protein, and axonomal transport culminating into apoptosis or other form of cell death (Glabe 2006; Rochet 2007).

Useful amyloid!!!

Amyloid formation by various non-pathological proteins indicates that it is a generic property of proteins. Nature has exploited this property to perform specialized functions in specific system. Proteinaceous fibril protein, curlein are used by Escherichia coli to colonize inert surface and mediate the binding to various host proteins. These proteins shows characteristic feature of amyloid having 6-12 nm in diameter, possessing rich β sheet structure and affinity toward congo red (CR) and thioflavin T (ThT) binding (Chapman et al., 2002). "Prion-like" property of self-perpetuating is observed in neuronal protein CPEB in *Aplysis*, where it helps in memory storage and synaptic plasticity (Kausik et al., 2003). Amyloid aggregates of silkmoth chorion protein in the egg shell have been observed as natural amyloid which helps in survival and development of the oocyte and embryo (Iconomidou et al., 2000). Mammalian systems are also not completely devoid of useful amyloids. Human eye protein crystallins which maintains refractive index exist predominantly as β pleated sheet *in vivo* and also exhibits CR and ThT sensitivity (Frederikse 2000). In spite of its notorious involvement in Alzheimer's diseases, rapid deposition of Aβ after severe head trauma highlights the possible involvement of these aggregates in maintaining vascular integrity of brain parenchyma against hemorrhage (Stefani 2004). All these finding indicate that amyloid can be physiologically useful provided it is regulated and operated under highly controlled condition.

Blocking the protein aggregation

Inhibiting the protein misfolding, their subsequent growth and deposition in different tissues is essentially required as therapeutic intervention against different protein misfolding diseases (PMDs). However, it is a major obstacle to decide which of the pathological mechanism to target for effective drug against different PMDs.

In the past few years significant progress has been made in development of therapeutic strategies against PMDs (Rochet 2007). These approaches includes (1) direct targeting the protein that undergo misfolding and aggregation (2) interfering with post-translational modification that promote misfolding and aggregation of proteins (3) upregulating the natural housekeeping mechanism.

In order to target fibrillogenic protein or peptide that lacks a stable fold under native condition, it is imperative to identify inhibitor that directly interferes with aggregation pathway. These inhibitors may be small molecules or peptides identified via structural based design or high throughput screening (Rochet 2007; Ross and Poirier 2004). Solid state NMR has elucidated the structure of Aβ 1-40 fibril at highest resolution, which helped to design peptide which can block Aβ fibril formation. Meredith and co-workers shown that peptide spanning residue 16-20 of Aβ with N methyl group at position 17 and 19 was potent inhibitor of Aβ fibrillisation (Sciarretta et al., 2006). The effectiveness of N methyl group was facilitated by (a) their solubility in water and not showing any tendency of fibril formation themselves; and (b) they adopt a stable extended conformation that bind to the end of developing fibril and 'cap' the growth process. In another study an analogue of human islet amyloid polypeptide (IAPP) with two N-methyl groups has been found to be a soluble, noncytotoxic and highly potent inhibitor of IAPP fibrillisation (Yan et al., 2005). In spite of potential inhibitory effect, peptide may not be an ideal drug candidate due to their immunogenicity, susceptibility to proteolysis, and weak bioavailability (Rochet 2007).

Another approach to identify small molecule that inhibits the formation of pathogenic protein aggregation is 'high throughput screening' (HTS). HTS have advantage over structural based method to identify chemical diversity of different 'hit' molecules. After screening the 3780 biologically active compounds using fluorescence-based assay in a cell-free system, Ingram and co-worker shown that 4,5-dianilinophthalimide (DAPH) not only inhibits Aβ fibrillisation but also disrupt preformed fibrils (Blanchard et al., 2004). An another compound N-(4-bromophenyl)-

3-(N-(4-bromophenyl)sulphamoyl) benzamide (C2-8) has been found to inhibit polyglutamine aggregation in Huntington's disease and suppress neurodegeneration *in vivo* (Zhang et al., 2005).

Stabilizing the native structure is another approach to reduce the likelyhood of misfolding and oligomerization in protein. Using transthyretin as a model protein it is observed that thyroxine (T4) greatly stabilizes the tetrameric structure of the protein and did not allow its dissociation into aggregation prone monomers (Johnson et al., 2005). Because T4 cannot be used as a useful therapeutic inhibitor due to its hormonal activity, binding of other compound like diclofenac, diflunisal and flufenamic acid were found to suppress TTR fibrillisation by binding to the native tetramer and inhibiting subunit dissociation under partially denaturing conditions (Johnson et al., 2005; Hammarstrom et al., 2003). These compounds may be used as a future drug against systemic amyloidosis and familial amyloid polyneuropathy. Amino acid arginine also stabilizes different proteins against aggregation by slowing protein-protein association reaction (Baynes et al., 2005).

Various post translational modifications reduce conformational stability of proteins by proteolysis, phosphorylation and oxidation thus, increases their propensity to misfold and aggregate. Controlling these modifications can be used to check protein self-association and subsequent pathogenesis. β- and γ- secretase help in successive proteolysis of amyloid precursor protein (APP) to yield fibrillogenic $A\beta_{1-40}$ or $A\beta_{1-42}$ peptide. MRK-560 suppresses amyloid plaque formation and Aβ generation in APP transgenic mice by inhibiting γ- secretase (Best et al., 2007). Since MRK-560 is orally bioavailable and can cross complex blood-brain barrier, it holds a new hope for the treatment of Alzheimer's disease. Hyperphosphorylation of multiple serine and threonine residue in tau protein by different kinase ultimately leads to neurodegeneration in animal model or humans (Wittmann et al., 2001; Le Corre et al., 2006). Inhibition of glycogen synthase kinase 3b (one of the tau kinase) with lithium or small molecule AR- A014418 decrease tau phosphorylation and can be used as a potential drug against tauopathies (Noble et al., 2005). Oxidative stress and protein aggregation are coupled phenomenon where protein oxidation generally promotes aggregation and protein aggregation populates reactive oxygen species (ROS) inside the cell. Thus, controlling or inhibition of oxidation through antioxidant has shown an early success for the treatment of patients suffering from Alzheimer's disease, Parkinson's disease or amyotrophic lateral sclerosis. Curcumin is one of the

antioxidant which can cross blood-brain barrier and prevent conversion of Aβ to toxic oligomers (Yang et al., 2005). Other antioxidants like myricetin, nordihydroguaiaretic acid, rosmarinic acid, tannic acid and α-tocopherol (vitamine E) suppress α-synuclein toxicity and human tauopathies (Masuda et al., 2006; Zhu et al., 2004; Ono and Yamada 2006).

Although all these antioxidants pose a great hope for different PMDs, a potential limitation of these compounds rest with the fact that they may block single species in aggregation pathway leading to accumulation of other intermediates which can make condition worse.

Enhancing the cellular quality control is an alternative option to regulate the widespread effect of aggregated proteins. Molecular chaperone are important factor in this regard which either repair the misfolded protein or degrade altered protein in association with ubiquitin-proteosome pathway or chaperone-mediated autophagy (Rochet 2007). There are several PMDs where neurodegeneration is closely associated with the impairment of chaperones, known as heat hock protein (HSP) (Muchowski and Wacker 2005). Cell culture model have shown that GRP78 and HSP70 binds and shield the APP from β/γ-secretase cleavage (Yang et al., 1998) thus reduce the secretion of pathogenic $A\beta_{1-40}$ and $A\beta_{1-42}$ fragment. Another molecular chaperone, HSP70 reduces the amount of aggregated α-synuclein species *in vivo* and *in vitro* and protect from α-synuclein-dependent toxicity (Klucken et al., 2004). Chaperone mediated inhibition of PolyQ toxicity has intensively explored in yeast, flies, worms and mice (Muchowski and Wacker 2005). HSP40 suppresses the formation of polyQ inclusion bodies and their toxicity (Jana et al., 2000; Kobayashi and Sobue 2001) whereas HSP70 repress apoptosis in protein misfolding disorders by inhibiting pro-apoptotic factor caspase3 and caspase9 (Zhou et al., 2001). Geldanamycin, a pharmacological agent which is known to modulate and enhance chaperone level, can be useful in the treatment of various PMDs (Rochet 2007; Ross and Poirier 2004). However, toxicity associated with geldanamycin and their inability to cross blood-brain barrier is questionable (Ross and Poirier 2004).

Additionally, macroautophagy (Iwata et al., 2005), immunotherapeutic approach (Monsonego and Weiner 2003; Kayed et al., 2003) and depletion of aggregating protein using RNA interference (Saito et al., 2005; Cooper et al., 2006) are other promising strategies against different protein misfolding disorders.

1.3 Work done by me

I undertook some basic and applied problems of protein science concerned with the non-native aspects of macromolecule.

First, I tried to investigate the local or residual structures in different denatured proteins. Fluorescence from the indole side chain in trp(s) was applied as a spectroscopic probe to detect structural and rotational dynamics surrounding the trp(s) residue in denatured proteins.

Conformational heterogeneity in denatured protein poses a greatest challenge to locate the residual structures. Conventional methods like circular dichroism, infrared spectroscopy are not effective in highlighting their presence. However, NMR is widely technique to locate these structures. I therefore tried to use less complicated and time saving technique to hunt residual structures in different denatured proteins.

Two different biophysical parameters namely, bimolecular fluorescence quenching rate constant (k_q) and steady-state anisotropy (r_{ss}) were used to monitor extent of exposure and rotational dynamics of trp(s) in a series of ten proteins subsequent to their overnight incubation in 6 M GdnCl at room temperature. Among ten proteins used in our investigation eight proteins namely, barstar, subtilisin carlsberg (SC), human serum albumin (HSA), melittin, myelin basic protein (MBP), glucagon, Ribonuclease T_1 (RNase T_1) and Trp-Met-Asp-Phe were having only one trp per polypeptide chain whereas bovine serum albumin (BSA) and hen egg white lysozyme (HEWL) were multi-tryptophan proteins. Bimolecular quenching constant (k_q) reflects the efficiency of quencher or the accessibility of the fluorophores to the quencher, whereas steady-state anisotropy (r_{ss}) on the other hand reveals the extent of rotational freedom and dynamics of fluorophore at their lifetime scale. Since r_{ss} depends upon both the lifetime and rotational correlation time of fluorophore

$$r_{ss} = \frac{r_o}{1 + \frac{\tau}{\theta}} \qquad 1.1$$

[where r_o, which is a constant is the initial anisotropy (anisotropy observed in the absence of other depolarizing processes like rotational diffusion or energy transfer), τ is fluorescence lifetime and θ is rotational correlation time of fluorophore], change in r_{ss} value can be attributed by change in either τ or θ.

We monitored surface accessibility of trp(s) in presence of extrinsic quencher iodide (KI) after overnight incubation of proteins in 6 M GdnCl at room temperature. Reduced k_q was observed in five proteins RNase T_1, BSA, melittin, barstar and HEWL as compared to model compound N-Acetyl-L-tryptophanamide (NATA). However, reduction in k_q was more pronounced in RNase T_1. Restricted rotational motion of trp(s) in same five proteins was also evident from increased r_{ss} value after nightlong incubation in denaturant. On the contrary, there was no change in emission maximum of the proteins except Trp-Met-Asp-Phe in same experimental condition.

Secondly, we attempted to inhibit the *in vitro* growth of HEWL aggregates using sodium dodecylsulfate (SDS), cetyl trimethylammonium bromide (CTAB) and disulphide breaking agent, 1,4 dithiothreitol (DTT) in alkaline condition.

Halting the growth of diffusible protein oligomers in solution phase is needed to be developed for an effective therapeutic approach against pathogenic protein aggregates (May et al., 2006). We applied sensitive fluorescence techniques to track the growth HEWL in pH 12.2 alone and in presence of detergents (SDS, CTAB) and DTT. Time-resolved anisotropy decay reveals the faster segmental motion of dansyl conjugated HEWL in presence of SDS, CTAB and DTT at pH 12.2 after ~24 hrs of incubation, compared to HEWL alone in pH 12.2 (control). However, this rotational freedom was more pronounced in presence of DTT. High r_{ss} value of control over the period of thirty ruled out any lag phase of HEWL in pH 12.2, whereas reduced r_{ss} in presence of additives for the same time span confirmed their effectiveness in suppressing the growth of large HEWL aggregates. Presence of amyloid like structure and hydrophobic interaction was monitored by enhanced ThT and ANS fluorescence. Substantial inhibitory action of CTAB and DTT against HEWL amyloid formation was observed by reduced ThT fluorescence however, inhibitory action of SDS was not possible to monitor due to background signal of ThT in presence of SDS. We also monitored HEWL secondary structure in month old incubated sample at pH 12.2 alone and in presence of additives at room temperature employing circular dichroism (CD). As enzymatic activity mirrors the native form of protein in any given sample, we monitored the time dependent HEWL activity at pH 12.2 buffer alone and in presence of SDS, CTAB and DTT. While revealing the importance of disulphide bond during the process of HEWL aggregation at alkaline condition, free thiol groups were found to increase for three days, and started decline after five days of incubation suggested their potential involvement in stabilization of lysozyme aggregates.

I extended my work of inhibiting HEWL aggregation at pH 12.2 with another approach. In this part of work lysozyme was preincubated overnight at room temperature with its competitive inhibitor N,N′,N″-Triacetylchitotriose (chitotriose) and N-Acetyl-D-glucosamine (NAG) before transferring to pH 12.2. After transferring to alkaline condition, reduced ANS and ThT fluorescence was observed at different time points in chitotriose incubated HEWL compared to sample at pH 12.2 without additive and in presence of NAG. Heterogeneity in HEWL aggregates was also observed in 12% SDS PAGE and we observed higher oligomers in 198 hrs old HEWL sample at pH 12.2 alone and in presence of NAG, but mostly monomeric species was observed at sample which was preincubated with chitotriose. Enzymatic activity of HEWL in same experimental conditions revealed ~75% activity in chitotriose incubated sample after 1500 minutes of incubation at alkaline condition which was nearly 24% in NAG incubated and almost zero in control (with no additives) for same time window.

While detecting HEWL amyloid in pH 12.2 in presence of additives, we came across a striking observation that enhanced ThT fluorescence was not an exclusive feature of amyloid. Negatively charged surfactant like SDS or cellular components also exhibits increased ThT fluorescence subsequent to their binding with positively charged dye. We monitored absorbance, fluorescence and steady-state anisotropy of ThT as a function of SDS concentration. Increments in all three parameters were observed up to 1.5 mM SDS which was saturated thereafter indicating their micellization. Surprisingly, absorption maximum of ThT was shifted in presence of SDS above its critical micellar concentration (CMC). When we tried to monitor the effect of positively charged CTAB or neutrally charged Triton X-100 and Tween 20 on the ThT absorption and emission spectra, we could not observed any changes over the wide concentration range of these surfactants. Thus comparing the absorbance and fluorescence of ThT with different surfactants, we observed that ThT selectively resides inside the anionic micelles like SDS instead of cationic and neutral micelles. We also tracked the mammalian cells employing ThT fluorescence subsequent to 450 nm excitation.

Chapter 2

Experimental techniques

Brief introduction to molecular spectroscopy

Spectroscopy is a branch of science which identifies and measures interaction of electromagnetic radiation (ER) with matter. These interactions can be ascribed by absorption, emission or scattering. The transition of matter from a lower energy state to a higher energy states is the basis of absorption spectroscopy. The molecular transition strongly depends upon the frequency of the radiation absorbed. For instance, X-ray radiation which oscillates at a high frequency is energetic enough to excite core electrons, whereas lower frequency ultraviolet and visible radiation only excites valence electrons. Lowest energy transitions occur in the vibrational and rotational levels of molecules and nuclei and are induced by infrared and radio waves. Emission spectroscopy, on the other hand, deals with the descent of an atoms or molecules from a higher energy state to a lower one. This transition is usually accompanied by the emission of radiant energy which can be measured by a variety of spectroscopic techniques specific to the frequency of the radiation. The various processes associated with the absorption and emission of radiation can be illustrated by Jablonski diagram (Figure 2.1).

Following the absorption of light, electrons are excited from the lowest energy level S_0 to higher energy levels either S_1 or S_2. The energy difference between the two states is equal to the energy of the incident photon. The electronic transition occurs very fast with the time scale of 10^{-15} seconds which is much faster than nuclear reorganization. Therefore, the higher energy states are achieved without any apparent change in the position of nuclei. This hypothesis is known as Franck-Condon principle. After absorption, a molecule returns to the ground state by radiative processes like fluorescence and phosphorescence and non-radiative processes such as vibrational relaxation, internal conversion, intersystem crossing, fluorescence quenching and other deactivation processes.

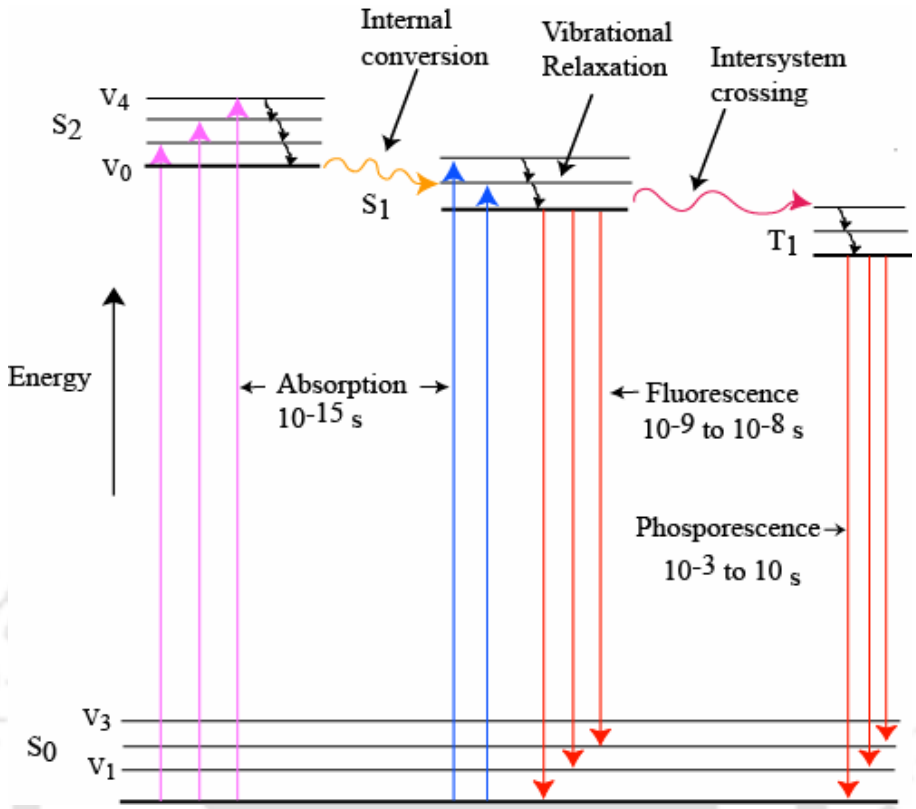

Figure 2.1 Jablonski diagram

2.1 Absorption

Absorptivity is the basic property of a chemical species to absorb light and is constant at a particular wavelength. When a molecule absorbs electromagnetic radiation, there is an induction of dipole which can be expressed as follows:

$$\mu_{ind} = \alpha \cdot \mathrm{E} \qquad 2.1$$

Where μ_{ind} is the induced dipole moment, α is the polarizability and E represents electric field strength of the light.

State of molecules changes subsequent to their interaction with light. For example, molecule with initial state a changes to state b subsequent to their interaction with light. This perturbation in states is outcome of altered distribution of electric charge of molecule in the presence of oscillating electric field E. The transition probability from state a to b is governed by transition dipole moment $\langle \Psi_b | \underset{\sim}{\mu} | \Psi_a \rangle$ abbreviated as μ_{ba}. Here Ψ_b and Ψ_a are the wavefunction of two states b and a. The

absorption intensity depends upon the rate at which energy is taken up from incident light. Transition rate (dP_b/dt) is product of two terms and can be written as

$$dP_b/dt = B_{ab}I(\nu) \qquad 2.2$$

Here B_{ab} is transition rate per unit energy density of radiation whereas $I(\nu)$ is the energy density on sample at frequency ν. B_{ab} can be expressed as follow:

$$B_{ab} = (2/3)(\pi/\hbar^2)\,|\langle \Psi_b \,|\, \underset{\sim}{\mu} \,|\, \Psi_a \rangle|^2 \qquad 2.3$$

The rate of energy transfer from light to molecules depend on the number of a to b absorption transition, number of b to a emission transition and on the energy per transition $(E_b - E_a = h\nu)$. E_b and E_a are energy associated with state a and b respectively ($E_b > E_a$), ν is the frequency of ER in hertz (seconds^{-1}) and h is Planck's constant (6.626 x 10^{-34} Joule•second). Now using equation 2.2, the rate of energy transfer can be written as

$$-dI(\nu)/dt = h\nu(N_a B_{ab} - N_b B_{ba})I(\nu) \qquad 2.4$$

Where N_a and N_b are the number of molecules per cm^3 in states a and b respectively, B_{ab} and B_{ba} are *Einstein coefficient for stimulated absorption and emission* respectively. For a simple two-state system, $B_{ab} = B_{ba}$.

When a radiation from given light source falls on solution containing a chromophore, it absorbs the light to a certain extent. The relationship between the amount of light absorbed and the concentration of the chromophore is expressed by Beer-Lambert law:

$$A = \log_{10}\frac{I_0}{I} \qquad 2.5$$

where A is the absorbance, I_0 is the intensity of the incident light, I is the intensity of the transmitted light. The absorbance is linearly related to the concentration of the solution which can be expressed as

$$A = \varepsilon(\lambda)\cdot c \cdot l \qquad 2.6$$

where ε is the molar extinction coefficient at given wavelength, c is the molar concentration of the absorbing molecule and l is the path length traveled by the light in solution.

2.2 Fluorescence

After spending the lifetime of the order of 10^{-9} seconds, excited electrons transit from the lowest vibrational level of first excited singlet state S_1 to the vibrational levels of S_0 with the emission of visible or ultraviolet light by a process called as fluorescence. Fluorescence is the emission of light accompanying a transition from a singlet excited state to singlet ground state. Owing to energy dissipation by vibrational relaxation and other non-radiative processes, fluorescence emission ends up with a higher wavelength of light compared to that initially absorbed. Since emission process is relatively slower than absorption, it reveals a lot about dynamics and interaction of fluorophore with other molecules in solution.

2.2.1 Factors affecting fluorescence intensity

Internal Conversion

In this process, excitation energy is lost by collision with solvent or by dissipation through internal vibrational modes. These types of transitions take place on the order of 10^{-12} seconds, and is represented in Figure 2.1 by a orange wavy arrow between S_2 with S_1. In general, rate of internal conversion (k_{ic}) has been observed to increase with increasing temperature. Therefore, the observed fluorescence decreases with the increase in temperature.

Intersystem crossing

Molecules in the S_1 state can also undergo a spin conversion to the first triplet state T_1. Conversion of S_1 to T_1 is called as intersystem crossing and is depicted as magenta wavy arrow (k_{isc}) in Figure 2.1. Excited triplet state T_1, in turn, convert to ground state either by phosphorescence or by internal conversion. Since transition from T_1 to singlet ground state is forbidden, rate constant for triplet emission are several orders of magnitude smaller than those for fluorescence.

Fluorescence quenching

Fluorescence quenching refers to any process that reduces the fluorescence intensity of a fluorophore. Collisional encounters or complex formation between fluorophore and quencher (Q) depopulates the excited state. Quenching can be a bimolecular process if it is occurring due to collision

$$S_b + Q \xrightarrow{k_q} S_a + Q \qquad 2.7$$

Where S_b and S_a are the excited and ground state energy level of a molecule. Since molar concentration of Q is usually excess over S_b, the actual observed rate is pseudo first order. The value of k_q can be measured by varying the concentration of quencher, [Q] and then monitoring the effect on quantum yield. Oxygen, I^- and acrylamide are common quenchers which depopulate the excited state of fluorophore by diffusion limited collision.

2.2.2 Fluorescence kinetics

Since internal conversion and intersystem crossing are two other deactivation phenomenon occurring at the same time frame as fluorescence, all molecules do not have equal opportunity to return to the ground state. So, two parameters namely fluorescence lifetime and quantum yield can be used to measure fluorescence with respect to the other processes.

The observed fluorescence lifetime τ_F, is defined as

$$\tau_F = \frac{1}{k_r + k_{ic} + k_{isc} + k_q[Q]} \qquad 2.8$$

k_r, k_{ic}, k_{isc} and kq represents rate of decay by fluorescence, internal conversion, intersystem crossing and fluorescence quenching respectively. Molar concentration of quencher is represented here as [Q].

The above expression can further be simplified as follow

$$\tau_F = \frac{1}{k_r + k_{nr}} \qquad 2.9$$

Where k_r is rate constant for radiative decay and k_{nr} is the sum of the rate constants for all non-radiative events.

Fluorescence efficiency or quantum yield, ϕ_F, is the ratio of the number of photons emitted to the number of photons absorbed. Because rate constant k_r and k_{nr} both depopulate the excited state, quantum yield is determined by the relative rate constants of the radiative and non-radiative processes by the following equation:

$$\phi_F = \frac{k_r}{k_r + k_{ic} + k_{isc} + k_q[Q]} = \frac{k_r}{k_r + k_{nr}} \qquad 2.10$$

The reciprocal of k_r is called as intrinsic or natural lifetime (τ_n), which describes the lifetime of fluorescence in the absence of the non-radiative processes.

$$\tau_n = \frac{1}{k_r} \qquad 2.11$$

Combination of equations 2.8 and 2.10 produce

$$\phi_F = k_r \times \tau_F \qquad 2.12$$

Thus, the relationship between quantum yield and lifetime can be obtain by combining equations 2.11 and 2.12

$$\phi_F = \frac{\tau_F}{\tau_n} \qquad 2.13$$

Interdependence between quantum yield and fluorescence lifetime suggest that decrease in the fluorescence lifetime results in decreasing quantum yield.

Fluorescence from excited samples can be measured either by steady-state or time- resolved techniques.

2.2.3 Steady-state fluorescence

In steady-state fluorescence, sample is illuminated with continuous beam of light and subsequent emission is observed thereafter. In steady-state there is equilibrium between population of fluorophores in the ground state and excited states. The fluorescence intensity which is measured using steady-state mode is an average glimpse of the molecules at their excited states condition. Changes in fluorescence intensity can arise due to changes in quantum yield of fluorophore owing to quenching and is a useful property to measure many biological phenomena. Emission maximum at particular wavelength in steady-state fluorescence spectrum reveals the Stokes shift and in case of indole chromophore, may indicate exposure and degree of polarity around fluorophore.

Fluorescence quenching

The decrease in fluorescence intensity of fluorophore is known as fluorescence quenching. It can be contributed by many processes like, excited state reaction, molecular rearrangement, energy transfer, ground state complex formation and collisional quenching. There are wide range of molecules which decrease

fluorescence intensity, acting as a quencher. Molecular oxygen is a commonly present quencher which reduces fluorescence intensity possibly by their paramagnetic nature which promote fluorophore to undergo intersystem crossing to the triplet state, whereas heavy atom like iodide exhibit their quenching behavior by spin-orbit coupling. Due to their larger size iodide is used to study surface accessibility of fluorophore in macromolecules.

There are two types of quenching phenomena 1) static quenching and 2) dynamic quenching

Static quenching

In static quenching, the fluorophore form a non-fluorescent complex with quencher. This process occurs in the ground state and does not depend upon diffusion or molecular collision.

Schematic showing static quenching

$$F + Q \rightarrow (FQ) \xrightarrow{h\upsilon} (FQ)^* \rightarrow (FQ) + heat$$

(non-fluorescent)

In the above scheme, F is a fluorophore, Q is a quencher and FQ is ground state complex formed after interaction between the fluorophore and quencher.

In the case of static quenching the lifetime of the sample is unchanged. Those fluorophores which are not complexed with quencher, are able to emit after excitation and show normal excited state properties. The reduced fluorescence from the sample is apparent because the quencher essentially reduces the population of fluorophores which can emit the light.

Collisional or dynamic quenching

Collisional quenching occurs when the excited fluorophore experiences contact with an atom or molecule that can facilitate non-radiative transition to the ground state. Common quenchers include O_2, I^-, Cs^+ and acrylamide.

Schematic showing dynamic quenching

$$F \xrightarrow{h\upsilon} F^* \rightarrow F^* + Q \underset{k_2}{\overset{k_0}{\rightleftarrows}} (F-Q)^* \xrightarrow{k(r)} F + Q + heat$$

After absorption of light, excited state of fluorophore F^* comes in contact with quencher (Q) with the bimolecular rate constant k_0. After effective collision with quencher, fluorophor quencher complex $(F\text{-}Q)^*$ is formed which can either proceed to

quenching with rate constant *k(r)* or break apart with rate constant k_2. Quenching efficiency E_Q can be written as

$$E_Q = \frac{k(r)}{k_2 + k(r)} \qquad 2.14$$

Since quencher concentration are generally in excess, *k(r)* is much larger than k_2 so that each encounter leads to quenching.

Unlike the static quenching where lifetime of fluorophore in invariable, dynamic quenching leads to a decrease in the lifetime of excited state. So, $\tau_0 / \tau = 1$ in the case of static quenching and greater than one in dynamic quenching. Here τ_0 and τ are the lifetime of fluorophore in absence and presence of quencher respectively.

Collisional quenching of fluorophore is described by the Stern-Volmer equation

$$\frac{F_0}{F} = 1 + k_q \tau_0 [Q] = 1 + K_{SV}[Q] \qquad 2.15$$

In above equation F_0 and F are the fluorescence intensities observed in the absence and presence of quencher respectively, k_q is bimolecular quenching constant, τ_0 is unquenched lifetime of fluorophore, and [Q] is the quencher concentration.

K_{SV} is the Stern-Volmer quenching constant and represented as

$$K_{SV} = k_q \tau_0 \qquad 2.16$$

In the simplest case, a plot of F_0/F versus [Q] should yield a straight line with a slope equal to K_{SV}. The bimolecular quenching constant k_q reflects the accessibility of the fluorophore to the quencher. For diffusion controlled quenching reaction, k_q is close to 1×10^{10} $M^{-1}s^{-1}$. This value is considered as maximum possible value in aqueous solution. Smaller value indicates the shielding of the fluorophore or a low quenching efficiency.

One can assume a linear Stern-Volmer plot if there is only one type of quenching. But it is true only if all fluorophores are fully exposed. Non-linear Stern-Volmer plots is evident in lactate dehydrogenase where purely collisional quenching by iodide indicates the presence of less accessible tryptophan compared to exposed one (Eftink and Selvidge 1982).

Steady-state fluorescence anisotropy

After excitation with vertically polarized light, emission from sample may be polarized or unpolarized. The extent of polarization of emission is used to calculate fluorescence anisotropy (*r*).

Steady-state anisotropy, which is time-averaged anisotropy decay over the intensity decay,

$$r_{ss} = \frac{\int_0^\infty r(t)I(t)dt}{\int_0^\infty I(t)dt} \qquad 2.17$$

reflects overall rotational motion of fluorophore. Because intrinsic or extrinsic dyes which are attached to macromolecules always exhibit local rotational motion in addition to depolarization through global Brownian tumbling of the macromolecule, it is however judicious to measure time-resolved anisotropy as well as that observed in the steady-state mode.

When a sample is illuminated with polarized light, those molecules with absorption transition dipole aligned parallel to the electric vector of the polarized excitation, have the highest probability of excitation. This phenomenon which is known as photoselection, populates polarized excited state of fluorophores. At their excited state life time (~10^{-9}s) Brownian rotational motion in fluorophores changes the extent of polarization and these changes can be detected in term of anisotropy as follows

$$r_{ss} = \frac{I_{||} - GI_{\perp}}{I_{||} - 2GI_{\perp}} \qquad 2.18$$

Here r_{ss} is steady-state anisotropy, $I_{||}$ and $I_{\perp}$ indicates the intensity of fluorescence emission when (A) both the excitation and emission polarizers are vertically oriented and (B) when emission polarizer is perpendicular to the excitation polarizer. The factor $G = \frac{I_{HH}}{I_{HV}}$ is the ratio of sensitivity of the detection system for vertically and horizontally polarized light. Anisotropy is an intensity ratiometric measurement and it is independent of the fluorophore concentration in the absence of artifacts.

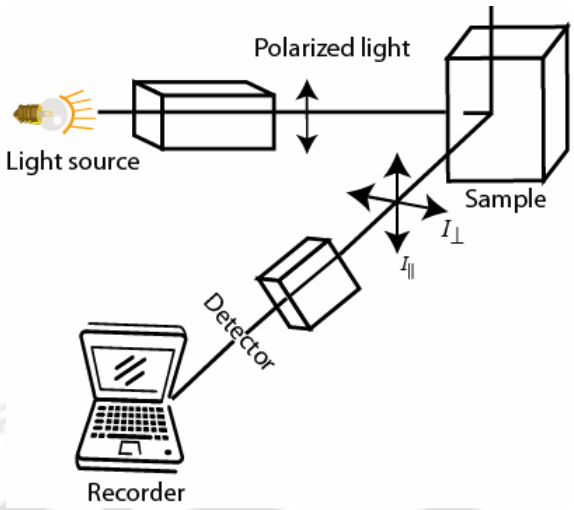

Figure 2.2 Schematic diagram for fluorescence anisotropy measurement

Since steady-state fluorescence offers time averaged information of molecules at their excited states, most of the molecular information available from fluorescence is lost during averaging process. To peep inside these events we require time-resolved fluorescence technique.

2.2.4 Time- resolved fluorescence

In time-resolved mode, the fluorescence intensity decay of a fluorophore is monitored as a function of time after excitation by a pulse of light. There are two methods for time-resolved measurements: 1) Time-domain method, where flash of light of ultra short duration is used to excite the sample and 2) frequency-domain method, where sample is excited with intensity modulated light, typically sine wave modulation. The brief description of only time-domain method is mentioned here as this was employed in several experiments in presented thesis.

In time-domain method the sample is excited with a pulse of light. The width of pulse should be as short as possible and preferably much shorter than decay time τ of sample. Generally pulse-width varies from nanosecond to picoseconds.

Time resolved intensity decay

Following the pulsed excitation, time dependent intensity decay of sample is measured using time correlated single photon counting (TCSPC) method. For the sample with single lifetime, intensity decay can be written as

$$I(t) = I_0 \exp(-t/\tau) \qquad 2.19$$

Here *I(t)* is intensity at any time *t*, I_0 is the initial intensity and τ is the fluorescence lifetime.

As mentioned earlier, fluorescence lifetime is the average amount of the time spent by fluorophore in their excited state before emission. This can be calculated by averaging *t* over the intensity decay of the sample.

$$< t >= \frac{\int_0^\infty tI(t)dt}{\int_0^\infty I(t)dt} = \frac{\int_0^\infty t\exp(-t/\tau)dt}{\int_0^\infty \exp(-t/\tau)dt} \qquad 2.20$$

After solving the equation 2.20 for a single exponential decay, the average time a fluorophore remains in the excited state is equal to the fluorescence lifetime τ.

$$\langle t \rangle = \tau \qquad 2.21$$

Now assume the case where decay consists of emission from more than one fluorophore or from the same fluorophore but in different environments, then decay is multi-exponential and individual lifetime is needed to be resolved. In these cases

$$I(t) = \sum_i \alpha_i \exp(-t/\tau_i) \quad \text{i} = 3 \qquad 2.22$$

Here α_i and τ_i indicates the i^{th} fractional amplitude and i^{th} lifetime respectively of the decay component. Sum of all fractional amplitudes is equivalent to unity, $\sum_i \alpha_i = 1$

From the above parameters mean fluorescence lifetime τ_m can be calculated as:

$$\tau_m = \sum_{i=1}^{n} \alpha_i \tau_i \quad \text{i} = 3 \qquad 2.23$$

Since steady-state observation is an average of the time-resolved phenomenon over the intensity decay of the sample, it is thus imperative to understand the relationship between these two events. For a fluorophore that exhibits a single decay time τ, intensity decay can be represented as

$$I(t) = I_0 e^{-t/\tau} \qquad 2.24$$

Now steady-state intensity (I_{ss}) can be related with the decay time as follow,

$$I_{ss} = \int_0^\infty I_0 e^{-t/\tau} dt = I_0 \tau \qquad 2.25$$

Being more sophisticated, time-resolved method is preferred over steady-state. It is independent of the concentration of the fluorophore and different lifetime(s) with their fractional amplitudes draw a real picture of microenvironment around the probe. Static and dynamic quenching, resonance energy transfer can be best studied using time-resolved measurement. Fluorescence lifetime imaging (FLIM) is increasingly used in cellular imaging and monitoring interaction of macromolecules inside the cells (Wallrabe and Periasamy 2005), since it afford a wide spectrum of lifetimes from 0.1 to 10 ns.

Time-resolved anisotropy decay

For single-exponential intensity decay the steady-state anisotropy (r_{ss}) may also be written in the form of Perrin equation (equation 1.1).

$$r_{ss} = \frac{r_o}{1 + \frac{\tau}{\theta}}$$

where r_o is initial anisotropy, τ is fluorescence life time and θ is rotational correlation time of fluorophore.

Initial anisotropy r_o of a fluorophore is given by

$$r_o = \frac{2}{5}\left(\frac{3\cos^2\beta - 1}{2}\right) \qquad 2.26$$

Where β is the angle between absorption and emission transition dipoles and depend upon excitation wavelength. The value 2/5 arises from photoselection for randomly oriented molecules in solution.

For a sample that contains mixture of different emitting species, average anisotropy $\bar{r}$ can be written as:

$$\bar{r} = \sum_i f_i r_i \qquad 2.27$$

where r_i indicate the anisotropies of the individual species, and f_i is the fraction of intensities of each species.

Time-resolved fluorescence depolarization on the nanosecond and sub-nanosecond time scales is a powerful technique to study rapid molecular motions in macromolecules. Time-dependent anisotropy *r(t)* provides information about size, shape and flexibility of macromolecules (Steiner 1991).

The anisotropy decay of a rotating spherical body following pulsed excitation is given by

$$r(t) = r_o e^{-t/\theta} = r_o e^{-6Dt} \qquad 2.28$$

As mentioned above, r_o is initial anisotropy at t = 0, θ is rotational correlation time of the sphere and D is the rotational diffusion coefficient. From here rotational correlation time, θ, can be obtained by Stokes-Einstein equation as follows

$$\theta = \frac{\eta V}{RT} \qquad 2.29$$

Where η is bulk viscosity, V is hydrodynamic volume of rotating unit, R stands for gas constant and T refers for temperature in Kelvin.

For a system with multiple fluorophores or single fluorophore in with multiple rotational components, the anisotropy decay at time t is multi-exponential and will be written as

$$r(t) = r_0 \sum_j \beta_j \exp(-t/\theta_j) \qquad j = 1 \text{ or } 2 \qquad 2.30$$

Where r_0 is the initial anisotropy in the absence of rotational diffusion, the θ_j are the individual correlation times and β_j are the fractional amplitudes of each correlation times in the anisotropy decay. Presence of multiple correlation times is common in macromolecules. Time-resolved fluorescence anisotropy data of fluorescent biomacromolecules generally originate from two types of motions 1) global motion, where overall movement of macromolecule is evident with a long correlation time and 2) segmental motion of probe, covalently bound with macromolecule, with shorter correlation time. Fluorescence anisotropy is commonly used for measuring protein–nucleic acid and protein–protein interactions (Rusinova et al., 2002; Hill and Royer 1997). Analyzing the movement in dansyl labeled antibody, Stryer and co-workers observed two types of motions. Fast segmental motion with 33 ns time scale was

observed due to the movement in F_{ab} whereas slow global movement of 168 ns was monitored due to rotational motion of whole antibody (Yguerabide et al., 1970). Time-resolved fluorescence anisotropy measurements of a dansyl probe in the active site of recombinant human factor VIIa exhibits global motion of whole protein with rotational correlation time of about 100 ns and segmental motion of the protease domain with rotational correlation time of about 14 ns (Waxman et al., 1993).

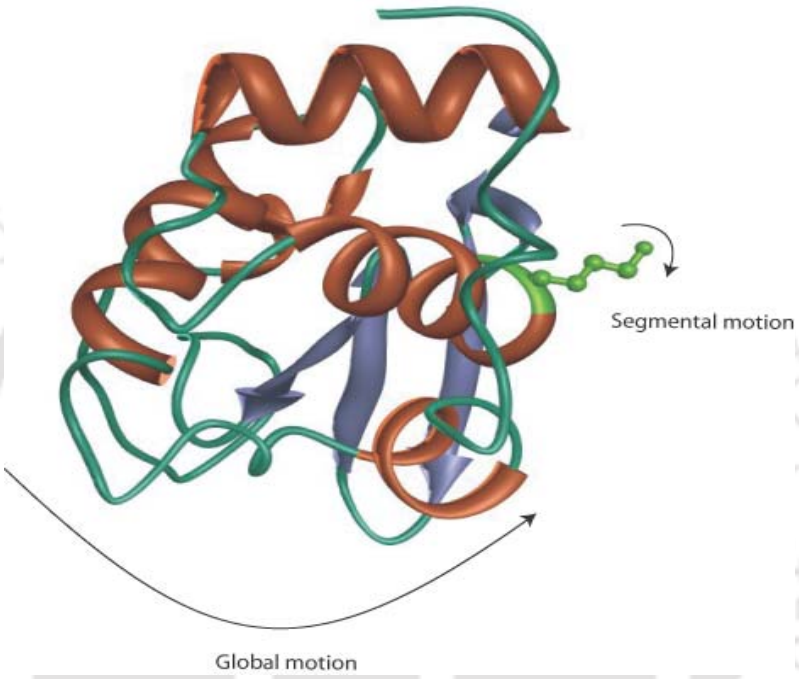

Figure 2.3 Figure depicting global and segmental motions in protein

Small molecules can also reveal multiple rotational components. The origin of multiple rotational correlation times arises due to non-spherical symmetry of fluorophore. If molecule is not spherical in nature, it will show different rate of rotation around each axis. Non-spherical molecules are described as a general ellipsoid or an ellipsoid of revolution. Most of the experiments are unable to divulge the shape of a general ellipsoid, most data are explained in term of ellipsoid of revolution. So, the anisotropy decay of non-spherical molecules is described in term of two form of ellipsoid of revolution A) prolate and B) oblate.

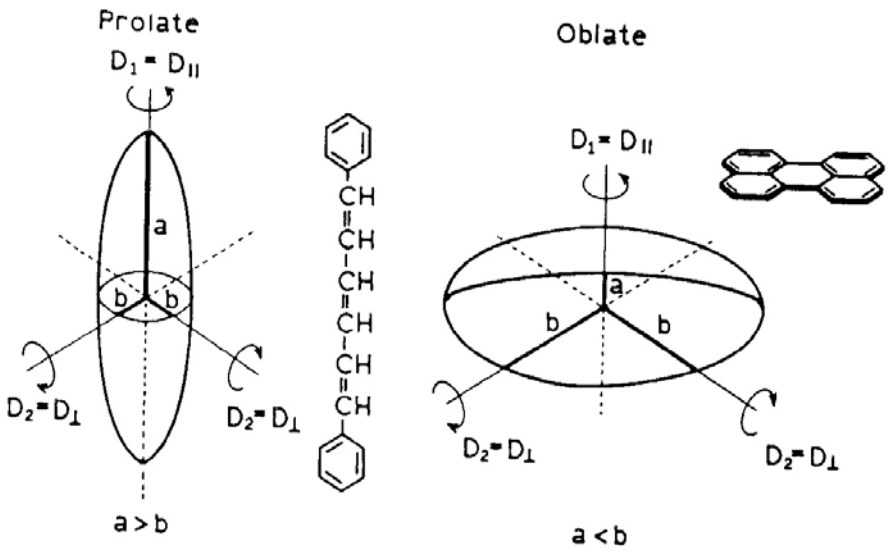

Figure 2.4 Prolate and oblate ellipsoide of revolution. The figure has been adapted from Principle in Fluorescence Spectroscopy by J. R. Lakowicz, second edition, 1999.

Theoretically, for a asymmetric body five correlation times are possible (Belford et al., 1972) however, in practices only three are expected to be distinguishable since two pairs of correlation times will be very close in magnitude and difficult to resolve (Small and Isenberg 1977).

2.2.5 Instrumentation for time-resolved fluorescence measurement

Time-domain fluorescence lifetime or anisotropy decay measurement involves a sensitive technique called *time-correlated single photon counting* (TCSPC). Working in time-domain mode, TCSPC measures the time interval between the exciting pulse and the emitted photon very accurately with a resolution of picoseconds. Repeating this "single photon experiment" several times gives the statistical distribution of arrival time of photons. This statistical distribution is then reconstructed to yield intensity decay of fluorophore(s).

The advantage of the TCSPC technique is the use of very low light levels. Less than one emitted photon per exciting pulse is sufficient. Being a digital technique, TCSPC contains essential components like light source, constant fraction discriminator (CFD), time-to-amplitude convertor (TAC), amplifier, photomultiplier tube (PMT), and multichannel analyzer.

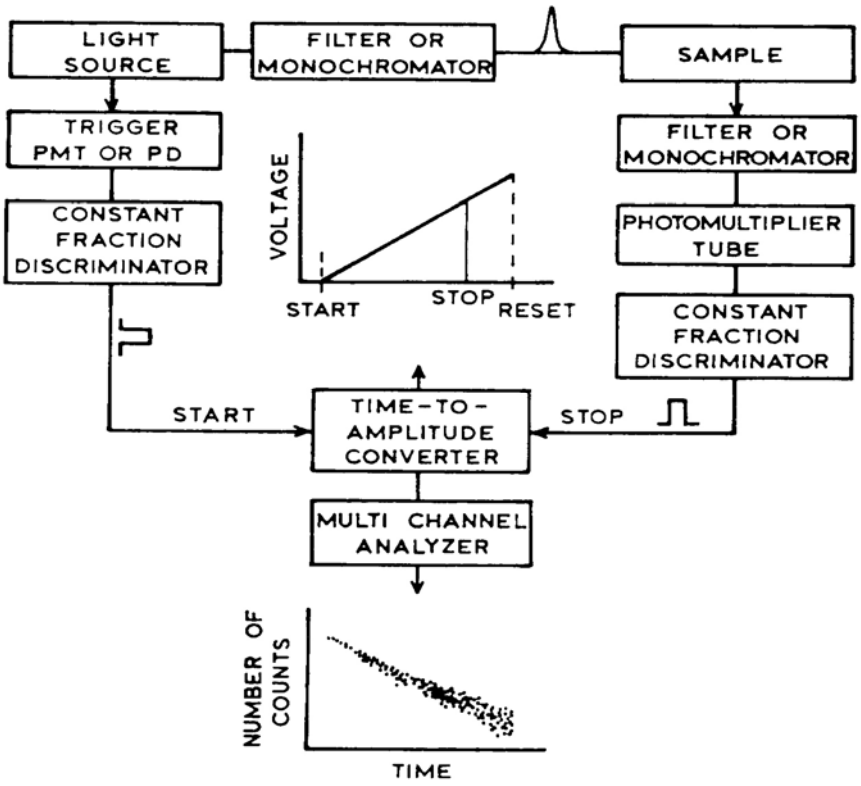

Figure 2.5 Setup for time-correlated single photon counting. The figure has been adapted from Principle in Fluorescence Spectroscopy by J. R. Lakowicz, second edition, 1999.

Depending on the emission yield, either forward or reverse mode of TCSPC can be employed. Forward mode counting implies the excitation pulse as a start TAC whereas, in reverse mode emission pulse is used to start TAC and excitation pulse is used to stop TAC.

The experiment starts with repetitive excitation of sample with pulsed light. The light source in our experimental condition was nanoLED with a pulse-width of 1.39 ns full wavelength half maximum (FWHM). The fluorescence intensity decay is collected at 54.7 degrees angle from the excitation polariser. This angle is also called as magic angle. Following the excitation, amplified emission signal is passed through constant fraction discriminator (CFD) which circumvent problems associated with pulse height variations and accurately measures the arrival time of the pulse. Now, each pulse is guided towards time-to-amplitude converter (TAC) which generate a voltage ramp that is proportional to the time between the excitation pulse and first arriving emitted photon. After arrival of the first photon from sample, multichannal analyzer (MCA) converts the voltage from TAC to the time channel using an analog

to digital converter (ADC). Summing over many pulses the MCA builds up a probability histogram of counts verses time channel. One should continue the experiment until about 10,000-15,000 counts in the peak channel are collected.

As stated earlier that in TCSPC less than one photon is detected per laser pulse, the detection rate is typically 1 photon per 20 excitation pulses. It is imperative to understand that why this statistic is required? Current electronics for TCSPC allows detection of first arriving photon. The dead time of these electronics is about 120 ns which are much longer than fluorescence decay. The dead time of electronics prevents detection of another photon resulting from same excitation pulse. Detection of larger number of photons leads to pile up and apparent decay becomes non-exponential.

Fluorescence time resolved intensity decay or anisotropy decay provide wealth of informations about fluorophore, like molecular environment, interaction with other molecules, size, shape and dynamics at their lifetime scale. However, analysis and interpretation of these data are little complex.

2.2.6 Analysis of time-resolved decay data

Time-resolved intensity decay analysis

Time-resolved fluorescence data acquired through TCSPC are moderately complex and cannot be evaluated by simple graphical methods. In intensity decay measurement there are three curves, instrument response function $L(t_k)$, measured intensity decay $N(t_k)$, and calculated intensity decay $N_c(t_k)$. These functions are in term of discrete time (t_k) because the counted photons are collected into channel each with known time t_k and width (Δt). Measured intensity decay $N(t_k)$, is a convolution of the instrument response function (IRF) with actual intensity decay, $N_c(t_k)$. The instrument response function (IRF) [$L(t_k)$] is the response of the instrument to sample having zero fluorescence lifetime. IRF is collected using dilute scattering solution such as magnesium hydroxide or colloidal silica without emission filter. It is important that this solution has NO FLUORESCENCE signal. This decay represents the shortest time that can be measured by instrument.

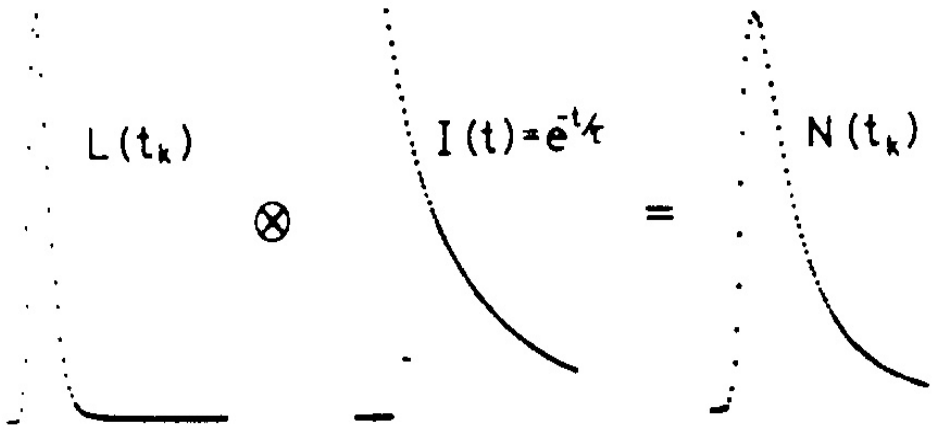

Figure 2.6 The figure represents the convolution of an impulse response function $I(t_k)$, lamp profile $L(t_k)$ to yield the measured decay $N(t_k)$. The intensity decay shown in the above figure corresponds to that of a mono-exponential decay. The figure has been adapted from Principle in Fluorescence Spectroscopy by J. R. Lakowicz, second edition, 1999.

The measured intensity decay $N(t_k)$ is the intensity decay of sample measured by TCSPC. The height on y-axis represents the number of photons that were detected within the time interval tk to $tk + \Delta t$, where Δt is width of timing channel. On a logarithmic scale, decay can be seen as straight line for the sample having single decay time.

$N_c(t_k)$ is the calculated data which is also called as fitted function. It is the convolution of IRF with impulse response function. For a sample with single-exponential decay the lifetime is the value of τ that shows best agreement between the measured data $N(t_k)$ and calculated fitted function $N_c(t_k)$.

The impulsive response function $I(t)$ is the δ-function response of instrument towards the δ-function excitation. Equation 2.19 and 2.22 which represents single and multi-exponential intensity decay respectively is example of impulsive-response function. Since most IRF are 0.5 to 2 ns wide and fluorescence lifetime also lies in nanosecond time scale, the measured intensity decay contains substantial contribution from IRF. The mathematical approach to extract the intensity decay data from measured data is called *iterative reconvolution*.

Although there are many methods to analyze TCSPC data, nonlinear least square analysis (NLLS) based on Marquardt's algorithm is extensively used to resolved complex decay obtained from many biophysical and biochemical events.

NLLS analysis is based upon some assumption like

1. All the experimental uncertainty is in the dependent variable (y-axis)
2. The uncertainties in the dependent variable (measured values) have a Gaussian distribution, centered on the correct value.
3. There are no systematic errors in either the dependent (y-axis) or independent (x-axis) variables.
4. The assumed fitting function is the correct mathematical description of the system. Incorrect models give incorrect parameters.
5. Each datapoints are each independent observations.
6. There is a sufficient number of datapoints so that parameters are overdetermined.

These assumptions are valid for TCSPC and thus least square is appropriate method of analysis.

A least square analysis starts with the model which is expected to be the best representation of the data. For a mono-exponential decay, $I(t) = I_0 \exp(-t/\tau)$ is assumed with guess values of I_0 and τ. These value is then convoluted with the IRF to yield the calculated or fitted decay, $N_c(t_k)$. Further, this calculated decay is compared with experimentally observed decay $N(t_k)$. These comparisons are endorsed by minimized value of χ^2, which is parameter to judge goodness-of-fit. It can be expressed as

$$\chi^2 = \sum_{k=1}^{n} \frac{1}{\sigma_k^2}[N(t_k) - N_c(t_k)]^2$$

$$= \sum_{k=1}^{n} \frac{[N(t_k) - N_c(t_k)]^2}{N(t_k)} \qquad 2.31$$

Since, χ^2 depend upon the numbers of datapoints, it is however not convenient to interpret. Another parameter called as reduced χ^2 (χ_R^2) is used.

$$\chi^2{}_R = \frac{\chi^2}{n-p} = \frac{\chi^2}{\upsilon} \qquad 2.32$$

Where n is number of datapoints, p is the number of floating parameters, and $\upsilon = n-p$ is the number of degree of freedom.

If measured and experimental data obtained from TCSPC are agreeing then χ_R^2 value will be near to unity. If the model does not fit the data then this value significantly exceed the unity. In this case new set of parameters are chosen by altering the older parameters. Process of convolution and matching are repeated iteratively until a χ_R^2 close to unity obtained and/or no further reduction in χ_R^2 is possible. This process is called as *iterative reconvolution*.

Apart from reduced χ^2, another parameter to monitor the quality of fit is the visual examination of residuals. The residuals are the difference between measured data and the fitted function. This difference yields the deviation. These deviations after being weighted by their standard deviation at each datapoint are plotted against time to obtain deviation plot.

Deviation (D_k) or difference between measured and calculated data is given as

$$D_k = \frac{I(t_k) - I_c(t_k)}{\sqrt{I(t_k)}} \qquad 2.33$$

For the good fit these values are randomly distributed around zero with a mean value near unity.

In our experiments we employed IBH DAS6 v6.1.48 decay analysis software to obtain lifetime from intensity decay data.

Time resolved anisotropy decay analysis

The anisotropy decays were analyzed based on the model below

$$I_{||}(t) = \frac{1}{3} I(t)[1 + 2r(t)] \qquad 2.34$$

$$I_{\perp}(t) = \frac{1}{3} I(t)[1 - r(t)] \qquad 2.35$$

$$r(t) = r_0 \sum_j \beta_j \exp(-t/\theta_j) \quad j = 1 \text{ or } 2 \qquad 2.36$$

When $r(t)$ is biexponential, θ_{fast} and θ_{slow} represents the local segmental motion of the labeled dye and overall tumbling (global motion) of the protein, respectively.

Nonlinear least square fitting based on Marquardt algorithm (Bevington and Robinson 1992) was performed to extract the best value for β_j and θ_j. $I_{\parallel}$ and $I_{\perp}$ were analyzed globally using the measured IRF. Additionally, anisotropy decay fits were constrained to yield steady-state anisotropy value that is close to the independently measured value using steady-state spectrofluorometer (Swaminathan et al., 1994; Feinstein et al., 2003).

Rotational correlation times from anisotropy decay data were extracted from *tani* software kindly provided by Dr. N. Periasamy, Tata Institute of Fundamental Research, Mumbai, India.

2.3 Electrophoresis

Electrophoresis is the electrokinetic phenomena describing the migration of a charged particle under the influence of an electric field. When a molecule with charge q, is placed in electric field with strength E, it experiences electrostatic Coulombic force equivalent to E_q. This is the force which drives the charged molecule towards the opposite electrode. Apart from electrostatic force, charged molecule also experiences an opposite frictional force that retard its movement. This frictional force is a measure of hydrodynamic size and shape of the molecule, the pore size of the medium in which electrophoresis is taking place and the viscosity of the buffer. So, the electrophoretic mobility (μ_e) can be described as follow,

$$\mu_e = \frac{\vartheta}{E} \qquad 2.37$$

Where ϑ is velocity of charged particle and E is the electric field strength. Many biomolecules like amino acid, protein, and nucleic acid possess ionisable groups which exist as electrically charged species either cation (+) or anion (-) at any given pH. Under the influence of electric field these charged species migrate either to cathode or anode depending upon the nature of their net charge. For example, agarose gel electrophoresis is used to separate nucleic acid while polyacrylamide gel electrophoresis is widely used to separate proteins according to their electrophoretic mobility.

Polyacrylamide gel electrophoresis

Electrophoresis in acrylamide gel is called as polyacrylamide gel electrophoresis (PAGE). Cross-linked polyacrylamide gels are prepared from the polymerization of

acrylamide monomer in the presence of N, N'-methylenebisacrylamide also known as bis-acrylamide. In the presence of free radical which is generated by ammonium persulphate and N,N,N', N'-tetramethylethylenediamine (TEMED), acrylamide monomer is polymerized in a long chain and bis-acrylamide help in polymerization by introducing second site for chain extension into growing chain. Subsequent to these events, a cross linked matrix with well defined structure is formed whose pore size depends upon the concentration of acrylamide and bis-acrylamide. There are two layers of gel namely stacking gel, and resolving or separating gel.

Stacking gel

The stacking gel consists of large pore size polyacrylamide gel. pH of this gel is around 6.8, about 2 pH units lower than that of electrophoresis buffer. These conditions enable the proteins to concentrate in stack and to form a thin starting zone in a few minutes before entering in resolving gel.

Resolving gel

Below the stacking gel is the resolving gel. The resolving gel is a small pore of polyacrylamide gel (3-30%) made with Tris buffer pH 8.8. In this gel, proteins separate according to their size. Generally 5 to 15% resolving gel can be used to separating different range of proteins. Below is the optimal resolution range of protein vs acrylamide concentration (Bollag et al., 1996).

Acrylamide Percentage	Separating Resolution
15% Gel	15 to 45 kD
12.5% Gel	15 to 60 kD
10% Gel	18 to 75 kD
7.5% Gel	30 to 120 kD
5% Gel	60 to 212 kD

Apart from stacking and resolving gel, running buffer of pH 8.3 is also a very important factor in electrophoresis.

There are different types of electrophoretic techniques to separate proteins in different condition.

1. Native gel electrophoresis– In this condition protein separation occurs in absence of any denaturing substance. This technique is particularly important if one wants to detect a particular protein in native condition.

2. SDS PAGE– Sodium dodecyl sulfate (SDS) polyacrylamide gel electrophoresis is commonly used technique to separate protein in presence of anionic detergent SDS in combination with a reducing agent.

How SDS PAGE works

The procedure for separating proteins by gel electrophoresis was formulated by Laemmli (Laemmli 1976). Sodium dodecyl sulfate is an ionic detergent that binds to the vast majority of proteins at a constant ratio of 1.4 gm SDS/gm protein. Owing to its anionic nature, SDS imparts a negative charge to all the proteins in sample. These charges abolish the inherent charge of the proteins and give every protein the same charge-to-mass ratio. Having the same charge-to-mass ratio and sieving properties of gels, mobility depends upon the molecular weight during SDS PAGE.

Before loading to stacking gel, protein sample is mixed with sample buffer containing SDS, β-mercaptoethanol (BME), bromophenol blue, glycerol, and Tris-glycine at pH 6.8 and boiled to dissociate the protein.

Protein separation by SDS PAGE is a complex phenomenon which takes place in different pH conditions with different ionic population. As described earlier, stacking gel and sample buffer have same pH of 6.8 whereas resolving gel have pH of 8.8 (all these components are buffered with Tris HCl, having chloride ions). Running buffer on the other hand is adjusted at pH 8.3 and contains glycine. Glycine is a weak acid and it can exist in either of two states, an uncharged zwitterion, or a charged glycinate anion (negatively charged). At low pH it is protonated and thus zwitterionic. At higher pH it is negatively charged.

After applying electric field, glycine ions in the running buffer moves away from the cathode (the negative electrode) and head toward the sample and the stacking gel. Here, owing to low pH (6.8) they lose most of their charge and slow down. Parallely, chloride ion in stacking gel and sample buffer also starts moving away from cathode. This creates a narrow zone of very high electrical resistance in the top of the stacking gel. Since, V = IR, the voltage increases to maintain constant current. The very high field strength thus makes the negatively charged proteins to move forward. So, all the proteins move in a compact band just behind the moving front of chloride ions, behind them, the glycine ions move slowly.

When the groups of ions enter the separating gel of pH 8.8, glycine becomes deprotonated and thus acquires more negatively charge. Increase in charge enhances

glycine mobility and it move ahead of protein-SDS complex. Since protein-SDS have complex have uniform charge to mass ratio, protein with higher molecular weight retains higher negative charge. This higher negative charge provides higher mobility of protein in SDS-PAGE gel which encounters increased frictional resistance. Under these conditions, sieving property of gel separates proteins according to their molecular weight. The negatively charged proteins continue to move towards anode (the positive electrode) and, because they have same charge per unit length, they travel into the separating gel under the applied electric field with the same mobility. Due to their small size, bromophenol blue is totally unretarded and therefore indicates the electrophoresis front.

Following electrophoresis, gel may be stained either with Comassie brilliant blue or silver stain to visualize the different protein bands.

Chapter 3

Material and methods

This chapter contains a list of the materials used and a detailed description of the procedure and experimental methods followed. It has been split into different sections.

SECTION 3.1

This section includes the chemicals used and procedures followed in the experiments that are described in the chapter 4 of the thesis.

3.1.1 Chemical used

N-acetyl-L-tryptophanamide (NATA), RNase T1 (Aspergillus oryzae), glucagon (mixture of bovine and porcine pancreas), melittin (bee venom), human serum albumin, bovine serum albumin, protease subtilisin carlsberg (bacterial), basic myelin (bovine brain), lysozyme (chicken egg white), Trp–Met–Asp–Phe–NH_2·HCl peptide and guanidine hydrochloride (GdnCl) were purchased from Sigma–Aldrich Chemicals Private Limited, New Delhi. Barstar employed here refers to the W38FW44F mutant which contains single Tryptophan residue, W53. It was isolated from a bacterial over-expression system as described previously (Swaminathan et al., 1996). Sodium hydroxide, sodium dihydrogen phosphate (NaH_2PO_4) and potassium iodide (KI) were procured from Merck Limited (Worli, Mumbai).

For UV-Visible absorbance and fluorescence measurement, quartz cuvettes with 1 cm path length from HELLMA was employed.

3.1.2 Solutions prepared

(A) Stock solution of proteins

Stock solutions of all proteins except melittin were prepared in 50 mM, pH 7, NaH_2PO_4 buffer buffer. Melittin was buffered at pH 8, Tris buffer to avoid tetramer formation. The concentrations of proteins were confirmed by measuring absorbance of their diluted solution in pH 7 buffer at 280 nm using Cary 100 spectrophotometer with double beam optics. The measured absorbance values were related to molar extinction coefficients of the proteins to determine their actual concentration. The absorbance of a 1 cm path length in a 1mg/ml protein solution at 280 nm is given by

$$(5700 \times n_{trp} + 1300 \times n_{tyr}) / M$$

Where M is molecular weight of protein, n_{trp}, and n_{tyr} indicates the number of tryptophan and tyrosine residues respectively in the protein. We used 5700 $cm^{-1}M^{-1}$ as molar extinction coefficients of tryptophan and 1300 $cm^{-1}M^{-1}$ as molar extinction coefficient of tyrosine.

(B) Stock solution of guanidine hydrochloride

8 Molar guanidine hydrochloride (GdnCl) solution was prepared in 50 mM, NaH_2PO_4 buffer, followed by pH adjustment at 7 using 10 N NaOH.

3.1.3 Denaturation of proteins

To ensure complete denaturation, all proteins were soaked in ~6 M GdnCl overnight (~12 hours incubation) at room temperature prior to the experiment. Protein concentrations were in the range 3–10 μM for quenching experiments and 25–60 μM for anisotropy experiments. For steady-state anisotropy measurement soaked samples without any additives were used while for quenching experiment KI was added to each sample. All experiments were performed at 293 K.

3.1.4 Fluorescence quenching experiment

Subsequent to overnight incubation in ~6 M GdnCl at room temperature, change in trp(s) fluorescence was observed in presence of a series of concentrations of iodide from 0 to 400 mM. The medium also contained 0·1 mM $Na_2S_2O_3$ to prevent the formation of I^{3-}. Steady-state fluorescence of all samples were measured using SPEX FluoroMax-3 fluorimeter purchased from Jobin Yvon Inc., USA, having automated Glan Thompson polarizers and a PMT operating at a voltage of 950 V in photon counting mode. The emission spectra of all samples were measured by exciting at 295 nm with 1 nm slit width and subsequent fluorescence emission was collected between 310–400 nm with 3 nm slit width. The integrated fluorescence is the average area of three independent emission spectra after subtracting the blank emission from sample containing KI, 6 M GdnCl but not protein.

The bimolecular quenching constant k_q was calculated from the Stern-Volmer equation as discussed earlier. For quenching experiments, the integrated fluorescence intensity between 340 and 380 nm was used to determine F_0/F since it gave a flat baseline free from Raman scatter and background fluorescence as obtained from blank.

3.1.5 Steady-state anisotropy measurement

For steady-state anisotropy measurement all samples were excited at 295 nm with 1 nm slit width and emission at 355 nm was collected with 5-10 nm slit width. All measurements were average of at least ten independent observations. All fluorescence measurements were carried out in quartz cuvettes. The background intensity from Raman scatter was observed to be negligible (less than 5%) compared to sample emission intensity under identical conditions as observed with blank samples. All the steady-state anisotropy data are G-factor corrected

SECTION 3.2

This section includes the chemicals used and procedures followed in the experiments that are described in the chapter 5 of the thesis.

3.2.1 Chemical used

Hen egg white lysozyme (HEWL) (L-6876), lyophilized cells of *Micrococcus Lysodeikticus* (ATCC 4698), Thioflavin T, 2,2'-dithiobis(5-nitropyridine), 8-Anilino-1-naphthalene sulfonic acid ammonium salt (ANS), Gly-Gly·HCl, Acrylamide, N,N'-methylenebisacrylamide, N,N,N', N'-tetramethylethylenediamine (TEMED), Glycerol and 1,4 Dithioerythritol was procured from Sigma-Aldrich Chemicals Pvt. Ltd., New Delhi. The dansyl probe, 2-Dimethylaminonaphthalene-6-sulfonyl chloride (D-23) was purchased from Molecular Probes (Eugene, Oregon, USA). PD-10 desalting columns containing sephadex G-25 for separating molecules with $M_r > 5000$ Da from those with $M_r < 1000$ were procured from Amersham Bioscience.

For UV-Visible absorbance and fluorescence measurement, quartz cuvettes with 1 cm path length was purchased from HELLMA.

Other chemicals like sodium dihydrogen phosphate, sodium bicarbonate ($NaHCO_3$), sodium dodecyl sulphate (SDS), dimethyl formamide (DMF) HPLC grade, ammonium persulfate (APS) were obtained from Merck Limited (Worli, Mumbai) and cetyl trimethylammonium bromide (CTAB) was procured from Amresco (Solon, Ohio, USA). All other chemicals employed were of analytical grade.

3.2.2 Reagents prepared

(A) Buffers used

50 mM, pH 7 phosphate buffer; 50 mM, pH 12.2 phosphate buffer; 100 mM, pH 9 bicarbonate buffer and 20 mM, pH 8.5 Gly-Gly buffer were prepared by

dissolving the respective salts in deionized water and respective pH was adjusted using pH meter by adding either 10 N NaOH or 10 N HCl.

(B) Stock solution of SDS, CTAB and DTT

Stocks solution 600 mM SDS (MW ~288), 200 mM CTAB (MW ~364) and 200 mM DTT (MW ~154) were prepared individually in 50 mM, pH 12.2 phosphate buffer.

(C) Thioflavin T (ThT) solution

Stock solution of ThT (~1 mg/ml) in deionized water was filtered through 0.45 µM syringe filter before estimation of the concentration in ethanol using extinction coefficient of 26,620 cm^{-1} M^{-1} at 416 nm (Wall et al., 1999). Stock solution was stored at 277 K and used within a month. Assay solutions were prepared by diluting the stock solution in 20 mM, pH 8.5 Gly-Gly buffer.

(D) 8-Anilino-1-naphthalene sulfonic acid (ANS) solution

Stock solution of ANS (~1 mg/ml) was prepared in deionized water and concentration was determined spectrophotometrically using 4950 cm^{-1} M^{-1} as the molar absorption coefficient at 350 nm (Weber and Young 1964). Stock solution was stored at 277 K.

(E) Reagents used in Tricine Sodium dodecylsulphate polyacrylamide gel electrophoresis

The acrylamide gels used are generally characterized by the total percentage concentration (%T) of both monomers (acrylamide and the crosslinker bisacrylamide) and the percentage concentration of the crosslinker (%C) relative to the total concentration %T.

- **Separating gel monomer** (49.5%, T 6% C)

Mixed 23.0 g acrylamide and 1.5 g *N, N'*-methylene-bisacrylamide in a total volume of 50 ml deionized water. Filtered the solution through a 0.45 µm filter and stored at 277 K protected from light. Discarded the solution after 30 days.

- ***Stacking gel monomer*** (49.5% T, 3% C)

Mixed 24.0 g acrylamide and 0.75 g *N, N'*-methylene-bisacrylamide in a total volume of 500 ml deionized water. Filtered the solution through a 0.45 µm filter and stored at 277 K protected from light. Discarded the solution after 30 days.

- **Anode buffer** (0.2 M Tris, pH 8.9)

Dissolved 12.11 g Tris base in 200 ml deionized water. pH of 8.9 was adjusted with 10 N HCl. After maintaining the final volume of 500 ml with deionized water, solution was filtered through a 0.45 µm filter and store at 277 K.

- **Cathode buffer** (0.1 M Tris, 0.1 M tricine, 0.1% SDS, pH 8.25)

Dissolved 6.05 g Tris base and 8.96 g tricine in a total volume of 500 ml deionized water. Filtered the solution through a 0.45 µm filter, added 0.5 g electrophoresis-grade SDS and stored at 277 K. It was not necessary to adjust the pH of this buffer.

- **Gel buffer** (3.0 M Tris, 0.3% SDS, pH 8.4)

Dissolved 90.8 g Tris base and 0.75 g electrophoresis-grade SDS in 100 ml deionized water. Adjusted the pH of the solution to 8.4 with 10 N HCl. Final volume of 250 ml was maintained by adding deionized water and store at 277 K.

- **Reducing sample buffer**

12% SDS (wt/vol), 6% mercaptoethanol (vol/vol), 30% glycerol (wt/vol), 0.05% Coomassie blue G-250, were mixed with 150 mM Tris-HCl, pH 7.0 phosphate buffer.

- **Gel fixing solution**

100 ml solution of 50% methanol, 10% acetic acid and 100 mM ammonium acetate was prepared.

- **Staining solution**

Staining solution was prepared by dissolving 0.025% (w/v) Coomassie Blue R-250 in a solution of 45% methanol, 45% deionized water, 10% glacial acetic acid.

- **Destain solution**

10% methanol, 10% glacial acetic acid and 80% deionized water were mixed to make Coomassie gel destain solution.

3.2.3 Procedure for labeling lysozyme with dansyl probe

The following procedure is recommended by Molecular Probes for labeling using amine reactive probe, dansyl chloride (Haugland 2002).

Initially, 3.5 mM solution of chicken egg white lysozyme was prepared in 1 ml of freshly prepared 100 mM, pH 9 bicarbonate buffer. 75 mM dansyl chloride solution was prepared by dissolving the probe in DMF. To the 1 ml lysozyme solution, 50 µl of the 75 mM dansyl chloride in DMF was added so that final concentration of amine reactive probe should be ~3.5 mM. So, the concentrations of the protein and dye were taken such that in the final mixture we have a ~1:1 ratio of the two components. Since lysozyme has 6 lysine residues with one $-NH_2$ in N

terminus, dansyl probe can react and covalently attach with anyone of these amines. Subsequent to the proper mixing of lysozyme with dansyl chloride, the reaction mixture was kept at 4^0C with constant stirring for three hours. After three hours of incubation, 1.5 ml pH 9 $NaHCO_3$ buffer was added to the reaction mixture to make final volume of 2.5 ml. The unlabeled fluorophores were separated from the labeled protein solution using an Amersham PD-10 desalting column previously equilibrated with 50 mM, pH 7 sodium phosphate buffer. Protein and dye concentrations were determined by using absorbance at 280 and 339 nm respectively. The molar extinction coefficient for the labeled probe at 339 nm is 3370 $cm^{-1}M^{-1}$ (Levi and Flecha 2003; Chen 1968). The molar ratio of the protein to dye in the dye conjugated protein was calculated to be ~1:1.

3.2.4 The aggregation reaction

Stock of lysozyme was freshly prepared in 50 mM, pH 7 phosphate buffer. For inducing aggregation this stock was diluted at least ten fold in 50 mM, pH 12.2 phosphate buffer.

3.2.5 Effect of SDS, CTAB and DTT on HEWL aggregation

To monitor the effect of additives on lysozyme aggregation, 14 mM SDS and 20 mM DTT from their respective stock solution were employed for 120 μM HEWL at pH 12.2 whereas for 3 mM CTAB (diluted from stock), protein concentration was kept at 80 μM owing to precipitation at higher concentration. Samples containing DTT were kept sealed to prevent air oxidation. All experiments were performed at 298 K.

3.2.6 Steady-state fluorescence anisotropy measurements

Steady-state fluorescence anisotropy measurements (G factor corrected and dark counts subtracted) were carried out using SPEX FluoroMax-3 fluorimeter purchased from Jobin Yvon Inc., USA, equipped with motorized Glan-Thompson polarizers and a PMT operating at a voltage of 950 V in photon counting mode. Dansyl labeled HEWL at different experimental conditions were excited at 370 nm with 1 nm slit width and emission at 444 nm was collected with a slit width between 4-8 nm. Background intensity from Raman scatter or buffer was negligible (< 5%) compared to sample emission intensity under identical conditions. Each steady-state anisotropy value measured is an average of at least three independent measurements.

3.2.7 Time-resolved fluorescence lifetime and anisotropy measurements

Nanosecond time-resolved fluorescence intensity and anisotropy decay was observed using the Fluorocube (IBH Glasgow, UK) employing time-correlated single photon counting (TCSPC) method. Instrument was equipped with motorized polarizers and an IBH TBX04 photon detection module. Samples were excited with pulses from 370 nm NanoLED having a temporal width of 1.3 ns (FWHM) and a repetition rate of 1 MHz. A neutral density filter (OD = 3) was used to attenuate excitation light. To block long wavelength contribution from 370 nm light source, Schott UG-1 filter was used. Emission was detected after passing it through a Schott 420 nm long pass filter to block excitation photons. Fluorescence intensity decay was collected in 1024 channels with a temporal resolution of 0.113 ns/channel. Peak counts were between 10000 and 15000 for all experiments. The fluorescence lifetime measurements were carried out with the emission polarizer at the magic angle position of 54.7^0. The time-resolved anisotropy measurements were performed with the emission polarizer parallel $(I_{\parallel})$ and perpendicular $(I_{\perp})$ to the orientation of the excitation polarizer.

3.2.8 Scattering experiment

To monitor the formation of lysozyme aggregates at different experimental conditions, 150 μM unlabeled lysozyme was incubated at 50 mM pH 7 and 50 mM, pH 12.2 buffer individually at 298 K. Light scattering intensity at 350 nm was observed using vertically polarized light from FluoroMax-3 fluorimeter spectrofluorometer equipped with motorized Glan-Thompson polarizers.

3.2.9 ANS binding assay

75 μM lysozyme was present in either 50 mM pH 12.2, 50 mM pH 12.2 with 20 mM DTT or 50 mM pH 7 phosphate buffer all containing 20 μM ANS. Samples were excited at 380 nm (slit width 1 nm) and subsequent emission between 400 and 600 nm (slit width 8 nm) was observed at different times using Jobin-Yvon Fluoromax-3 spectrofluorometer. Background intensity from Raman scatter or buffer was negligible (<5%) compared to sample emission intensity under identical conditions. The integrated fluorescence is the average area of three independent emission spectra after subtracting the blank emission. The values reported are averaged over multiple sets of experiments. ANS experiment was not possible in

presence of SDS and CTAB owing to background fluorescence from micelles even without protein.

3.2.10 Thioflavin T binding assay

Protein (incubated in pH 12.2 with or without additives [3 mM CTAB or 20 mM DTT] or pH 7 for a specified duration) was diluted with ThT (in pH 8.5 buffer) in a manner such that molar ratio of protein to ThT was ~1:2 as described previously (Wall et al., 1999). The protein was typically ~12 μM in the assay medium. Samples were excited at 450 nm with 1 nm slit width and subsequent emission between 470 and 550 nm was observed at 5 nm slit width using the Jobin-Yvon Fluoromax-3 spectrofluorometer at different time intervals. Other conditions and procedures are similar to those mentioned for ANS binding assay. Again, with 14 mM SDS, ThT experiment was not possible due to background fluorescence even without protein.

3.2.11 Estimation of free thiol groups

A 3 mM stock of DTNP [2,2'-dithiobis(5-nitropyridine)], was freshly prepared in dimethyl sulfoxide (DMSO). In the 100 mM pH 7 reaction buffer, 50 μM of DTNP was mixed with 6 μM or 12 μM of HEWL (diluted from 120 μM HEWL in pH 12.2 buffer). After 15 minutes of proper mixing, formation of the product, 5-nitropyridine-2-thione was confirmed from the characteristic absorption peak near 387 nm using Varian Cary 100 spectrophotometer employing double beam optics. The concentration of free thiol groups was determined by calibrating the absorbance at 387 nm with a standard plot generated using known concentrations of L-cysteine amino acid (0-100 μM) under identical conditions.

3.2.12 Circular Dichroism spectroscopy

CD spectra of month long incubated HEWL at pH 12.2 with or without 14 mM SDS, 3 mM CTAB and 20 mM DTT was recorded using a Jasco J-715 spectropolarimeter equipped with peltier controlled cell holder. Spectra at 298 K were collected using a rectangular quartz cell of 1 cm pathlength from 200-300 nm with a bandwidth of 1 nm, response of 1 sec and a scan speed of 20 nm/min. All spectra were recorded by diluting the incubated 120 μM HEWL samples by ~60 fold in 50 mM pH 7 buffer. The spectra could not be measured at pH 12.2, owing to large absorption by buffer alone at wavelengths below 230 nm. All the displayed spectra are blank subtracted and averaged over at least four scans.

3.2.13 HEWL assay

The HEWL activity was performed as described by Davies et al. Stock solution of *M. lysodeikticus* (2.34 mg/ml) was freshly prepared in water and diluted finally to 78 µg/ml in assay buffer (50 mM pH 7 phosphate buffer, ionic strength 0.05). 120 µM HEWL incubated in pH 12.2 alone or with 14 mM SDS, 20 mM DTT or 80 µM HEWL with 3 mM CTAB were diluted such that final concentration of protein in assay medium containing *M. lysodeikticus* was 70 nM. Lysozyme activity at different time points after incubation was determined by measuring the initial rate of decrease (slope for the first 30 s) in the absorbance at 450 nm at 298 K using Cary 100 double beam spectrophotometer. The activity recovered from different incubation conditions were expressed as percentage of activity with respect to that of freshly made native lysozyme at the same concentration in the same assay buffer.

3.2.14 Tricine-Sodium dodecyl sulphate polyacrylamide gel electrophoresis

16% Tricine-SDS-PAGE was performed as described by Schagger.

Stacking gel (4.0% T, 3.0% C)

In a 50-ml conical tube, 0.8 ml of stacking gel monomer, 2.5 ml of gel buffer, and 6.7 ml deionized water were mixed. 50 µl freshly prepared 10% ammonium persulfate and 10 µl TEMED were also added to the mixture. Solution was gently mixed and used immediately.

Separating gel (16.5% T, 6.0% C)

In a 50-ml conical tube, 10.0 ml of separating gel monomer, 10.0 ml of gel buffer, 3.1 ml glycerol, and 6.9 ml deionized water were mixed. 100 µl freshly prepared 10% ammonium persulfate and 20 µl TEMED were also added to the mixture. Solution was gently mixed and used immediately.

Gel was polymerized using vertical electrophoresis apparatus (Bio-Rad) with 0.75 mm spacer. After polymerizing the stacking and separating gel, upper (cathode) and lower (anode) buffer chambers were filled with the appropriate buffers. Protein samples incubated for 16 days at pH 12.2 with or without 14 mM SDS, 3 mM CTAB and 20 mM DTT were mixed individually with sample buffer and ~29 µg protein sample was employed to electrophoresis at 10 mA constant current for nearly 120 minutes. Gel was treated with gel fixing solution for one hour followed by staining with 0.025 % (w/v) Coomassie brilliant blue with multiple destaining.

3.2.15 Peptide bond absorption

To monitor peptide bond absorption in 120 μM HEWL at pH 12.2 for different time periods, samples were diluted 300 fold in deionized water and absorbance between 190 nm and 220 nm was collected using Varian Cary 100 spectrophotometer employing double beam optics with a quartz cuvette of path length 1 cm. Absorbance of fresh HEWL in deionized water and pH 12.2 buffer alone was also recorded with same dilution.

SECTION 3.3

This section includes the chemicals used and procedures followed in the experiments that are described in the chapter 6 of the thesis.

3.3.1 Chemical used

Hen egg white lysozyme (HEWL) (L-6876), lyophilized cells of *Micrococcus Lysodeikticus* (ATCC 4698), Thioflavin T, 8-Anilino-1-naphthalene sulfonic acid ammonium salt (ANS), Gly-Gly-HCL, Acrylamide, N,N'-methylenebisacrylamide, N,N,N', N'-tetramethylethylenediamine (TEMED), N,N′,N″-Triacetylchitotriose, N-Acetyl-D-glucosamine, bovine serum albumin and Dalton marker VII-L was procured from Sigma-Aldrich Chemicals Pvt. Ltd., New Delhi.

Other chemicals like sodium dihydrogen phosphate, ammonium persulfate (APS) and sodium dodecyl sulphate were obtained from Merck Limited (Worli, Mumbai). All other chemicals employed were of analytical grade.

For UV-Visible absorbance and fluorescence measurement, quartz cuvettes with 1 cm path length was purchased from HELLMA.

3.3.2 Reagents prepared

(A) Buffers used

50 mM, pH 7 phosphate buffer; 10 mM, pH 7.3 phosphate buffer; 50 mM, pH 12.2 phosphate buffer and 20 mM, pH 8.5 Gly-Gly buffer were prepared by dissolving the respective salts in deionized water and respective pH was adjusted using pH meter by adding either 10 N NaOH or 10 N HCl.

(B) Thioflavin T and ANS stock solution

Stock solution of ThT and ANS were prepared same as described in section 3.2.2, C and D respectively.

(C) Stock solution of N,N′,N′′-Triacetylchitotriose (chitotriose)

50 mM stock solution of chitotriose was freshly prepared by dissolving ~3.8 mg chitotriose in 120 µl deionised water.

(D) Stock solution of N-Acetyl-D-glucosamine (NAG)

250 mM stock solution of NAG was freshly prepared by dissolving ~7.0 mg NAG in 120 µl deionised water.

(E) Reagents used in Sodium dodecyl sulphate polyacrylamide gel electrophoresis (SDS-PAGE)

- **Acrylamide solution**

Mixed 3.0 g acrylamide and 0.8 g *N, N′*-methylene-bisacrylamide in a total volume of 100 ml deionized water. Filtered the solution through a 0.45 µm filter and stored at 277 K protected from light. Discarded the solution after 30 days.

- **Stacking buffer** (0.5 M Tris, 0.4% SDS, pH 6.8)

Dissolved 6.05 g of Tris base in a total volume of 100 ml deionized water. After adjusting the pH at 6.8 with 10 N HCl, 0.4 g SDS was added and dissolved completely. Filtered the solution through a 0.45 µm filter and stored at 277 K.

- **Resolving buffer** (1.5 M Tris, 0.4% SDS, pH 8.8)

Dissolved 91.0 g of Tris base in a total volume of 500 ml deionized water. After adjusting the pH at 8.8 with 10 N HCl, 2.0 g SDS was added and dissolved completely. Filtered the solution through a 0.45 µm filter and stored at 277 K.

- **SDS running buffer**

2X SDS running buffer was prepared by dissolving 6 g Tris, 28.8 g glycine and 2 g SDS in a total volume of 1 liter deionized water. After adjusting the pH at 8.3 solution was stored at room temperature. During the time of experiment this solution was diluted to 1X with deionized water.

- Reducing sample buffer, staining solution and destain solution was prepared as described in section 3.2.2, E.

3.3.3 Preincubation of N,N′,N′′-Triacetylchitotriose (chitotriose) and N-Acetyl-D-glucosamine (NAG) with HEWL

Stock of HEWL was prepared in deionized water. Before inducing the aggregation, lysozyme was diluted ~5 fold in 10 mM, pH 7.3 phosphate buffer. 100 µl of chitotriose or NAG from their respective stocks were added individually to HEWL solution at 10 mM pH 7.3 phosphate buffer such that molar concentration of

chitotriose was ~17 fold and molar concentration of NAG was ~83 fold excess over lysozyme. Both the samples were kept overnight at room temperature (298 K).

3.3.4 Binding of chitotriose or NAG with HEWL

Binding of chitotriose with HEWL was confirmed by collecting the difference spectra of HEWL-chitotriose complex at pH 7.3 buffer. After overnight incubation, absorption spectra of 50 µM HEWL with 850 µM chitotriose was collected between 240 nm to 350 nm using Varian Cary 100 spectrophotometer. Spectra of HEWL-chitotriose complex was subtracted from 50 µM HEWL spectra under identical conditions.

Binding of HEWL-chitotriose was also confirmrd by trp(s) fluorescence after night long incubation. After overnight incubation, trp(s) emission spectra of 2 µM HEWL with 34 µM chitotriose was collected between 295 nm to 475 nm subsequent to excitation at 280 nm employing Jobin-Yvon Fluoromax-3 spectrofluorometer. Fluorescence from lysozyme (2 µM) without chitotriose, but identical otherwise, was also collected in parallel.

3.3.5 The aggregation reaction

After overnight incubation at room temperature, lysozyme aggregation was induced by diluting the incubated protein-chitotriose/NAG complex at least 3-4 times in 50 mM, pH 12.2 phosphate buffer. Effect of low protein concentration on HEWL aggregation in presence chitotriose or NAG was observed by diluting protein-inhibitor complex ~15 fold in aggregation inducing buffer. To validate the effect of tri sugar or single sugar on HEWL aggregation, control samples which contained no chitotriose/NAG but were identical otherwise were run in parallel. All experiments were performed at 298 K.

3.3.6 ANS binding assay

After night long incubation of protein-chitotriose/NAG complex, 75 µM lysozyme (either with 1.25 mM chitotriose or 6.25 mM NAG) was transferred to 50 mM pH 12.2 and 50 mM pH 7 phosphate buffer individually, containing 20 µM ANS. Other procedures are similar to section 3.2.9.

3.3.7 ThT binding assay

Time dependent kinetics of HEWL amyloid formation either in presence or absence of additives was monitored by the ThT binding assay as described earlier (Wall et al., 1999).

Protein (incubated in pH 12.2 with or without chitotriose/NAG for a specified duration) was diluted with ThT (in pH 8.5 buffer) in a manner such that molar ratio of protein to ThT was ~1:2. The protein was typically ~10 µM in the assay medium. To monitor any contribution of chitotriose or NAG themselves on ThT fluorescence, low concentration of HEWL either with chitotriose or NAG was also employed for ThT experiment. Other procedures are similar to section 3.2.10.

3.3.8 Sodium dodecyl sulphate polyacrylamide gel electrophoresis

Stacking gel (5%)

In 20 ml conical flask, 0.67 ml acrylamide solution, 1.0 ml of stacking gel buffer, and 2.3 ml deionized water were mixed. 50 µl freshly prepared 10% ammonium persulfate and 10 µl TEMED were also added to the mixture. Solution was gently mixed and used immediately.

Separating gel (12%)

In 20 ml conical flask, 4.0 ml acrylamide solution, 2.5 ml of separating gel buffer, and 3.5 ml deionized water were mixed. 50 µl freshly prepared 10% ammonium persulfate and 5 µl TEMED were also added to the mixture. Solution was gently mixed and used immediately.

Gel was polymerized using vertical electrophoresis apparatus (Bio-Rad) with 0.75 mm spacer. After polymerizing the stacking and separating gel, upper (cathode) and lower (anode) buffer chambers were filled with the running buffer (pH 8.3). 198 hrs old HEWL incubated at pH 12.2 with or without chitotriose/NAG were mixed individually with sample buffer and ~21 µg protein sample was employed to electrophoresis at constant voltage at 180V. Mixture of BSA and HEWL and Dalton marker VII-L were employed individually as standard molecular weight marker. Subsequent to electrophoresis, gel was stained with 0.025% (w/v) Coomassie brilliant blue followed by multiple distaining.

3.3.9 HEWL assay

HEWL activity in different experimental conditions was performed as described in section 3.2.13. 100 µM HEWL incubated at pH 12.2 with or without chitotriose/NAG were diluted such that final concentration of protein in assay medium containing *M. lysodeikticus* was 70 nM. Other procedures are same as section 3.2.13.

SECTION 3.4

This section includes the chemicals used and procedures followed in the experiments that are described in the chapter 7 of the thesis.

3.4.1 Chemical used

Hen egg white lysozyme (HEWL), Thioflavin T, Gly-Gly.HCl, Tween 20, Rhodamine 101 and pyrene were procured from Sigma-Aldrich Chemicals Pvt. Ltd., New Delhi. Sodium dodecyl sulphate (SDS) and Triton X-100 were obtained from Merck Limited (Worli, Mumbai) and Sisco Research Laboratories (Mumbai), respectively while Cetyl trimethylammonium bromide (CTAB) was procured from Amresco (Solon, Ohio, USA). All other chemicals employed were of analytical grade.

3.4.2 Reagents prepared

(A) Buffer prepared

50 mM, pH 7 phosphate buffer; 50 mM, pH 12.2 phosphate buffer and 20 mM, pH 8.5 Gly-Gly buffer were prepared by dissolving the respective salts in deionized water and respective pH was adjusted using pH meter by adding either 10 N NaOH or 10 N HCl. For 5X phosphate buffered saline (PBS) solution, 0.10 gm potassium chloride, 4.0 gm sodium chloride, 0.10 g potassium dihydrogen phosphate, and 0.57 gm sodium dihydrogen phosphate were dissolved in a total volume of 100 ml deionized water. After adjusting the pH at 7.4 by adding 2 N HCl followed by autoclave, 1X solution was used.

(B) ThT stock solution

Stock solution of ThT was prepared same as described in section 3.2.2 C.

(C) Pyrene stock solution

Initially 50 mM pyrene (MW ~202) was prepared in methanol (HPLC grade). It was then diluted to 50 µM in methanol and used as stock solution. In all the experimental conditions pyrene was finally diluted to 2 µM.

(D) Stock solution of SDS, CTAB, Triton X-100 and Tween 20

50 mM stock solution of SDS and CTAB, 10 mM stock solution of Triton X-100 (MW ~647) and Tween 20 (MW ~1228) were prepared in 20 mM, pH 8.5 Gly-Gly buffer.

3.4.3 Absorption of ThT with different surfactants

To monitor absorbance of ThT in presence of different surfactants, 20 µM ThT was employed in 20 µM-10 mM SDS, 5mM CTAB and 2 mM Triton X-100 and Tween 20. Spectra were collected between 300 nm to 500 nm using Cary 100

spectrophotometer with double beam optics. All spectra were subtracted from blank containing respective concentration of surfactants without ThT.

3.4.4 Emission of ThT with different surfactants

To monitor emission of ThT in presence of different surfactants, 20 μM ThT was employed in 0.25 mM-10 mM of SDS/CTAB and 2 mM Triton X-100/Tween 20. All samples were excited at 450 nm with 1 nm slit width and subsequent emission between 470 nm to 550 nm with 5 nm slit width was collected using Fluoromax-3 spectrofluorometer. All spectra were average of three independent observations after subtracting the blank emission containing respective concentration of surfactants without ThT.

3.4.5 Determination of Critical Micellar Concentration (CMC) of surfactants

Pyrene fluorescence emission and its peak III to peak I vibronic band intensity ratio was used to determine Critical Micellar Concentration of SDS, CTAB, Triton X-100 and Tween 20 at 20 mM pH 8.5 Gly-Gly buffer. 2 μM pyrene was mixed with a series of concentrations of surfactants. For SDS and CTAB concentration was ranged from 0 mM-10 mM while for Triton X-100 and Tween 20 it was varied from 0 μM-2000 μM. All samples were excited at 310 nm with 1 nm slit width and subsequent emission between 350 nm to 450 nm with 1 nm slit width was collected using Fluoromax-3 spectrofluorometer. All spectra were average of three independent observations after subtracting the blank emission containing respective concentration of surfactants without pyrene.

3.4.6 Quantum yield calculation

Quantum yield of Rhodamine 101 was used as a standard fluorophore to calculate quantum yield of ThT in presence of 5 mM SDS. Absorbance of Rhodamine 101 in ethanol, ThT in pH 8.5, and ThT with 5 mM SDS in pH 8.5 was observed at 450 nm. Absorbances in all samples were below 0.05. For emission spectrums, all samples were exciting at 450 nm with 1 nm slit width and fluorescence emission between 470 nm to 800 nm was collected with 10 nm slit width. The integrated fluorescence is the average area of three independent emission spectra after subtracting the blank emission.

Quantum yield was calculated using following equation

$$\frac{F_{ref}}{F_{sample}} = \frac{\phi_{ref}}{\phi_{sample}} \times \frac{Ab_{ref}}{Ab_{sample}} \qquad 3.1$$

Where

F_{ref} = Integrated fluorescence of reference compound (Here Rhodamine 101)

F_{sample} = Integrated fluorescence of sample

ϕ_{ref} = Quantum yield of reference compound (For Rhodamine 101 it was 1.0)

ϕ_{sample} = Quantum yield of sample

Ab_{ref} = Absorbance of reference at 450 nm

Ab_{sample} = Absorbance of sample at 450 nm

Quantum yield of ThT in 5 mM SDS was observed to be ~3.5 times higher compared to that observed at pH 8.5 buffer.

3.4.7 Mammalian cell culture

HT29 (human colon adenocarcinoma) and BHK-21 (baby hamster kidney) cells obtained from National Centre for Cell Science, India, were maintained in Dulbecco's Modified Eagle's (DMEM) medium supplemented with 10% fetal bovine serum (FBS), 50U/mL penicillin and 50 mg/mL streptomycin in a humidified atmosphere in 5% CO_2 at 310 K.

3.4.8 Fluorescence microscopy

Fluorescence images were recorded using a laser scanning confocal microscope (LSM 510, Carl Zeiss, Germany) employing the 458 nm Argon line for exciting ThT. The plated cells were washed with PBS (pH 7.4) three times before addition of 50 μM ThT to eliminate fluorescence contributions from the growth media. After addition of ThT, the cells were incubated for 15 minutes at room temperature before collecting images to allow for partitioning of the dye into the cell. The images were collected under a open pinhole (840 μm) using a 20x objective (0.50 NA) after filtering the emission using a 475-525 nm band pass filter to block excitation photons.

3.4.9 Lysozyme fibril formation

(A) HEWL fibril at acidic condition was prepared as described previously (McAllister et al., 2005). 10 mg/ml lysozyme was incubated at 80 mM NaCl; 70 mM glycine–HCl (pH 2.7). After 13 days of incubation at 333 K, sample was centrifuged at 5000 rpm for 5 minutes and supernatant was used for AFM imaging.

(B) HEWL fibril at alkaline condition was prepared by incubating 120 μM protein at 50 mM, pH 12.2 phosphate buffer at 298 K for 8 days.

3.4.10 Atomic force microscopic imaging

For AFM image of HEWL in different experimental conditions, the samples were diluted nearly 10 fold in incubating buffer and added to freshly cleaved mica in presence of 10 mM Mg^{2+}. After few minutes of incubation, mica was rinsed with deionized water to remove unabsorbed sample and dried under nitrogen gas. AFM images were acquired on Picoplus microscope (Molecular Imaging, USA) under non contact or MAC MODE. The oscillation amplitude during measurement was 71.64 KH_Z while scan speed was 2.0 lines/second.

Chapter 4

Employing the fluorescence anisotropy and quenching kinetics of tryptophan to hunt for residual structures in denatured proteins

Native structure of protein is critical for its functional identity. Under extreme conditions i.e. high temperature, extreme pH, high concentration of guanidine hydrochloride or urea, proteins loose their native conformation and become denatured (Mirsky and Pauling 1936; Dill and Shortle 1991). Thus, denaturation abolishes the structural and functional features of the protein. It has been observed that even at extreme denaturation conditions some proteins are not fully unstructured but retain some local structures. Persistence of local native-like ordered structures in protein under extreme denaturing conditions are known as *residual structures* (McCarney et al., 2005).

Residual structures has drawn wide attention in past decades due to their potential involvement in many biophysical and biochemical processes. Residual structures are believed to act as a nucleation site from where protein folding is likely to originate (Shortle 1993; Miranker and Dobson 1996). By initiating the folding process these structures reduce the Levinthal search and allow energetically favorable interactions that help protein to attain their native conformation. Apart from their involvement in folding process, recent evidences suggest that residual structures modulate the process of protein aggregation (Mishima et al., 2006). Presence of short and long range interaction, particularly clusters of hydrophobic residues are evident in amyloidogenic proteins. Ueda and co-worker reported that out of six hydrophobic clusters, W62G which reside in cluster 5, retards the amyloid fibril formation of reduced hen egg white lysozyme at acidic condition (Mishima et al., 2007).

Owing to the conformational heterogeneity detail characterization of denatured states of protein and so the residual structures is quite formidable. However, NMR, small angle scattering and fluorescence spectroscopy has been explored to elucidate the information about these structural ensembles (Neri et al., 1992; Seetharaman et al., 2002; Kohn et al., 2004; Garcia et al., 1995; 1998). The important aspect of residual structures is the presence of hydrophobic clusters. However, there are several reports where presence of trp(s) has been reported in these clusters (Neri et al., 1992; Tafer et al., 2004; Pearce et al., 2004; Crowhurst et al.,

2002; Seetharaman et al., 2002). The elegant work of Schwalbe and co-workers has shown that presence of trp(s) in hydrophobic clusters stabilize non-native form of lysozyme by long range interaction which is abolished by replacement of trp[62] to glycine (Gly) (Seetharaman et al., 2002).

Understanding the importance of denatured state to the protein folding problem, we wish to investigate if alternative approaches other than NMR can be employed to locate residual structures in denatured protein. The work reported here is an attempt to address the above question.

As involvement of trp in residual structures has been reported earlier, we took advantage of the ubiquitous presence of trp(s) to locate these native-like structures in different denatured proteins. The fluorescence from the indole side chain in trp is a convenient spectroscopic probe for the structure and rotational dynamics surrounding the trp(s) residue in protein (Beechem and Brand 1985). Different fluorescence techniques namely fluorescence quenching, fluorescence anisotropy, FRET, emission maximum of fluorophore has been widely exploited to reveal structure and dynamics of protein (Eftink 1991; Lakshmikanth and Krishnamoorthy 1999; Steiner 1991; Chen and Erickson 2005).

We employed two different biophysical parameters namely, bimolecular fluorescence quenching rate constant (k_q) and steady-state anisotropy (r_{ss}) to monitor extent of exposure and rotational dynamics of trp(s), respectively in a series of ten proteins subsequent to their overnight incubation in 6 M GdnCl at room temperature. Among ten proteins used in my investigation eight proteins namely, barstar, subtilisin carlsberg (SC), human serum albumin (HSA), melittin, myelin basic protein (MBP), glucagon, Ribonuclease T_1 (RNase T_1) and Trp-Met-Asp-Phe possessed only one trp per polypeptide chain whereas bovine serum albumin (BSA) and hen egg white lysozyme (HEWL) were multi-tryptophan containing proteins. The bimolecular fluorescence quenching rate constant (k_q) of indole by extrinsic quenchers like iodide reveals the surface accessibility of indole to the quencher and how deep it is buried in the protein. In this regard we employed iodide as a quencher since 1) it selectively quenches surface exposed trp residue(s) in a protein (Lakshmikanth and Krishnamoorthy 1999) and 2) unlike acrylamide (Garcia et al., 1998) it is free from static quenching, making it a convenient quencher for steady-state fluorescence studies. Steady-state anisotropy (r_{ss}) on the other hand reveals the extent of rotational freedom and dynamics of trp side chain during their fluorescence lifetime (Steiner

1991). Since r_{ss} depends upon fluorescence lifetime and rotational correlation time of fluorophore as described in equation 1.1, change in r_{ss} can be meaningfully correlated with rotational motion of fluorophore only when fluorescence lifetime remains almost invariant under the same experimental condition. Thus, k_q and r_{ss} are sensitive indicators of any structural propensity surrounding trp probe.

As stated earlier that out of ten proteins used in my investigation eight proteins namely, barstar, SC, HSA, melittin, MBP, glucagon, RNase T_1 and Trp-Met-Asp-Phe possessed only one trp per polypeptide chain, it makes unambiguous interpretation of the data possible at molecular level.

Figure 4.1 shows the Stern–Volmer plot observed for quenching of model compound NATA and eight single trp proteins by iodide in the presence of 6 M GdnCl after nightlong incubation at room temperature. Results are also presented for two multi-tryptophan proteins namely, lysozyme (with six tryptophans) and bovine serum albumin (with two tryptophans). Linear variation of F_0/F against iodide concentration in model compound NATA, indicates that quenching is purely dynamic in nature which is consistent with previous report (Maity and Jarori 2002). The presence of static component in quenching would have resulted in an upward curvature owing to the quadratic dependence of F_0/F on quencher concentration.

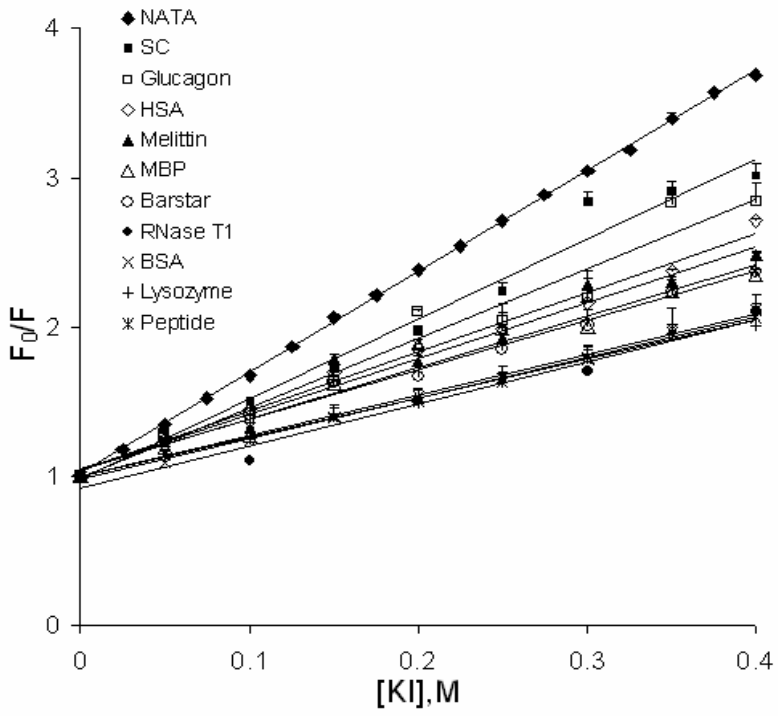

Figure 4.1 Stern-Volmer plot indicating fluorescence quenching of trp(s) in different proteins by iodide in presence of 6 M GdnCl.

The Stern–Volmer constant, K_{SV} calculated from the slope of the fitted straight line and bimolecular quenching constant k_q was calculated from equation 2.16 as follow:

$$K_{SV} = k_q \tau_0$$

where τ_0 is unquenched lifetime of fluorophore. The unquenched fluorescence lifetime of trp in above mentioned proteins (except BSA and tetrapeptide) at 6 M GdnCl was obtained from the earlier work of Swaminathan et al., 1994.

Fluorescence lifetime measurement of tryptophans in BSA and tetrapeptide under same experimental conditions were performed using 295 nm nanoLED source to excite trp(s). Intensity decay measurements were carried out in an IBH fluorocube using the TCSPC method, equipped with motorized Glan-Thompson polarizer and an IBH TBX04 photon detection module. Upon excitation at 295 nm, emission from sample was collected at magic angle (54.7^0) to eliminate the polarization effect on lifetime measurements. Emission was collected through a WG-320 cut-on filter to separate the fluorescence signal from the scattered light. The lifetime(s) were determined by *iterative reconvolution*. Tryptophan lifetime in BSA and tetrapeptide at 6 M GdnCl after overnight incubation was consistent with an earlier measurement performed elsewhere. Initially, in absence of 295 nm light source in our lab, this experiment was performed at Tata Institute of Fundamental Research (TIFR), Mumbai. Table 4.1 shows the mean fluorescence lifetime of BSA and tetrapeptide Trp–Met–Asp–Phe at 6 M GdnCl. Lifetime value obtained from this experiment was used to calculate k_q shown in Table 4.3.

Table 4.1 Fluorescence lifetime of BSA and Tetrapeptide at 6 M GdnCl as obtained from TIFR. (Multiple measurements of BSA and peptide was collected here)

S.No	Conditions	τ_1 (ns)	α_1	τ_2 (ns)	α_2	τ_3 (ns)	α_3 (ns)	χ^2	Mean Lifetime (τ_m) ns
1	BSA 1	0.61	0.25	2.38	0.54	4.53	0.21	0.95	2.38
2	BSA 2	0.63	0.23	2.33	0.54	4.50	0.23	1.04	2.44
3	BSA 3	0.54	0.23	2.16	0.51	4.28	0.26	0.98	2.35
4	Peptide 1	0.40	0.53	1.19	0.41	3.09	0.06	1.09	0.89
5	Peptide 2	0.39	0.51	1.13	0.42	2.98	0.07	1.09	0.89
6	Peptide 3	0.40	0.55	1.28	0.41	3.58	0.04	1.40	0.89

Later on the same experiment with 295 nm source was performed in our laboratory and we obtained nearly same mean fluorescence lifetime of BSA and tetrapeptide, as we obtained from TIFR, Mumbai. Table 4.2 shows the mean fluorescence lifetime of BSA and Trp–Met–Asp–Phe after overnight incubation at 6 M GdnCl .

Table 4.2 Fluorescence lifetime of BSA and Tetrapeptide at 6 M GdnCl as obtained by us. (Multiple measurements of BSA and peptide was collected here)

S.No	Conditions	τ_1 (ns)	α_1	τ_2 (ns)	α_2	τ_3 (ns)	α_3 (ns)	χ^2	Mean Lifetime (τ_m) ns
1	BSA 1	0.02	0.11	1.05	0.20	3.13	0.69	1.18	2.37
2	BSA 2	0.09	0.04	1.22	0.27	3.31	0.69	1.22	2.61
4	Peptide 1	0.04	0.21	0.48	0.29	1.30	0.51	1.09	0.81
5	Peptide 2	0.07	0.11	0.50	0.33	1.32	0.56	1.08	0.91

As evident from Table 4.3, the Stern-Volmer constant for NATA was 6.76 M^{-1} which was similar to the value obtained earlier (6.81 M^{-1}) when NATA was incubated at 3.8 M GdnCl in presence of iodide (Alston et al., 2008). The F_0/F data corresponding to proteins SC and glucagon appear relatively more scattered about their linear regression fit compared to the rest of the proteins in Figure 4.1. However, the value of k_q for SC and MBP are fairly consistent with the values obtained from earlier report (Lakshmikanth and Krishnamoorthy 1999) where k_q value of $2{\cdot}0 \times 10^9$ and $1{\cdot}24 \times 10^9$ $M^{-1}s^{-1}$ were obtained for SC and MBP respectively in presence of 6 M GdnCl. Compared to earlier reported value of k_q with wild type barstar (containing three tryptophans) where value of 1.0×10^9 $M^{-1}s^{-1}$ was observed (Swaminathan 1995), we observed 1.52×10^9 $M^{-1}s^{-1}$ with mutant barstar W38FW44F. It is thus apparent from Table 4.3 that all proteins employed in the study possess a lower k_q compared to a tiny molecule like NATA and the tetrapeptide Trp–Met–Asp–Phe. Decrease in k_q was prominent in RNase T1, which displays a value lower than 50% of the value that observed with NATA, indicating the structural propensity around tryptophan in this protein. Melittin, barstar, BSA and lysozyme also display fairly low values for the bimolecular quenching constant in comparison to the rest of proteins. The lower k_q value in these proteins compared to NATA and tetrapeptide Trp-Met-Asp-Phe indicates the significant amount of shielding from iodide and this is likely to arise if residual structures exist in the vicinity of trp in the above mentioned proteins. Nevertheless, the hindrance posed by the long flexible swollen polypeptide to the

diffusional encounter with iodide, especially when tryptophan is located in the middle of the chain (as in MBP, SC and HSA in Table 4.3) appears negligible.

Table 4.3 Fluorescence quenching, steady-state anisotropy and emission spectrum parameters of proteins in 6 M GdnCl after overnight incubation at 298 K.

Sample	K_{SV} (M^{-1})	τ_m* (ns)	kq ($M^{-1}s^{-1}$)	r_{ss}	Chain length	λ_{max} Emission (nm)	Position of W in the chain
NATA	6.76	2.84	$2.38 \times 10^9 \pm 3.62 \times 10^8$	0.014 ± 0.004	1	352	1
Melittin	3.73	2.43	**1.53×10^9** $\pm 4.24 \times 10^7$	**0.062 ± 0.002**	26	352	19
Glucagon	4.67	2.06	$2.27 \times 10^9 \pm 2.12 \times 10^7$	0.048 ± 0.003	29	350	14
Barstar	3.29	2.16	**1.52×10^9** $\pm 1.25 \times 10^8$	**0.095 ± 0.004**	89	350	53
RNase T1	2.80	2.66	**1.05×10^9** $\pm 9.9 \times 10^7$	**0.091 ± 0.004**	104	348	59
MBP	3.45	1.78	$1.94 \times 10^9 \pm 4.58 \times 10^7$	0.058 ± 0.007	169	350	115
SC	5.34	2.40	$2.23 \times 10^9 \pm 3.54 \times 10^7$	0.053 ± 0.005	274	352	112
HSA	3.98	1.96	$2.03 \times 10^9 \pm 4.95 \times 10^6$	0.084 ± 0.005	585	350	213
BSA	2.75	2.4	**1.15×10^9** $\pm 3.51 \times 10^7$	**0.091 ± 0.002**	583	348	134, 213
Lysozyme	2.63	1.66	**1.58×10^9** $\pm 6.11 \times 10^7$	**0.102 ± 0.002**	129	348	28, 62, 63, 108,111,123
Trp-Met-Asp-Phe	2.70	0.90	$3.03 \times 10^9 \pm 2.36 \times 10^8$	0.045 ± 0.006	4	344	1

*Majority of these values were obtained from previous work (Swaminathan et al., 1994)

Table 4.3 also shows the steady-state fluorescence anisotropy (r_{ss}) for the indole ring in eight single trp proteins, two multi-tryptophan proteins and NATA. For steady-state anisotropy measurement, protein samples at 6 M GdnCl were excited at 295 nm and emission at 355 nm was collected using L-format method. Steady-state anisotropy (r_{ss}) value of 0·014 observed for NATA was consistent with a rotational correlation time ~0·15 ns as calculated from Perrin equation using r_0 = 0·27419 (Lakowicz 3rd Ed, 2006). For a small molecule like NATA this value is expected in mildly viscous solution of GdnCl. For the tetrapeptide also (mean fluorescence lifetime ~0·90 ns) r_{ss} value of 0·045 is consistent with a fast rotational motion. The

observed r_{ss} values in melittin, barstar, RNase T1, BSA, and lysozyme was significantly higher compared to NATA and tetrapeptide. As discussed earlier, r_{ss} depends upon fluorescence lifetime and rotational correlation time of fluorophore, there was no major change in trp lifetime in denatured proteins studied here. Almost constant fluorescence lifetime of trp between 1.7 to 2.7 ns (Swaminathan et al., 1994) clearly indicates that change in r_{ss} in above mentioned proteins are due to the rotational dynamics of trp in denatured states. Thus, Table 4.3 shows agreement between two independent parameters, k_q and r_{ss}. The lower bimolecular quenching constant and higher steady-state anisotropy which reveals the residual structure around trp in RNase T1 has been reported earlier using temperature dependent NOE (Matsuura et al., 2004). Takahashi and co-workers observed that helical region in RNase T1 unfolds at a lower temperature compared to β-sheet B containing tryptophan at 59 (W59). Like many other trp in hydrophobic clusters, W59 in RNase T1 is also buried in a hydrophobic core in the native protein. Among the other single trp containing proteins, melittin and barstar too exhibited a relatively ordered trp as evident from lower k_q and a moderately large r_{ss} in proportion to their chain length. The W53 in barstar is also known to be buried in the hydrophobic core (Swaminathan et al., 1996). Previous reports have also indicated the presence of residual structure around W53 in barstar (Bhavesh et al., 2004; Wong et al., 1999; Saxena et al., 2006). Using cold denaturation of barstar at 3 M urea, Wong et al. reveal residual structure population at the second helices and near the end of the second β-strand of native barstar. Their results suggested that first and second helices of barstar are potential initiation site for folding process. Saxena et al. by employing time-resolved FRET using W53 as a donor in different barstar mutant and showed that the fraction of unfolded molecules having native-like compactness is insignificant in the total population of unfolded molecules.

In lysozyme, which has six tryptophans, we observed low k_q and a higher r_{ss} suggesting the presence of residual structures. Presence of these native-like structures in denatured lysozyme involving trp(s) has been shown by Schwalbe and co-workers. Using NMR they showed that four of the six tryptophans in lysozyme are indeed part of hydrophobic clusters in 8 M urea. They also demonstrated that W62 play a critical role in stabilizing all hydrophobic clusters by long-range interaction (Seetharaman et al., 2002)

Melittin which is almost similar in size to peptide glucagon, shows a significantly higher r_{ss} and lower k_q in contrast to glucagon. This strengthens the possibility that trp in melittin is part of a residual structure.

It is however interesting to compare the data obtained from BSA and HSA which are nearly similar in polypeptide chain but have different tryptophan residues. HSA possess only one trp per polypeptide chain wheras BSA has two tryptophans. While the sole trp in HSA has a k_q ~2·0 × 10^9, the overall k_q of two tryptophans in BSA was observed ~1·1 × 10^9 $M^{-1}s^{-1}$. In both cases the position of tryptophan residues in the polypeptide are well in the interior. The r_{ss} observed for BSA is marginally higher compared to HSA, but importantly the mean fluorescence lifetime for BSA is also higher suggesting a slower r_{ss} compared to HSA. Based on these observations it is likely that at least one of the tryptophan residues in BSA is part of a residual structure.

The wavelength corresponding to fluorescence emission maximum for indole side chain in denatured proteins forms yet another parameter to estimate the exposure of the indole ring to the solvent. Buried tryptophan in native protein exhibit emission maximum near 308 nm while in solvent exposed condition it is nearly 350 nm (Alston et al., 2008). We monitored the solvent exposure of trp(s) in all proteins by observing emission maximum after nightlong incubation at 6 M GdnCl. Subsequent to excitation at 295 nm all proteins in our study except tetrapeptide, revealed emission maxima between 348 and 352 nm in the denatured state. In case of tetrapeptide emission maximum was nearly 344 nm (Figure 4.2 and Table 4.3).

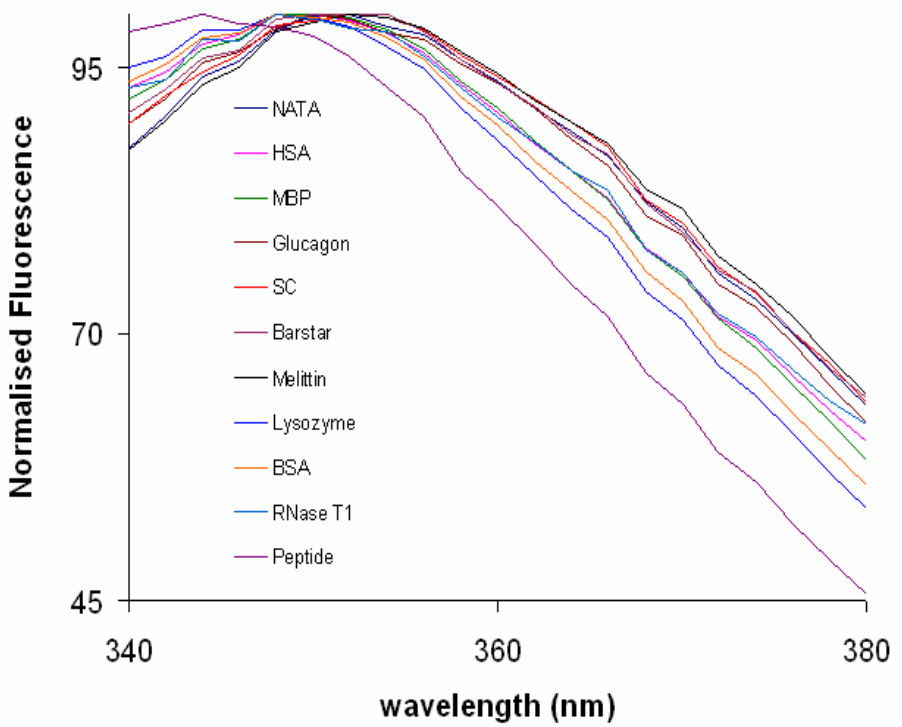

Figure 4.2 Corrected fluorescence emission spectra of trp(s) in different proteins in presence of 6 M GdnCl.

The observed fluorescence emission maximum in all proteins was close to that observed for NATA (352 nm), indicating that indole is solvent exposed in all the proteins after overnight incubation at 6 M GdnCl. On the contrary, observations from quenching data reveals that the indole in RNase T1, BSA, melittin, barstar and lysozyme is not freely accessible to a large anion like iodide. Steady-state anisotropy data also suggests the likelihood of residual structure around trp in above mentioned proteins. The absence of correlation between indole emission maxima and rate of iodide quenching is clearly evident in the case of the tetrapeptide, which has the lowest emission maximum and highest bimolecular quenching constant. Therefore trp(s) emission maximum is not a useful probe for locating residual structures.

Thus, iodide quenching and steady-state anisotropy experiments provide a superior alternative to locate residual structures in denatured protein compared to fluorescence emission maxima.

Experiment at a glance

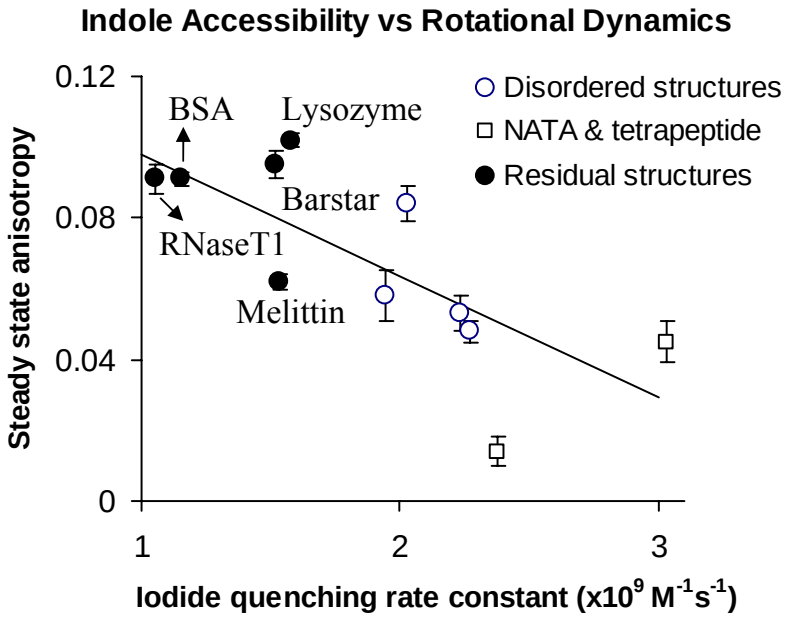

Figure 4.3 The correlation between two independent structural parameters of tryptophan side chain in ten denatured proteins is highlighted. Tryptophan residues present in hydrophobic clusters are likely to possess low biomolecular iodide quenching rate constant and high anisotropy compared to N-Acetyl-L-tryptophanamide, Trp-Met-Asp-Phe-NH_2 peptide and other disordered tryptophans in proteins.

Conclusions:

(1) Fluorescence bimolecular quenching rate constant and steady-state anisotropy of trp, can serve as useful parameters to search and locate residual structures in the vicinity of trp in denatured proteins.

(2) Tryptophan emission maximum, on the other hand is not so conclusive for revealing residual structures in denatured proteins.

(3) It is likely that trp(s) is a part of residual structure in BSA, RNase T1, Lysozyme, Barstar and Melittin after night long incubation at 6 M GdnCl.

Chapter 5

Effect of SDS, CTAB and DTT on the size, dynamics, activity and growth of soluble lysozyme aggregates

Protein misfolding and aggregation has invited attention from large pool of scientists in recent years not only owing to their potential involvement in many neuropathic and nonneuropathic diseases like Alzherimer's disease or diabetes type II (Chiti and Dobson 2006) but also due to the reduced recovery of recombinant proteins in biotechnology industries (Carrio and Villaverde 2002). Insoluble protein aggregates like amyloid fibrils are associated with a wide range of diseases that arise due to degeneration of nerve cells. Although the exact molecular mechanism leading to protein aggregation is still elusive, it is a popular belief that protein has to unfold at least partially for eliciting their self-association (Chiti and Dobson 2006). Aggregated proteins are characterized by cross beta sheet structure and wealth of information suggests that early soluble oligomers otherwise known as "protofibrils" are real culprits in various protein misfolding disorders (PMDs) (Stefani 2004; Kayed et al., 2003; Ross and Poirier 2004). Employing cell culture model of Huntington's disease, it has been shown that inclusion body formation supports neuronal survival whereas small oligomers of Huntington protein cause significant cell death (Arrasate et al., 2004).

Pathogenicity of soluble oligomers are not only restricted to disease related proteins. Prefibrillar aggregates from non disease related proteins has also been found toxic towards cultured fibroblasts and neurons, while, mature fibrils were not cytotoxic in nature (Bucchiantini et al., 2002; Sirangelo et al., 2004).

Inhibiting protein misfolding and controlling the growth of their pathogenic species are urgently required as therapeutic intervention against different PMDs. Past few years have witnessed significant progress in development of therapeutic strategies against PMDs (Rochet 2007). Meredith and co-workers inhibited Aβ fibrillization employing small peptide spanning residue 16-20 of Aβ with some modifications (Sciarretta et al., 2006), whereas an analogue of human islet amyloid polypeptide (IAPP) has been found to be a potent inhibitor of IAPP fibrillization (Yan et al., 2005). Stabilizing the native structure of protein is an alternative approach to reduce

their misfolding and oligomerization. Thyroxine (T4) is known to stabilize the tetrameric structure of transthyretin, thus prevent its dissociation into aggregation prone monomers (Johnson et al., 2005). Different small molecules like ligand, substrate or enzyme inhibitors are known to selectively bind to the native protein conformer and prevent its structural fluctuation leading to misfolding and aggregation (Rochet 2007; Loo and Clarke 2007; Papp and Csermely 2006). Various post translational modifications (Wittmann et al., 2001; Best et al., 2007), use of antioxidants (Masuda et al., 2006) and chaperone-mediated autophagy (Muchowski and Wacker 2005) are other approaches against various PMDs.

Understanding the pathogenic behavior of soluble protein oligomers, and urgent need to inhibit their growth in solution, we used hen egg white lysozyme (HEWL) as a model protein and studied the growth of aggregates and their subsequent inhibition at pH 12.2.

Hen egg white lysozyme is structurally a well characterised protein capable of cleaving glycosidic linkage. Owing to its small size (129 residues) and excellent solubility in water, it can serve as a model protein to investigate the protein folding/misfolding phenomenon (Trexler and Nilsson 2007). HEWL is a globular protein with overall dimensions of 4.5 nm x 3.0 nm x 3.0 nm (Blake et al., 1965). Eight cysteine residues with four disulphide bonds makes HEWL an extremely stable protein. In spite of having ~60% sequence homology with human lysozyme, which causes systemic nonneuropathic amyloidosis (Pepys et al., 1993), HEWL is non-amyloidogenic in nature. Aggregation and amyloid fibril formation in HEWL under acidic condition has been extensively explored (Krebs et al., 2000; Frare et al., 2004; McAllister et al., 2005). Amyloid formation in lysozyme was observed at pH 2.7 and 57^0C after incubation for 10 days using AFM (McAllister et al., 2005) whereas Dobson and co-workers has shown that a peptide corresponding to residues 49—64 from the β-domain of HEWL readily forms fibrils at pH 4.0 (Krebs et al., 2000). Compared to acidic conditions only few reports are available where self-association of lysozyme at alkaline condition has been studied. Equilibrium-sedimentation experiments have shown that hen egg white lysozyme undergoes reversible pH dependent self-association at 1 mM concentration (Sophianopoulos and Van Holde 1961), where monomers are populated below pH 4.5 and higher aggregates between pH 9.8 and 11 (Sophianopoulos and Van Holde 1964). Recently, Yousefi and co-workers observed lysozyme fibril formation in presence of SDS (0.1—2.5 mM) at pH

9.2 (Mohavedi et al., 2007). They also observed β-cyclodextrin as an effective inhibitor of lysozyme fibrillization at alkaline pH.

Owing to few reports describing HEWL aggregation at alkaline condition, we took this condition as a challenge and tried to monitor the growth of HEWL aggregates with or without additives using different biophysical and biochemical techniques. In earlier work we demonstrated that HEWL shows aggregation tendency at pH 12.2 (Homchaudhuri et al., 2006), in the present work we explored if small molecules like anionic surfactant sodium dodecyl sulphate (SDS), cationic surfactant cetyl trimethylammonium bromide (CTAB) and disulphide breaking agent 1,4 Dithioerythritol (DTT) can inhibit HEWL aggregation at alkaline condition?

We began our study to monitor the growth of aggregates by measuring the scattering intensity from unlabeled HEWL at pH 7 and pH 12.2. Then dansyl labeled lysozyme was used to monitor the growth of protein aggregates with or without additives at pH 12.2 employing steady-state and time-resolved fluorescence anisotropy technique. Fluorescence anisotropy, owing to its sensitivity and specificity is a unique technique to observe fluorophore dynamics in solution at nanosecond time-scale (Lakowicz,3rd Ed, 2006). We used long lifetime fluorescent probe, dansyl chloride (~15 ns) to monitor the slow overall tumbling motion of large multimeric aggregates as shown by us earlier (Homchaudhuri et al., 2006). Steady-state fluorescence anisotropy (r_{ss}) gives a time integrated average value of the rotational motion of molecule in the excited state, while time-resolved anisotropy decay data yields multiple rotational motions experienced by the fluorophore in the excited state in term of their rotational correlation time, ϕ_i. Subsequently, unlabeled lysozyme was used to monitor the exposure of hydrophobic patches and kinetics of fibril formation at different experimental condition employing ANS and thioflavin T fluorescence respectively. Secondary structural feature in different experimental condition was monitored by circular dichroism spectroscopy while involvement of disulphide bonds during aggregation process was expounded by estimating free thiol groups. Later on, we also monitored the catalytic activity of HEWL with or without additives in pH 12.2 at different time points. These investigations elucidated the underlying molecular mechanisms during the process of HEWL aggregation under alkaline condition including the inhibitory effect of different additives.

5.1 Light scattering experiment

After monitoring the growth of dansyl conjugated HEWL at pH 12.2, we tried to observe the same phenomenon with unlabeled lysozyme in same experimental condition. This experiment was also imperative to rule out the possibility that covalent modification of the amino group induces HEWL aggregation. Figure 5.1 shows the light scattering intensity of 150 µM unlabeled lysozume at pH 7 and pH 12.2. Increase in scattering intensity upto 360 minutes of pH 12.2 incubated HEWL indicates the formation of aggregates, while at pH 7, fairly constant values reflects the presence of monomeric lysozyme. This finding from scattering experiment supports our steady-state observations where lysozyme showed aggregation tendency at pH 12.2 and also rules out the likelihood of covalent modification promoting oligomerization under this condition.

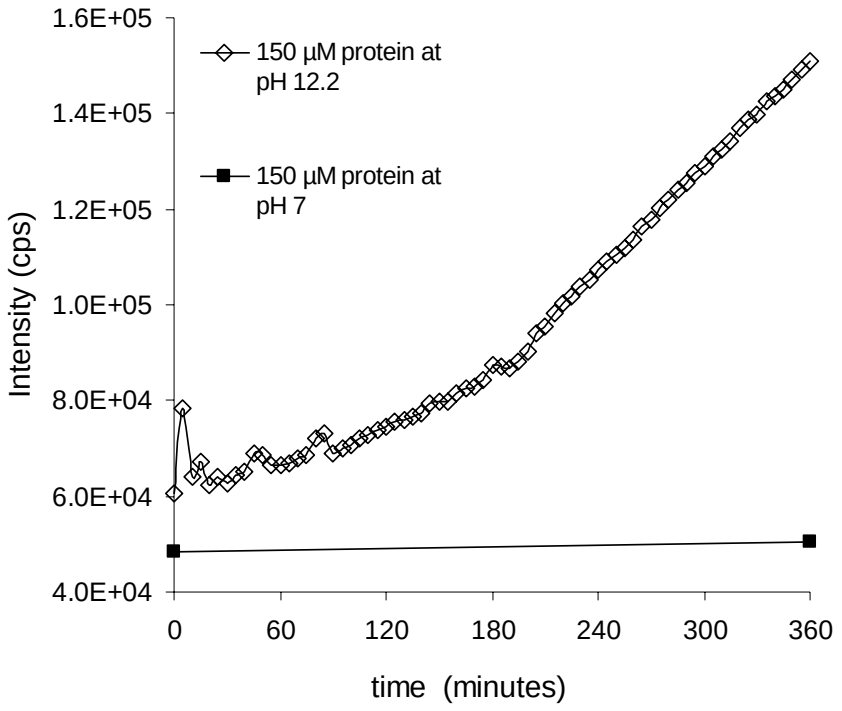

Figure 5.1 Formation of aggregates in solutions of unlabeled lysozyme (150 µM) monitored by light scattering using vertically polarized light at 350 nm.

Since scattering signals are prone to contamination, we did not extended the scattering experiments to monitor the effect of SDS, CTAB and DTT on the growth of HEWL aggregates. Scattering signal from additives can interfere with the signals from protein and make the observations more complicated.

5.2 Steady-state fluorescence anisotropy at short times with 40 µM labeled HEWL

Steady-state anisotropy measurement of 40 µM dansyl labeled lysozyme at pH 12.2 alone (CONTROL) or in presence of 14 mM SDS, 3 mM CTAB or 20 mM DTT was performed at 298 K. To monitor the effect of lower temperature on HEWL aggregation, steady-state anisotropy (r_{ss}) of a sample at 283 K (without additives but identical otherwise) was also run in parallel. Figure 5.2 shows the variation in r_{ss} of 40 µM dansylated HEWL as a function of time after exposure to alkaline pH under different conditions. In the absence of any additive, r_{ss} value of ~0.08 was observed initially, showing gradual increase with time upto ~0.15 over the period of 360 minutes and constant thereafter as observed after a night long (~12 hours) incubation (referred onward as 'overnight incubation') at room temperature.

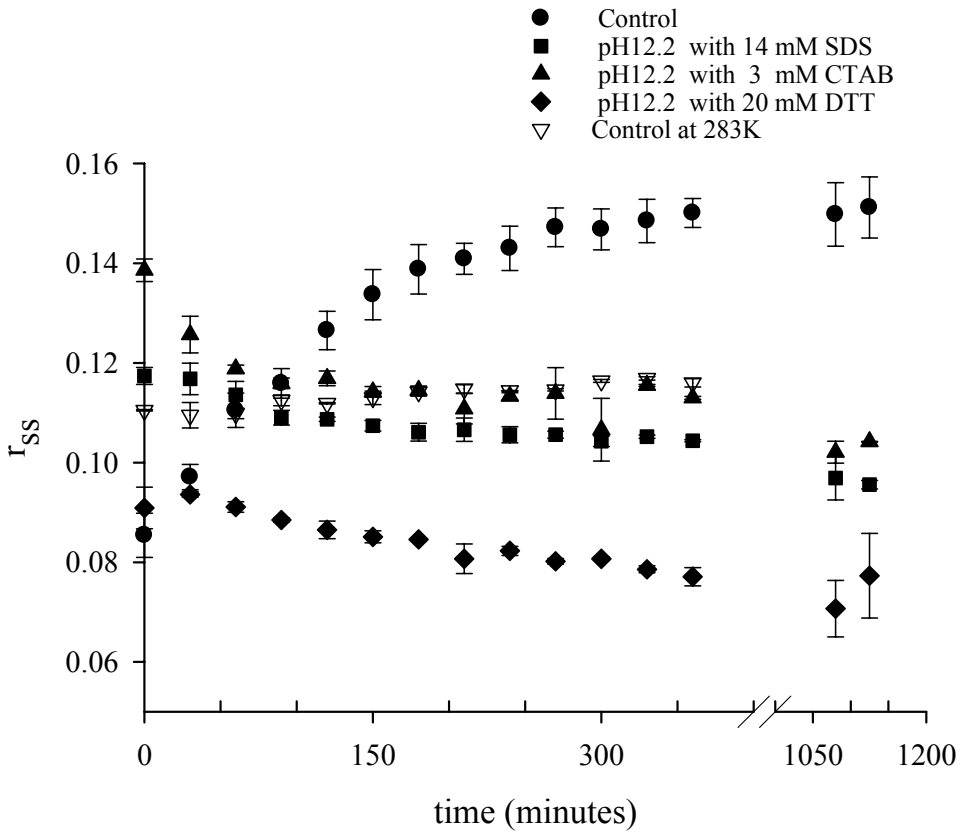

Figure 5.2 Change in steady-state anisotropy of 40 µM dansyl labeled lysozyme in the presence and absence of different additives at pH 12.2 is plotted against time. All measurements except one were performed at 298 K.

In the presence of 14 mM SDS in the medium, the r_{ss} begins at ~0.12 and displays a minor dip at ~120 minutes followed by a plateau like profile over the

period of ~1200 minutes. In the presence of 3 mM CTAB in the medium, the r_{ss} which was initially at ~0.14 shows a rapid fall to ~0.12 by 120 minutes. Subsequently a fairly uniform profile is maintained by r_{ss} with time. Similar to SDS, a minor dip in r_{ss} was evident after overnight incubation. In the presence of 20 mM DTT also there was a gradual decrease in r_{ss} starting from ~0.09 initially to ~0.07 after overnight incubation. Thus, in contrast to the control (absence of additive) no increase in r_{ss} was observed in the presence of SDS, CTAB and DTT. Since steady-state anisotropy serves as quick indicator of fluorophore rotational motion, higher r_{ss} in control indicates the growth of HEWL aggregates with time while significantly lower value of r_{ss} with SDS, CTAB and DTT clearly indicates their effectiveness against oligomerization of HEWL at pH 12.2.

The experiments above were carried out at 298 K. Next we look at the influence of lower temperature. Steady-state anisotropy of dansyl probe conjugated HEWL incubating at 283 K in the absence of any additive indicates the almost constant value (0.110-0.116) throughout the six hours period, indicating no significant change in the size or dynamics of the protein. We also tried to monitor the same experiment at 338 K but due to precipitation this experiment was not possible to perform.

After observing significant difference in r_{ss} of dansyl labeled HEWL in control and in presence of additives, we proceeded toward time-resolved measurements. Since r_{ss} is a function of fluorescence lifetime and the rotational correlation time of the fluorescent probe, we then performed time-resolved fluorescence intensity decay and anisotropy decay of the dansyl conjugated HEWL to measure the fluorescence lifetime and rotational correlation times respectively of dansyl probe in different experimental conditions.

5.3 Time-resolved fluorescence measurement

We used different concentrations of dansyl labeled HEWL at pH 7, pH 12.2 alone or in presence of SDS, CTAB or DTT to observe concentration dependent change in lifetime of dansyl probe in given set of experiments. These experiments were necessary to perform since time-resolved anisotropy measurements involved 120 μM HEWL whereas r_{ss} measurements were with 40 μM HEWL. 40 μM and 120 μM protein was employed to pH 12.2 alone or in presence of SDS and DTT. With 3 mM

CTAB, protein concentration was 40 and 80 μM because any higher concentration of protein showed precipitation probably due to formation of electroneutral complex.

Table 5.1 Fluorescence lifetime of 40 μM dansyl labeled lysozyme in different experimental conditions.

S.No	Conditions	t mins	τ_1 (ns)	α_1	τ_2 (ns)	α_2	τ_3 (ns)	α_3 (ns)	χ^2	Mean Lifetime (τ_m) ns
1	pH 7	0	8.4	0.12	14	0.86	0.22	0.01	1.2	13.0
2	pH 7	1600	6.4	0.18	14.6	0.8	0.58	0.02	1.5	12.8
3	pH 12.2	0	5.7	0.14	14.7	0.83	0.45	0.03	1.7	13.0
4	pH 12.2	1600	7.0	0.20	14.2	0.80	0.53	0.03	1.5	12.8
5	pH 12.2, 14 mM SDS	0	6.9	0.13	13.0	0.85	0.35	0.02	1.4	11.9
6	pH 12.2, 14 mM SDS	1600	6.6	0.13	13.6	0.85	0.5	0.02	1.3	12.4
7	pH 12.2, 3 mM CTAB	0	5.1	0.23	13.0	0.74	0.88	0.08	1.4	10.9
8	pH 12.2, 3 mM CTAB	1500	5.2	0.14	13.6	0.85	0.34	0.01	1.4	12.3
9	pH 12.2, 20 mM DTT	0	5.7	0.14	12.1	0.83	0.71	0.03	1.1	10.8
10	pH 12.2, 20 mM DTT	1600	5.7	0.12	11.8	0.84	0.06	0.03	1.4	10.6

Table 5.2 Fluorescence lifetime of 120 μM and 80 μM labeled lysozyme with SDS, DTT and CTAB respectively. Lifetime of 20 μM protein at pH 12.2 is also shown.

S.No	Conditions	t mins	τ_1 (ns)	α_1	τ_2 (ns)	α_2	τ_3 (ns)	α_3 (ns)	χ^2	Mean Lifetime (τ_m) ns
1	pH 7	0	14	0.24	11.3	0.75	0.2	0.01	1.4	11.84
2	pH 7	1600	5.3	0.02	12.0	0.87	0.6	0.01	1.2	11.5
3	pH 12.2	0	5.8	0.17	13.0	0.8	0.13	0.03	1.3	11.4
4	pH 12.2	1600	6.1	0.17	13.1	0.81	0.36	0.02	1.3	11.6
5	pH 12.2, 14 mM SDS	0	5.0	0.06	12.0	0.92	0.60	0.02	1.4	11.3
6	pH 12.2, 14 mM SDS	1600	7.7	0.04	11.8	0.95	0.11	0.01	1.5	11.5
7	pH 12.2, 3 mM CTAB	0	4.0	0.34	10.8	0.6	0.56	0.07	1.4	7.8
8	pH 12.2, 3 mM CTAB	1500	4.2	0.25	11.2	0.7	0.41	0.05	1.3	8.9
9	pH 12.2, 20 mM DTT	0	4.7	0.1	11.2	0.87	0.31	0.03	1.5	10.2
10	pH 12.2, 20 mM DTT	1500	19	0.09	9.52	0.9	2.34	0.01	1.6	10.3
11	20 μM, pH 12.2	0	5.4	0.11	14.0	0.86	0.32	0.03	1.3	12.6
12	20 μM, pH 12.2	1500	6.0	0.10	13.0	0.89	0.25	0.03	1.6	12.2

Analysis of time-resolved fluorescence intensity decay revealed the presence of three lifetimes in all experimental conditions (Table 5.1 and 5.2). Mean fluorescence lifetime of dansyl tagged HEWL at pH 7 and pH 12.2 (11-13 ns) was consistent with earlier reported values (Homchaudhuri et al., 2006) however, occurrence of three lifetime components reflects the structural heterogeneity of lysozyme in solution (Wang et al., 2002; 2004). Table 5.1 and 5.2 shows the lifetime data obtained by analyzing the intensity decay profiles under different conditions.

Figure 5.3 depicts the mean fluorescence lifetime (τ_m) of labeled protein at pH 7, pH 12.2 alone or presence of additives over the period of more than 1400 minutes.

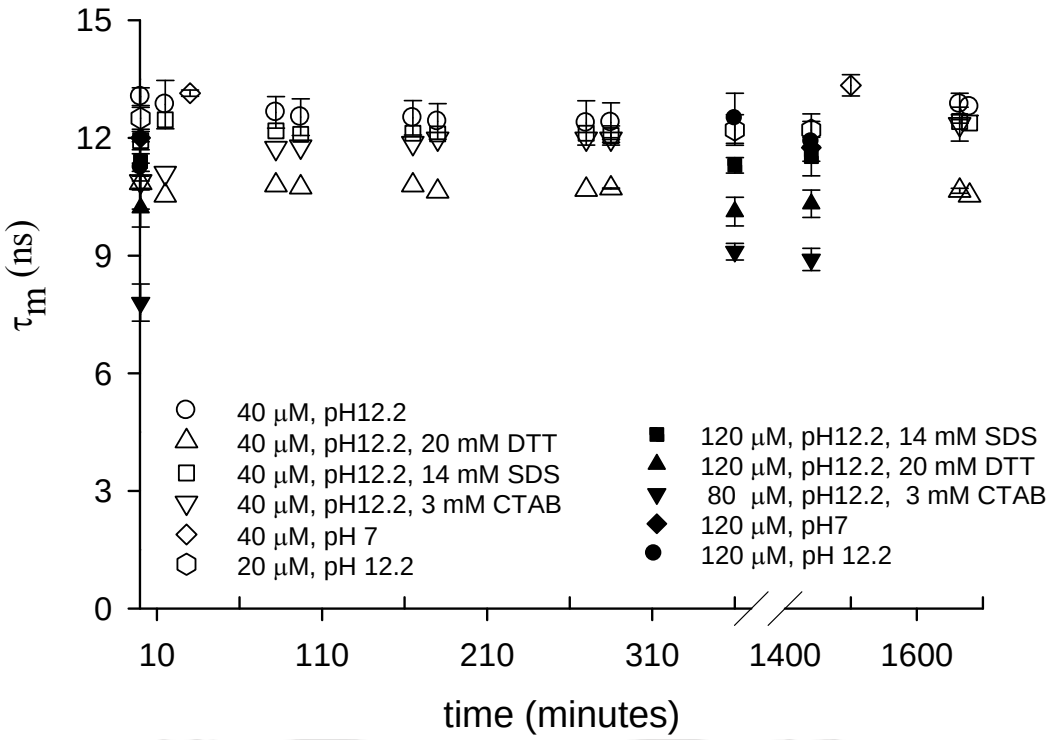

Figure 5.3 Variation in the mean fluorescence lifetime, (τ_m) of dansyl labeled lysozyme at different concentrations, in presence and absence of different additives at pH 7 and pH 12.2 is shown against time. τ_m was calculated using the formula $\sum_{i=1}^{3} \alpha_i \tau_i$,where τ_i and α_i correspond to the i^{th} lifetime and its fractional amplitude, respectively. In all experimental conditions the maximum relative errors for mean lifetime values were between 2% to 7%.

As evident from Table 5.1, 5.2 and Figure 5.3, mean fluorescence lifetime of danyl probe either with 40 μM or 120 μM protein with or without additives at pH 12.2 was almost constant between 10.3 ns to 12 ns. However, in case of 80 μM protein with 3 mM CTAB, a reduced lifetime was observed. Figure 5.3 also shows that 20

μM protein also have same mean lifetime as observed for higher concentrations of proteins. Thus concentration dependent changes in mean lifetime can be ruled out in these cases. The changes in fluorescence lifetime of dansyl probe in presence of CTAB may arise from binding and subsequent electrostatic interaction between positively charged CTAB with negatively charged HEWL at pH 12.2 (Chatterjee et al., 2002). This interaction seems to be more pronounced at higher protein concentration where with 80 μM protein, mean lifetime reduces to ~8.5-9.0 ns compared to 40 μM (11-12 ns). Fairly invariant fluorescence lifetime over the period of ~1500 minutes indicates that the rise in r_{ss} may not be attributed to change in lifetime however, it was likely that rotational correlation time shall contribute to these changes. The invariance of lifetime data during 0-1500 minutes clearly validates the use of r_{ss} to monitor the aggregation of dansyl labeled HEWL. Subsequently we performed time-resolved anisotropy decay measurements to obtain insight into the molecular dynamics of protein in control and in presence of additives.

5.4 Time-resolved anisotropy decay measurements

Time-resolved fluorescence anisotropy decay measurements were performed with 80-120 μM of dansyl labeled HEWL at 30 minutes, 360 minutes and ~1400 minutes subsequent to their incubation at pH 12.2 with or without 14 mM SDS, 3 mM CTAB and 20 mM DTT. Since we were interested in larger protein aggregates, higher protein concentration was chosen to specifically magnify the effect of different additives on the progress of aggregation**.** Anisotropy decay data were analyzed and different correlation times were extracted indicating segmental and global motion of probe and protein molecule respectively during the process of aggregation and their subsequent inhibition. Figure 5.4 depicts the anisotropy decay of labeled lysozyme at different experimental conditions while Table 5.3 shows the data extracted from anisotropy decay analysis. Anisotropy decay at different time points in Figure 5.4 has been indicated by different colors. Black, at t = 30 minutes; blue, at t = 360 minutes; red, at t = ~1500 minutes after incubation.

Figure 5.4A shows the time-resolved fluorescence anisotropy decay of dansyl tagged 120 μM HEWL at pH 7 after 30 minutes and 1600 minutes of incubation at 298 K. No significant change in the rate of anisotropy decay was visible between the two observations widely separated in time. Importantly, the anisotropy r(t), decays to zero after ~20 ns, indicating absence of residual anisotropy (r_∞). The decay fitted well

to a single exponential with a rotational correlation time ~4 ns (see Table 5.3, items 1-2), accounting for tumbling of the whole protein that is fully monomeric. This value is consistent with previously reported value (3.8 ns) for native lysozyme (Vos et al., 1987). Therefore, the overall 3D structure of the protein in the native state is intact and unchanged during the long duration of incubation. This was in agreement with our earlier results (Homchaudhuri et al., 2006).

Anisotropy decay of 120 μM HEWL in pH 12.2 at different time points is shown in figure 5.4B. While observing r(t) longer time (~30 ns), which we termed as residual anisotropy (r_∞) there was small but significant r_∞ (~0.03) at 30 minutes. As time progresses, this value rises significantly (>0.10) at 360 minutes and remains constant till next day (1500 minutes). Analysis of anisotropy decay profile revealed the presence of two correlation times at 30, 360 and 1500 minutes of incubation (Table 5.3, items 3-5). Looking at the fast rotational component, a value of ~2.4 ns (amplitude of 0.44) was observed at 30 minutes. Subsequently at 360 minutes this component is slowed down (~5 ns) and it remains fairly slow (~5 ns) thereafter at 1500 minutes, although a minor increase in the amplitude of this component (0.26 to 0.38) was seen after overnight incubation. Thus, changes in fast component which indicates the segmental motion of dansyl probe (attached to ε-amino group of L-lysine residue in lysozyme) indicates that probe that was initially fast and free, became slow and hindered later on as time progresses. While observing the slow component which reflects the global motion of protein, correlation time of ~10 ns with amplitude 0.56 was obtained after 30 minutes of incubation. This ~10 ns component may arise from the global tumbling of a small oligomeric HEWL or from an extended topology of a misfolded monomer. After 360 minutes this component increased significantly to ~73 ns (0.74) and ~60 ns (0.62) after 1500 minutes, indicating the formation of large multimeric HEWL aggregates and their reorganization after overnight incubation. So, six hours exposure to alkaline pH appears sufficient to trigger formation of large aggregates in HEWL. We used this condition as a control for different manoeuvres that follow to inhibit the process of aggregation.

Figure 5.4C shows the effect of 14 mM SDS on HEWL aggregation at pH 12.2. The anisotropy decay data indicates r_∞ value of ~0.04 after 30 minutes which decreased to ~0.02 after 360 minutes and remain almost constant after 1500 minutes of incubation. The details of the fits obtained from these traces are displayed in Table 5.3 (items 6-8). After 30 minutes fast segmental motion of 2.1 ns was observed with

an amplitude of 0.29. This value was slightly increased to 2.4 ns at 360 minutes and 2.8 ns at 1500 minutes with higher amplitude (0.55-0.58). This reflects the fairly unrestricted segmental mobility of dansyl group at later times. While looking to slow component, we observed 9.4 ns (0.71) correlation time at 30 minutes which was similar to that observed with control at same time point. At 360 and 1500 minutes, this value was constant with ~14 ns (0.45-42), indicating an oligomeric HEWL with loose molecular packing perhaps with bound SDS micelles. These observations clearly indicate that SDS inhibits progress of HEWL aggregation at pH 12.2.

Figure 5.4D depicts the influence of 3 mM CTAB on the kinetics of HEWL aggregation at alkaline condition. Residual anisotropy at 30 minutes shows the value of ~0.05 which was reduced to ~0.03-0.02 at 360 and 1500 minutes respectively. Fitted parameters for each of the traces are shown in Table 5.3 (items 9-11). Fast component of ~2.2 ns with 0.48 amplitude was monitored after 30 minutes, which showed faster segmental motion of ~1.5 ns with amplitude of 0.45 after 360 minutes and remain almost constant thereafter upto 1500 minutes of observations. Slow component also exhibited decreasing trends with ~14 ns at 30 minutes to ~12 ns after 360 minutes then ~10 ns after 1500 minutes of incubation with marginal increase in amplitude. These results suggest that HEWL exists as a loosely packed oligomer, whose aggregation propensity is diminished in prolonged presence of CTAB.

To rule out any contribution of solution viscosity for slow overall tumbling (10-14 ns) of the protein in presence of 14 mM SDS or 3 mM CTAB, we performed bulk viscosity measurements using Ostwald's viscometer and observed no significant change in solution viscosity in presence of these surfactants.

Figure 5.4E shows the influence of 20 mM DTT on the growth kinetics of lysozyme aggregates in solution at pH 12.2. Residual anisotropy of <0.05 at 30 ns after 30 minutes of incubation indicates fast anisotropy decay. This value was exhibiting a decreasing trend at 360 and 1400 minutes. Table 5.3 (items 12-14) display the details of the fits obtained by these traces. Fast component of ~1.2 ns was observed after 30 minutes of incubation, which increased marginally to ~1.9 ns at 360 minutes and 1.4 at 1400 minutes. Amplitude of fast motion was also raised from 0.45 to 0.64 and finally to 0.81. This observation indicates increasing freedom for segmental motion in presence of DTT. Slow component between 7-8 ns with concomitant decrease in amplitude (0.55 to 0.19) was observed for same time span indicating the elongated monomeric form of HEWL. These observations indicate that

inhibitory effect of DTT is emphatic on HEWL oligomerization, compared to SDS and CTAB.

In order to investigate the influence of low monomer concentration on dynamics of the aggregates, we carried out experiments with 20 μM lysozyme at pH 12.2. Figure 5.4F reveals the anisotropy decays observed at 30, 360 and 1500 minutes of exposure to alkaline pH. At 30 minutes of incubation, r_∞ was nearly zero which marginally increased to ~0.02 after 1500 minutes reflecting the slow progress of aggregation. The decay parameters are listed in Table 5.3, items 15-17.

Compared to higher monomer concentration (120 μM protein), the amplitude for the fast segmental motion (0.55) at 30 minutes is significantly higher indicating a relatively unhindered mobility. As time progresses, this rotational component becomes noticeably faster (~1.3 ns) retaining significant amplitude quite unlike the ~5 ns component at higher monomer concentration where segmental motion is slowed down and restricted as time progresses. The slow component shows a value around 11-12 ns at 360 minutes and later, indicating a small oligomer in contrast to the large multimeric aggregate (~60 ns) observed at higher monomer concentration. It is thus, apparent that a low monomer concentration has a critical impact on the aggregation growth kinetics as would be expected for a concentration dependent phenomenon.

It is thus clear from Figure 5.4 and Table 5.3 that the rotational correlation times of dansyl probe obtained from anisotropy decays serve as an excellent indicator of the process of HEWL aggregation. The reduced rotational correlation times in presence of 14 mM SDS, 3 mM CTAB and 20 mM DTT compared to pH 12.2 control clearly indicates the effectiveness of these molecules in arresting the growth of HEWL aggregates at alkaline pH.

The figures obtained during the analyzing the anisotropy decays are shown in Figures 5.5 to 5.8.

Table 5.3 Decay parameters recovered from fits to anisotropy decay curves in Figure 5.4

	Condition	t mins	r_0 [a]	r_{ss} [b]	ϕ_1 [c] (ns)	ϕ_2 [c] (ns)	α_1 [d]	α_2 [d]	χ^2 [e]
1	pH 7	30	0.18	0.04	4.1	--	1.0	--	1.5
2	pH 7	1600	0.18	0.05	4.0	--	1.0	--	1.5
3	pH 12.2	30	0.29	0.10	2.4	10	0.44	0.56	1.2
4	pH 12.2	360	0.29	0.20	4.9	73	0.26	0.74	1.5
5	pH 12.2	1500	0.27	0.17	4.8	58	0.38	0.62	1.4
6	pH 12.2, 14 mM SDS	30	0.25	0.10	2.1	9.4	0.29	0.71	1.3
7	pH 12.2, 14 mM SDS	360	0.23	0.09	2.4	14	0.55	0.45	1.3
8	pH 12.2, 14 mM SDS	1500	0.23	0.08	2.8	14	0.58	0.42	1.5
9	pH 12.2, 3 mM CTAB	30	0.27	0.14	2.2	14	0.48	0.52	1.1
10	pH 12.2, 3 mM CTAB	360	0.29	0.12	1.5	12	0.45	0.55	1.3
11	pH 12.2, 3 mM CTAB	1500	0.29	0.10	1.3	10	0.51	0.49	1.2
12	pH 12.2, 20 mM DTT	30	0.26	0.08	1.2	7.5	0.45	0.55	1.4
13	pH 12.2, 20 mM DTT	360	0.20	0.05	1.9	8.4	0.64	0.36	1.4
14	pH 12.2, 20 mM DTT	1400	0.24	0.05	1.4	7.1	0.81	0.19	1.6
15	pH 12.2, 20 µM	30	0.21	0.06	2.4	8.9	0.55	0.45	1.4
16	pH 12.2, 20 µM	360	0.25	0.07	1.3	11	0.49	0.51	1.2
17	pH 12.2, 20 µM	1500	0.28	0.08	1.4	12	0.57	0.43	1.9

[a]initial anisotropy; [b]steady-state anisotropy calculated from fit; [c]rotational correlation time(s); [d]fractional amplitudes associated with correlation time; [e]reduced chisquare for the fit. The errors in the values reported for ϕ_1 are within 10%, while those for ϕ_2 are 5%, based on results from multiple experiments.

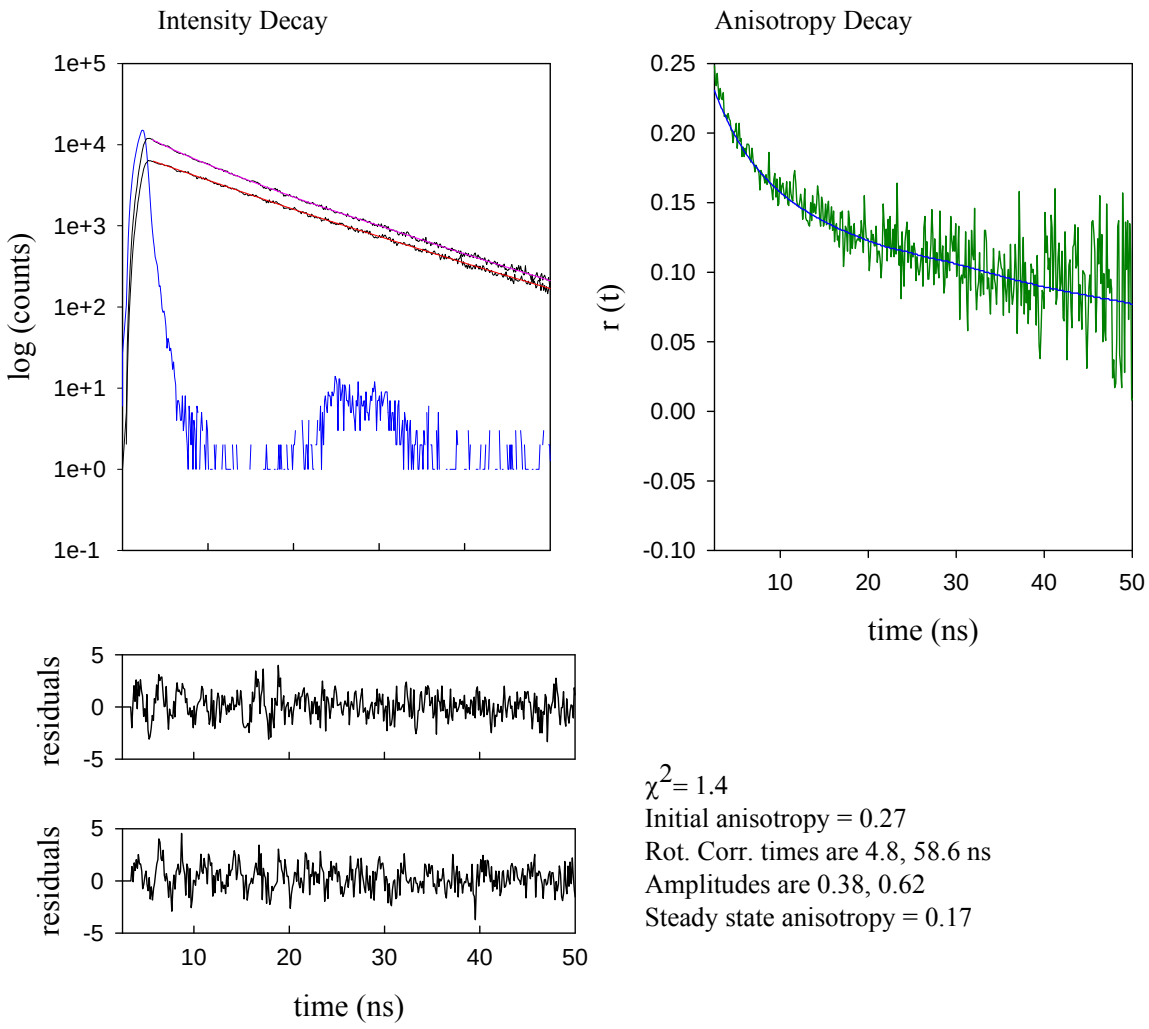

Figure 5.5 The plots shown above correspond to (i) IRF (blue); (ii) measured I_{par} (black); (iii) fitted I_{par} (pink); (iv) measured I_{per} (black); (v) fitted I_{per} (red). The measured anisotropy decay is shown in dark green and fitted anisotropy decay is depicted by blue curve. The corresponding residuals are shown in black curves below the intensity decay plots. Upper residual represents for parallel intensity decay (I_{par}) while lower residual represents for perpendicular intensity decay (I_{per}).

Anisotropy Decay of 120 μM dansyl labeled lysozyme in pH 12.2 buffer containing 14 mM SDS at t = 1500 minutes

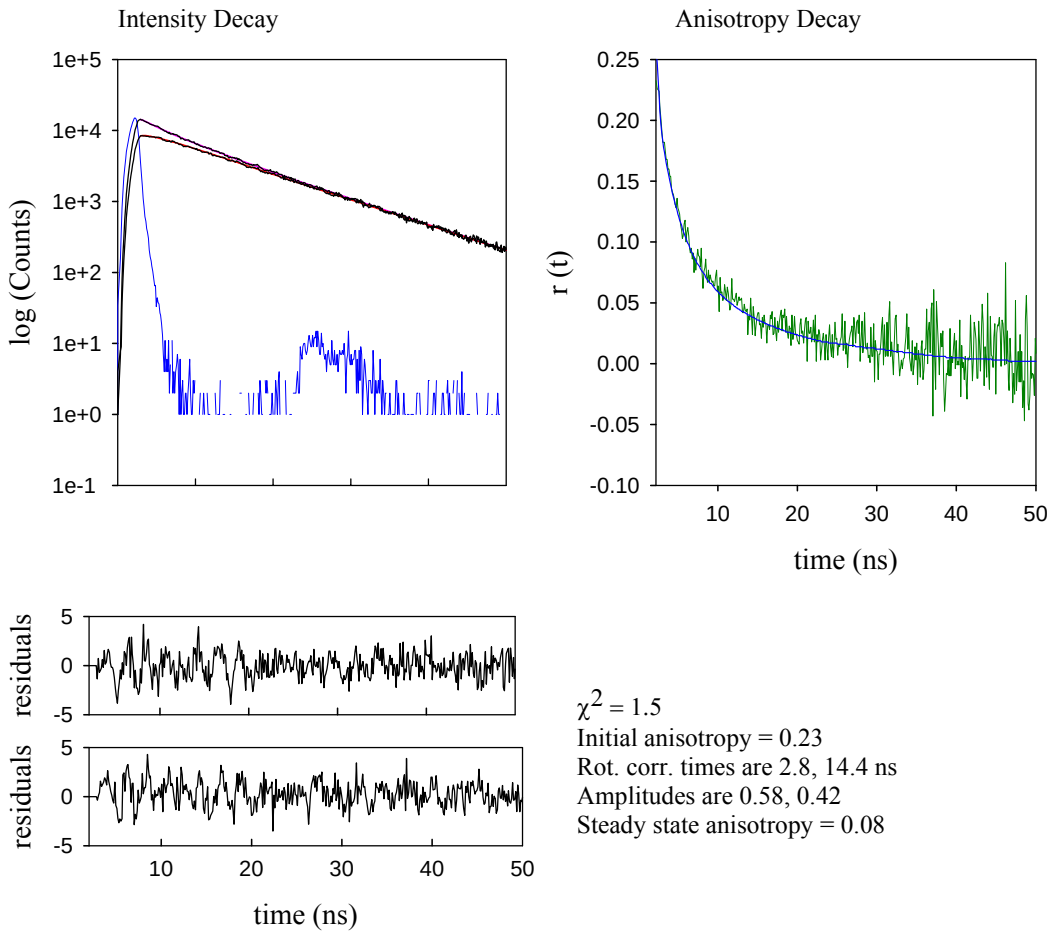

Figure 5.6 The details of curves are same as depicted in Figure 5.5.

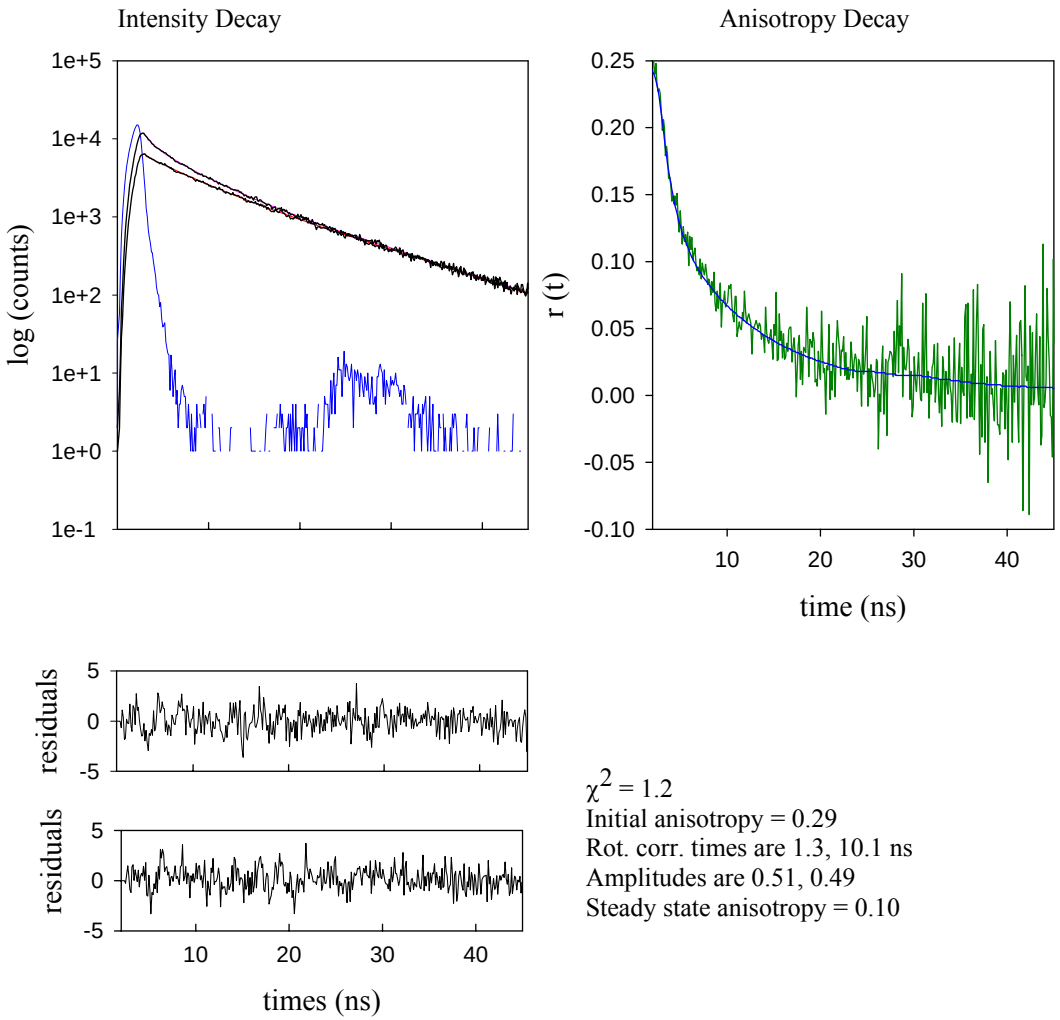

Figure 5.7 The details of curves are same as depicted in Figure 5.5.

Anisotropy Decay of 120 μM dansyl labeled lysozyme in pH 12.2 buffer containing 20 mM DTT at t = 1400 minutes

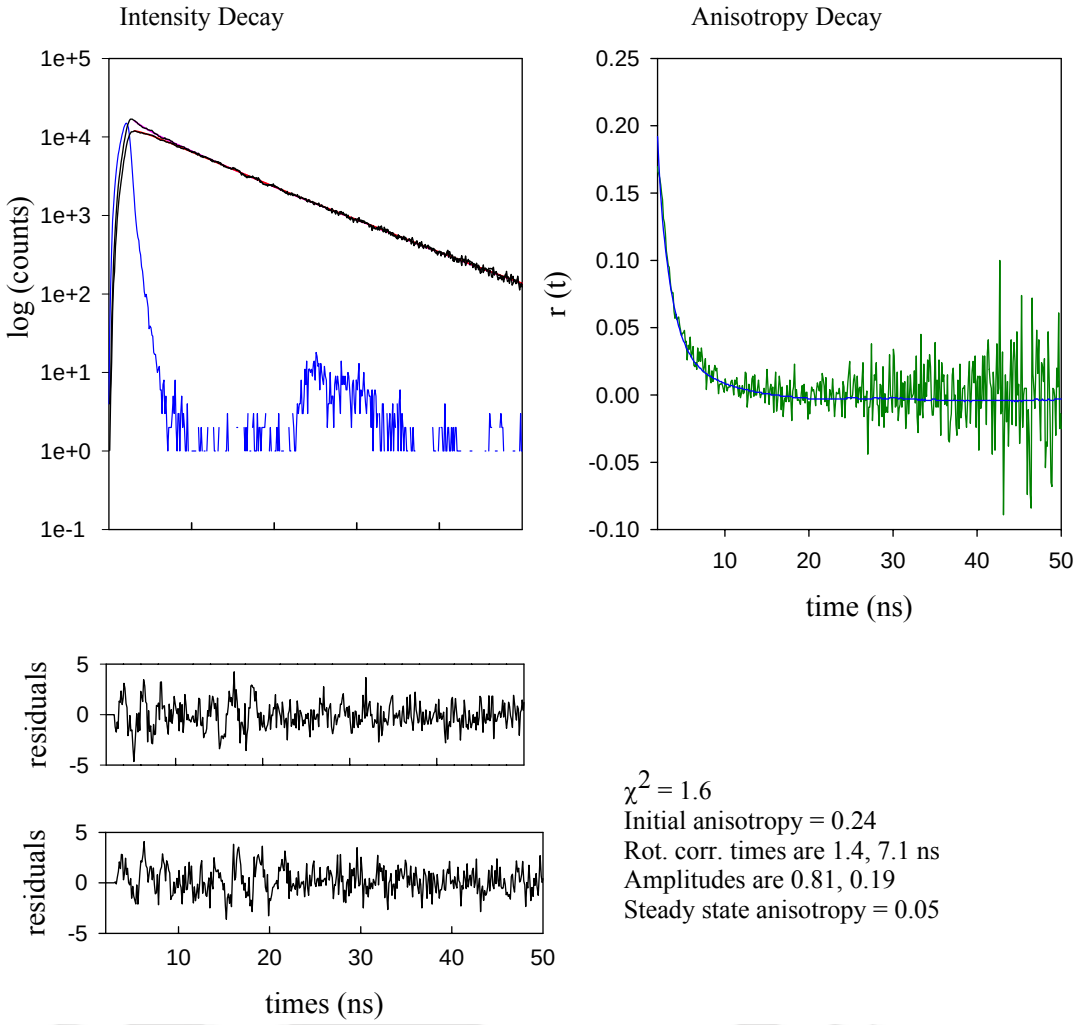

Figure 5.8 The details of curves are same as depicted in Figure 5.5.

5.5 Steady-state fluorescence anisotropy at longer time duration

Steady-sate and time-resolved fluorescence anisotropy discussed in Figure 5.2, 5.4 and Table 5.3 were confined to a time window spanning from 0 to ~1500 minutes only. However, there are reports where lag period of several days or week has been observed before onset of aggregation (Giri et al., 2007; McAllister et al., 2005). Keeping this fact in mind, we extended our observations to longer time periods to monitor the same under our experimental conditions. For this purpose we employed the r_{ss} once again to 80-120 µM dansyl labeled protein at pH 7, pH 12.2 with or without 14 mM SDS, 3 mM CTAB and 20 mM DTT. Figure 5.9 shows the variation in r_{ss} of dansylated HEWL as a function of time under different conditions stated above.

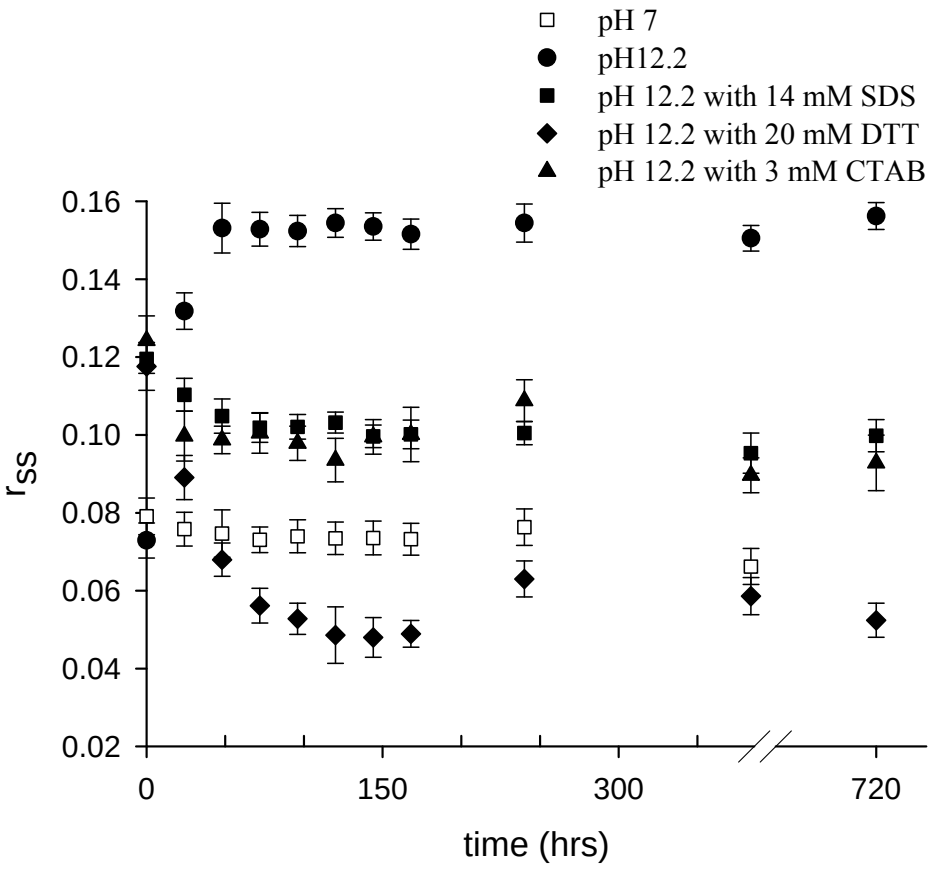

Figure 5.9 Steady-state fluorescence anisotropy of 80-120 µM dansyl labeled lysozyme at pH 12.2, in the presence of different additives is plotted against time duration of incubation at 298 K.

At pH 7, the r_{ss} starts from ~0.08 and remains fairly constant around 0.07 for several days till 384 hours, suggesting no change in protein oligomeric state. At pH 12.2 in the absence of any additive, r_{ss} starts from ~0.07 and reaches to ~0.15 in 48

hours and remain constant around ~0.15 for 720 hours of observation, suggesting that the aggregates are stable and intact as time progresses from days to weeks. At pH 12.2 in the presence of 14 mM SDS, the r_{ss} starts from ~0.12 decreases to ~0.10 after 72 hours and remains constant thereafter for 720 hours. At pH 12.2, in the presence of 3 mM CTAB, the r_{ss} starts from ~0.12 but drops to ~0.10 in 48 hours and remains between 0.10-0.11 for several days, stabilizing around ~0.09 later on indicating their restricted growth. At pH 12.2 in presence of DTT, the r_{ss} starts from ~0.12 and drops steeply and steadily to ~0.05 after 120 hours. This value was constant between 0.05-0.06 for several weeks thereafter reflecting a monomeric *like* state as observed with dansylated HEWL at pH 7.

From these observations it is apparent that all the additives employed are effective in halting the growth of HEWL aggregates over several weeks. While the effect of surfactants, SDS and CTAB are similar to earlier times, the dramatic influence of DTT in halting aggregation is noteworthy and appears potent enough at long times too.

5.6 Circular Dichroism spectroscopy

Circular dichroism (CD) is a well known technique to monitor the secondary structure in protein. To obtain further molecular details on the aggregation process, we performed CD measurement of HEWL under alkaline incubation with or without SDS, CTAB or DTT. Since direct CD measurement at pH 12.2 was not possible owing to large amount of absorption by buffer alone in the far ultraviolet region, HEWL at different experimental environment was diluted to 50 mM pH 7 phosphate buffer at the time of measurement. Figure 5.10 shows CD spectra of HEWL under the conditions employed in this study after incubation for 37 days at room temperature.

At pH 7 a characteristic spectrum for α-helices in the protein is seen with a negative band at 208 nm and a shoulder near 222 nm, which was consistent with earlier CD spectra of HEWL at pH 7 (Tanaka et al., 1975). At pH 12.2 in absence of additives, there was a pronounced decrease in helical content relative to pH 7, as evident with the decrease in molar ellipticity over a wide range of wavelengths. In presence of 3 mM CTAB or 20 mM DTT at pH 12.2, the protein appears further less helical. In presence of 14 mM SDS, the helical content appears much more than observed with HEWL at pH 12.2, while it is a shade more than at pH 7. These

observations are consistent with the earlier reports where SDS promotes helix formation in protein (Parker and Song 1992; Bisaglia et al., 2006).

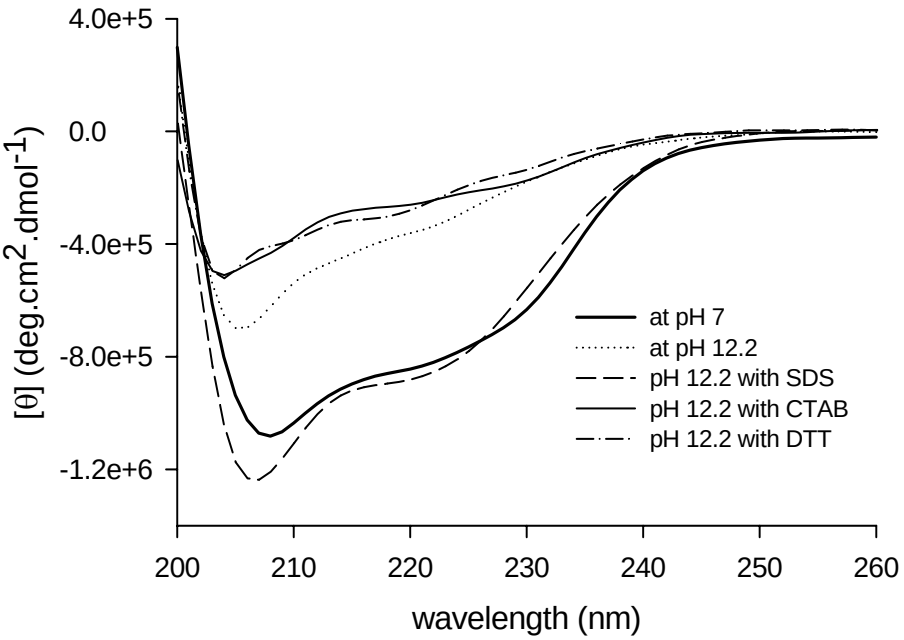

Figure 5.10 The far ultraviolet CD spectra of HEWL ((Molar ellipticity vs wavelength) after incubation for 37 days under the different conditions employed is shown here.

The CD data of HEWL with SDS show agreement with steady-state anisotropy and time-resolved anisotropy decay data. The ~14 ns rotational correlation time of dansyl probe in presence of SDS and its high r_{ss} after 720 hours of incubation is consistent with the ordered helical structures observed by CD. In presence of 3 mM CTAB or 20 mM DTT also, CD data was consistence with anisotropy data. The ~7 ns and ~10 ns rotational correlation time observed in aggregates in presence of DTT and CTAB respectively, along with their low r_{ss} after 720 hours, reflect relatively more unfolded structures observed in CD, compared to pH 12.2 alone or in presence of SDS. Contrary to the hallmark of amyloid exhibiting cross β-sheet, we could not observed these characteristics in CD spectra of HEWL at pH 12.2 (Figure 5.10). It is possible that amyloid fibrils constitute a minor fraction in a mixture of globular aggregates and amyloid fibrils that exist at pH 12.2 after several weeks of incubation.

Previous studies on change in secondary structure of HEWL as a function of pH have revealed two structural transitions. The first transition occurs at acidic pH (McAllister et al., 2005), between 3.8 and 2.0, accompanied by a small reduction in α-

helical content whereas second transition occurs at alkaline pH (Hameed et al., 2007), between 11 and 13, accompanied by a pronounced decrease in mean residue ellipticity similar to our observations at pH 12.2. Hameed et al. proposed that at pH 12.75 HEWL exists as a partly reversible molten globule state, while at pH 13.2 it is irreversibly unfolded.

5.7 ANS fluorescence

The ~10 ns tumbling time of HEWL coupled with fast segmental motion (~2.4 ns) immediately after exposure to pH 12.2 (Table 5.3, item 3) hints at a significant unfolding of the protein in alkaline pH compared to pH 7. It is thus likely that exposed hydrophobic regions of protein may act as driving force for aggregation process. 8-Anilino-1-naphthalene sulfonic acid ammonium salt (ANS) is widely used dye for the characterization of exposed hydrophobic pockets in partially folded protein intermediates (Semisotnov et al., 1987). It has also been used to monitor the process of fibril formation (Souillac et al., 2002).

To detect the exposure of hydrophobic regions during the course of HEWL aggregation and their inhibition, ANS fluorescence was monitored in pH 7, pH 12.2 and pH 12.2 with 20 mM DTT soaked lysozyme at different time points. In presence of SDS and CTAB, ANS experiment was not possible owing to background fluorescence arising from ANS bound to micelles of SDS/CTAB. Figure 5.11A and 5.11B depicts ANS fluorescence spectrum and integrated fluorescence intensity respectively with HEWL in different experimental conditions. Figure 5.11B reveals that in contrast to pH 7, the ANS fluorescence rises gradually in the first six hours coinciding with the growth of HEWL aggregates at pH 12.2. After day long incubation, a steep rise in ANS fluorescence was evident before saturation. This finding indicates the successive exposure of hydrophobic surfaces of HEWL during aggregation. Exposure of hydrophobic regions at alkaline condition may be the reason for the inhibition of HEWL aggregates in presence of amphipathic molecules like SDS and CTAB. It is quite likely that SDS and CTAB shall favorably bind to these available hydrophobic regions in HEWL thereby not only diminish their exposure to polar solvent but also halt the aggregation. Since isoelectric point of HEWL is ~11.3 (Wetter and Deutsch 1951), at pH 12.2, it is likely that hydrophobic interaction predominate between negatively charged HEWL and SDS while with CTAB, electrostatic interactions may play a major role (Chatterjee et al., 2002). The

concentration of surfactants employed in our experiments are 10-fold higher than the cmc of SDS (1.36 mM) and CTAB (0.27 mM) in pH 12.2 buffer as measured using pyrene III/I peak ratio (Figure 5.12A and 5.12B). Figure 5.11B also reveals that in presence of DTT there was no increase in ANS fluorescence. It is apparent that in presence of DTT, hydrophobic regions of HEWL are not exposed at alkaline condition thus limiting their interactions leading to aggregation. This observation was consistent with anisotropy data where DTT was found to arrest the aggregation process.

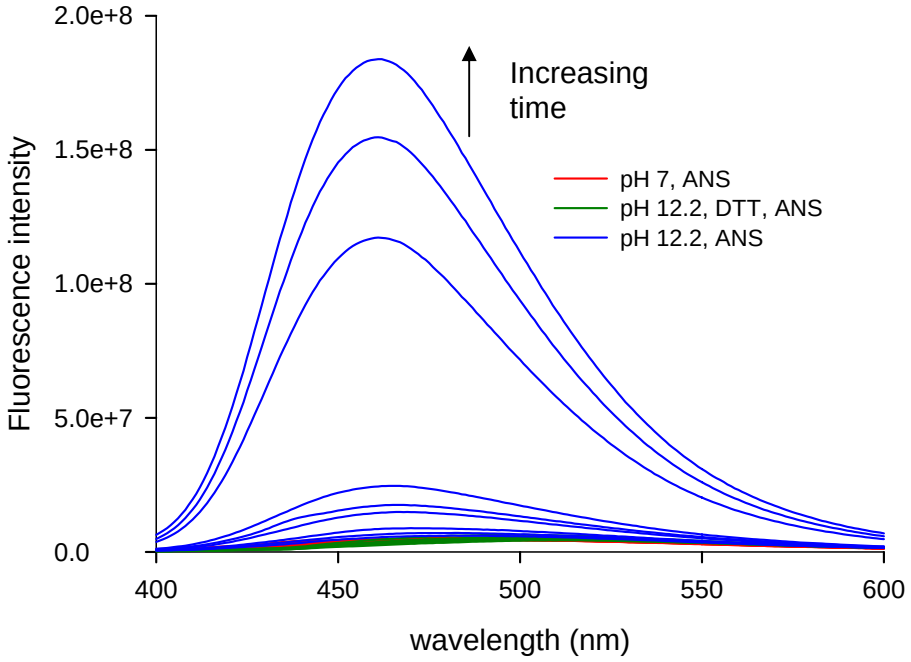

Figure 5.11A Change in fluorescence intensity of 20 µM ANS with 75 µM HEWL in different experimental conditions at different time intervals after incubation is shown above. Curves from top to bottom at different time points are based on emission maximum at 460 nm. Integrated fluorescence intensity of same spectra with specific time points is depicted below.

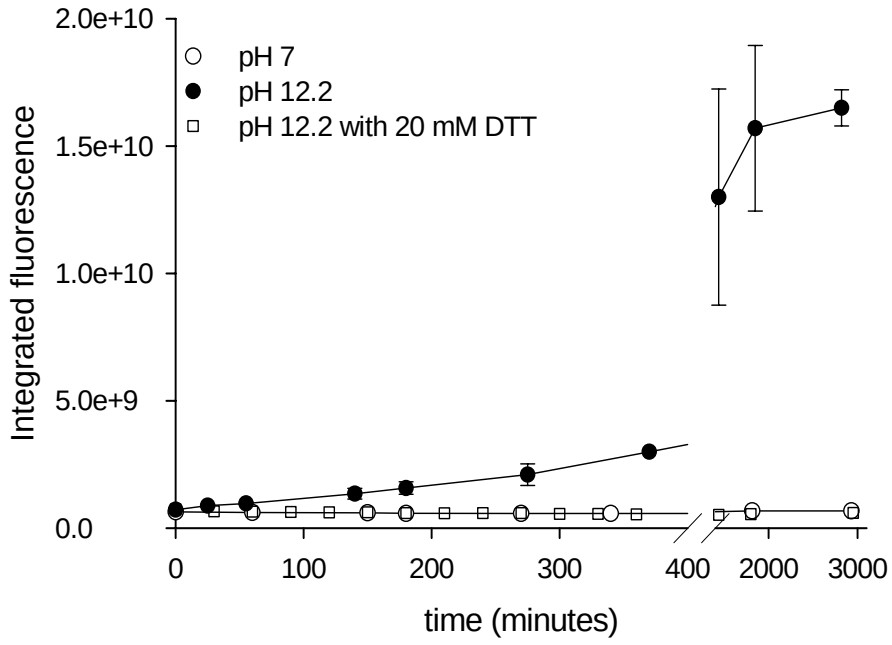

Figure 5.11B Integrated ANS fluorescence intensity in presence of HEWL at different experimental conditions is shown here.

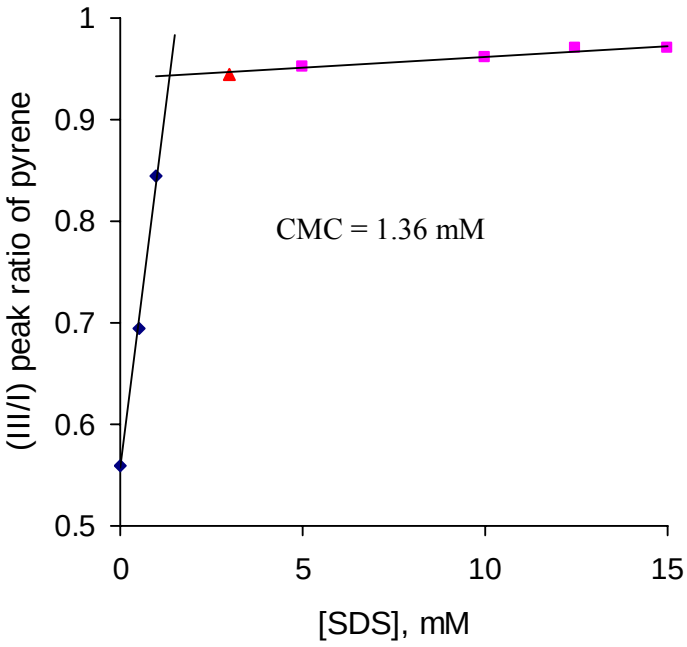

Figure 5.12A Determination of critical micellar concentration (CMC) for SDS using pyrene III/I intensity ratio in 50 mM pH 12.2 phosphate buffer.

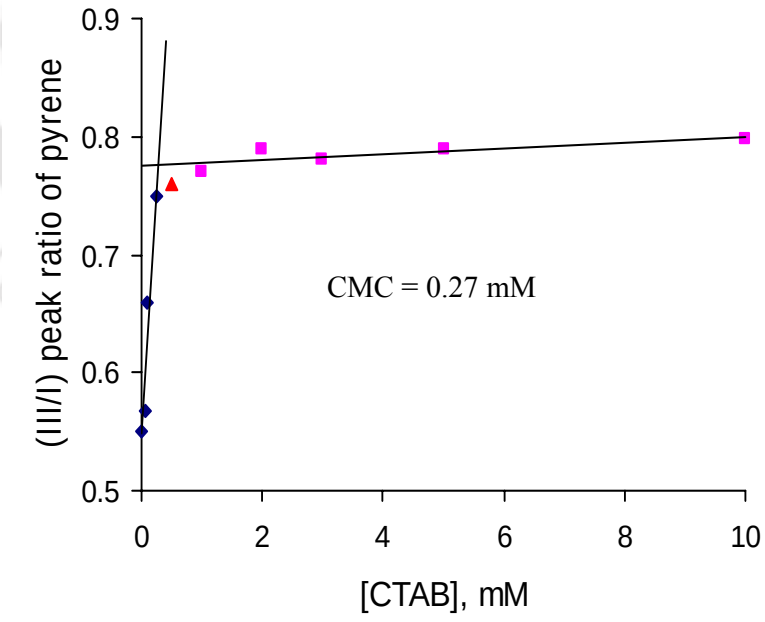

Figure 5.12B Determination of critical micellar concentration (CMC) for CTAB using pyrene III/I intensity ratio in 50 mM pH 12.2 phosphate buffer.

5.8 Thioflavin T fluorescence

ThioflavinT (ThT) is a commonly used probe to detect amyloid fibrils (Vassar and Culling 1959; Levine 1993). To ascertain the amyloid characteristic of aggregates, ThT fluorescence was measured to pH 7, pH 12.2 and pH 12.2 with 3 mM CTAB and 20 mM DTT soaked lysozyme at different time points. Again, with 14 mM SDS, ThT experiment was not possible to perform due background ThT fluorescence arising from SDS micelles alone.

Figure 5.13A and 5.13B shows the fluorescence spectrum and integrated fluorescence intensity respectively of ThT with HEWL at different experimental conditions at different time points subsequent to incubation. We could not obtain data prior to 50 hours owing to precipitate formation by HEWL when transferred to pH 8.5 medium from pH 12.2. Compared to pH 7 incubated HEWL, where ThT fluorescence intensity was almost constant with time, higher intensity and a gradual rise in ThT fluorescence for pH 12.2 sample was observed as time progresses, hinting at saturation around ~150 hours. It is thus apparent that that amyloid-like aggregates are being formed on prolonged exposure to alkaline pH but not at neutral pH.

In case of lysozyme at pH 12.2 with additives, it is evident from Figure 5.13B that thioflavin T fluorescence intensity is 5—10 fold less when HEWL was incubated with either 3 mM CTAB or 20 mM DTT for same time window as monitored for lysozyme at alkaline condition without additives. With these observations we may conclude that presence of either CTAB or DTT is effective in preventing the formation of amyloid-like aggregates of HEWL at alkaline pH.

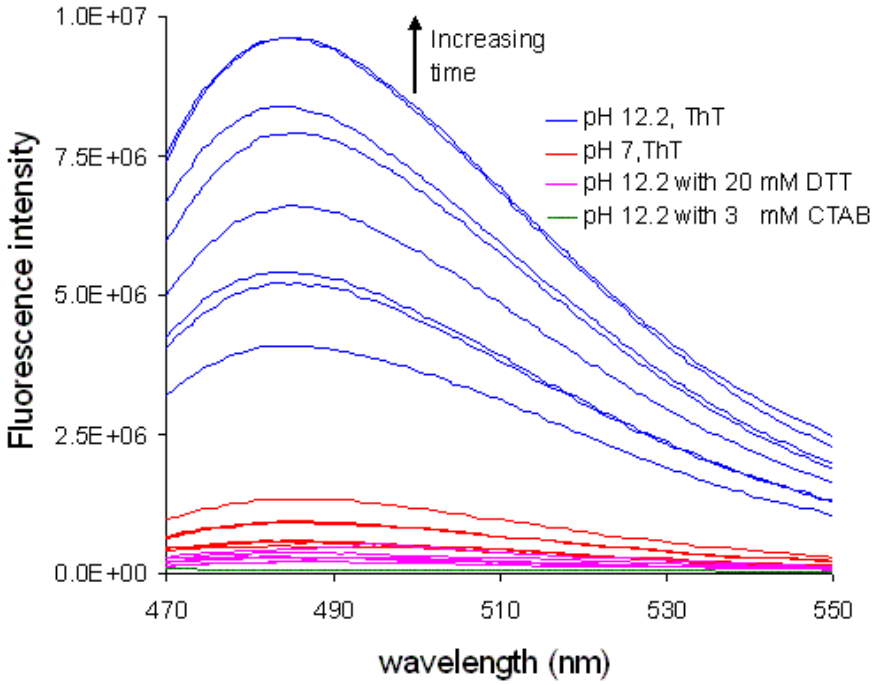

Figure 5.13A Change in fluorescence intensity of ThT with HEWL in different experimental conditions at different time intervals after incubation is shown above. Curves from top to bottom at different time points are based on emission maximum at 550 nm. Integrated fluorescence intensity of same spectra with specific time points is depicted below.

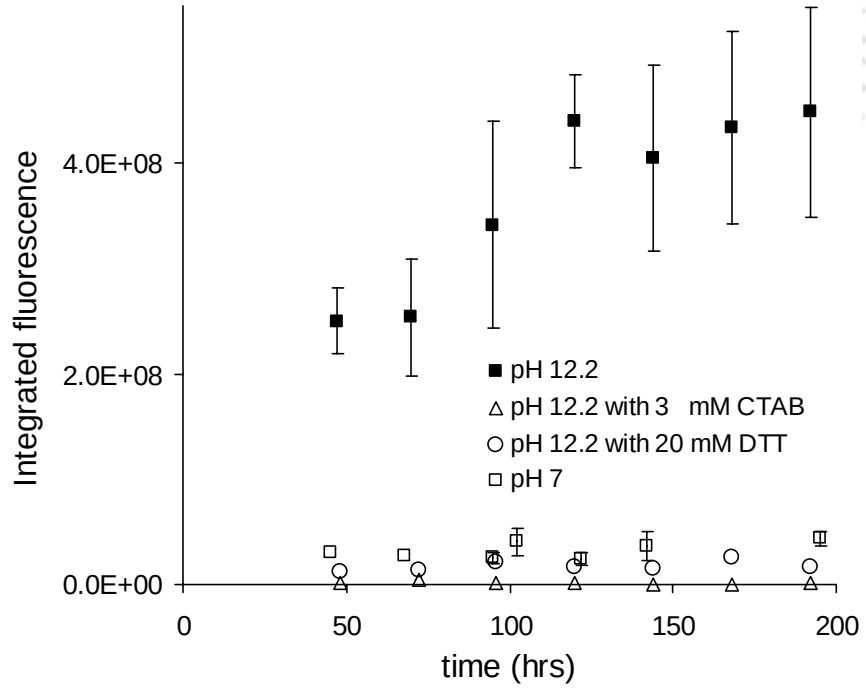

Figure 5.13B Integrated ThT fluorescence intensity with HEWL at different experimental conditions at different time points is shown here.

5.9 Estimation of free thiol groups

The potent inhibitory influence of DTT in arresting lysozyme aggregation is a salient result from our experiments. Contrary to popular belief where disruption of disulphide bonds are known to promote aggregation (Smith and Radford 2001; Maeda et al., 2007), we have shown that reduction of disulphide bond restrict the growth of HEWL aggregates at alkaline pH. Earlier, it have been shown that disulfide bonds can get cleaved under alkaline conditions (Anderson and Wetlaufer 1975), subsequently these may get oxidised again with a different cysteine thiol groups leading to disulfide scrambling and intermolecular disulfide bonds. To ascertain this phenomenon in our condition, we estimated the concentration of free thiol present in 6 µM HEWL after different periods of incubation at pH 12.2. Figure 5.14B shows the gradual rise in levels of free thiol in the first three days of incubation. After three days ~41 µM thiol (nearly ~85% of eight thiol groups) in HEWL appears free. Subsequently, the thiol levels showed saturation for 3-5 days and display gradual decrease after five days of incubation.

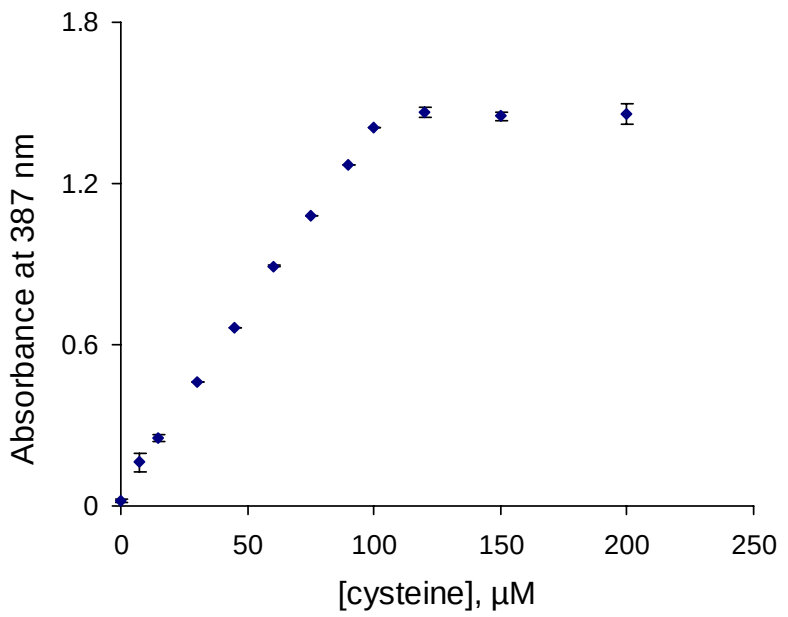

Figure 5.14A Standard curve of L-cysteine using 50 µM 2,2′-dithiobis(5-nitropyridine) is shown. Absorbance of reaction mixture was monitored at 387 nm after 15 minutes of mixing. After 100 µM cysteine there was saturation in absorbance.

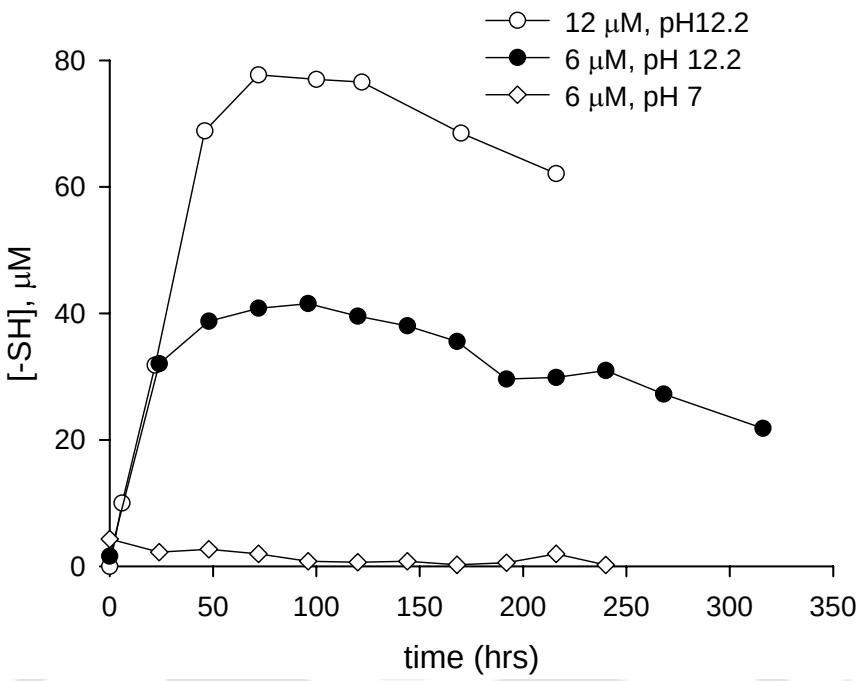

Figure 5.14B Estimation of free thiol groups in HEWL (diluted from 120 μM) at different time points subsequent to incubation at pH 12.2 and pH 7 using 50 μM DTNP is shown.

Figure 5.14B also indicate that the saturation does not arise from stoichiometric limitations as an identical trend, saturating at 78 μM thiol (~81% of eight thiol groups) was obtained with 12 μM HEWL. The decrease after five days indicates fresh disulfide bond formation, part of which could perhaps be of intermolecular nature due to proximity among HEWL molecules in the aggregate. On the contrary, all disulphide bonds were observed to be intact in pH 7 incubated protein.

To ascertain the importance of late disulfide bond formation in aggregates, we added 20 mM DTT to HEWL samples at pH 12.2 after 120 hours and observed ThT fluorescence in control and DTT samples. Figure 5.15 shows no significant change in ThT fluorescence either in control or in presence of DTT over the period of fifteen days.

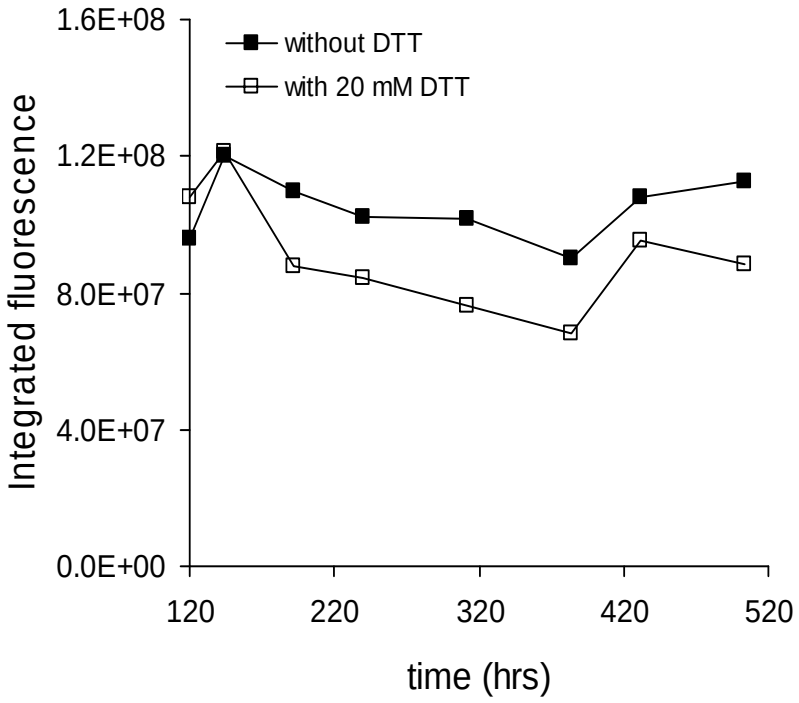

Figure 5.15 Effect of DTT added after 120 hours of incubation to pre-formed HEWL aggregates at pH 12.2 is shown using thioflavin T fluorescence.

It is thus apparent that DTT is critically effective against HEWL aggregation ONLY if employed from beginning.

Observation from Figure 5.14B indicate that at least one thiol from every HEWL monomer may be involved in fresh disulphide bonds after three days, making it likely that they are intermolecular in nature. These disulfide bonds may be critical for the assembly and growth of aggregates. Once these disulphide bonds are formed, aggregates become tightly packed and assembled, preventing DTT or DTNP or OH^- from gaining any access to the inner core of the aggregate (Figure 5.15 and 5.14B).

5.10 HEWL activity

Demonstrating the enzymatic activity is a true indicator of the native form of protein. In earlier experiments we observed that SDS, CTAB and DTT were efficient in halting the growth of lysozyme aggregates at alkaline condition. We then extended our work to see if the native protein can be recovered subsequent to incubation at pH 12.2 either in presence or absence of additives. Figure 5.16 shows the percentage HEWL activity under different experimental conditions at different time points.

Activity was compared against a freshly made native HEWL sample of identical concentration whose activity was normalized to 100%.

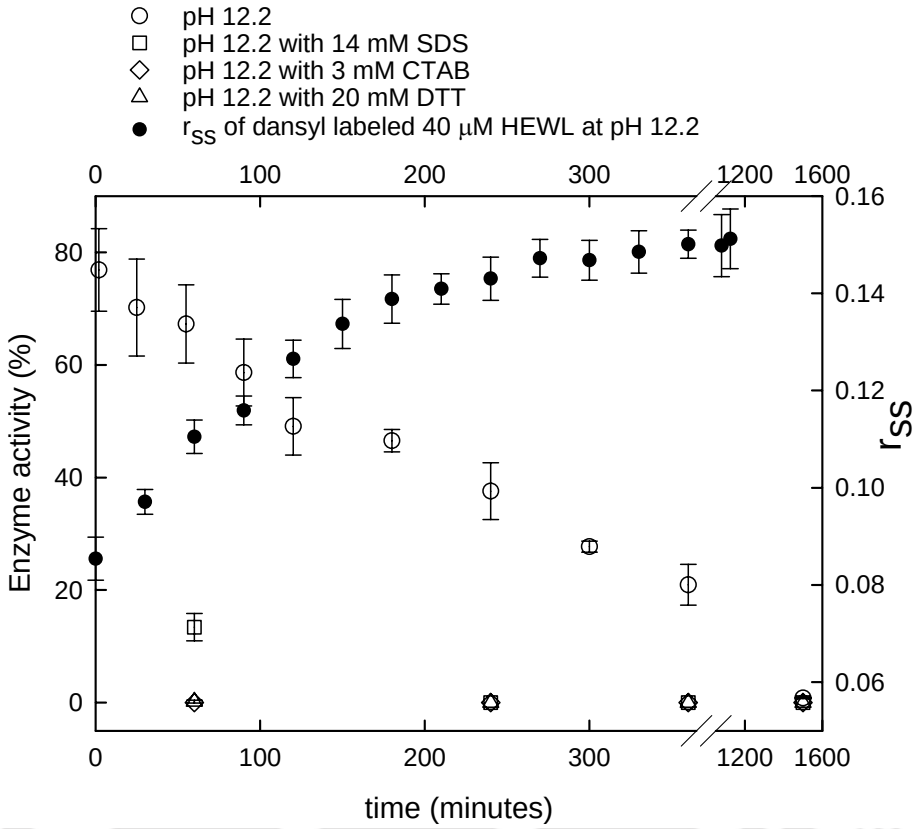

Figure 5.16 Percentage recovery of HEWL activity after incubation at different experimental conditions at different time points is shown. Steady-state anisotropy of 40 μM protein at pH 12.2 is also shown.

Figure 5.16 shows that while ~70% activity was recovered after the first one hour of incubation, this value was decreased to ~20% after 6 hours and later dropping to zero after 24 hours. This observation was consistent with our earlier steady-state data where irreversibility in lysozyme aggregation was observed after 60 minutes (Homchaudhuri et al., 2006) of incubation. Gradual decrease in catalytic activity coupled with concomitant increase in steady-state anisotropy of lysozyme at pH 12.2, as shown in Figure 5.16 indicate the growth in aggregate population with decrease in native HEWL population. Since enzymatic activity is proportional to the concentration of native form of protein in the medium, decrease in activity clearly reflects the formation of soluble aggregates, a process that is observed to be slow but irreversible in nature.

In presence of additives, Figure 5.16 shows that except with 14 mM SDS at 30 minutes, none of the additives could help in recovering any activity either after 1 hour

or after 15 days of incubation (Figure 5.17). Initially, minor recovery of HEWL activity with SDS indicates weakly bound surfactants with protein which was consistent with fast dansyl dynamics (~9.4 ns) observed at 30 minutes of incubation (Table 5.3, item 6) while, in presence of CTAB, HEWL was tightly bound (~14 ns, Table 5.3, item 9) to oppositely charged surfactants through electrostatic interaction. Figure 5.17 also indicates the stability of HEWL at room temperature where nearly 80% activity was recovered from pH 7 soaked lysozyme after 15 days of incubation.

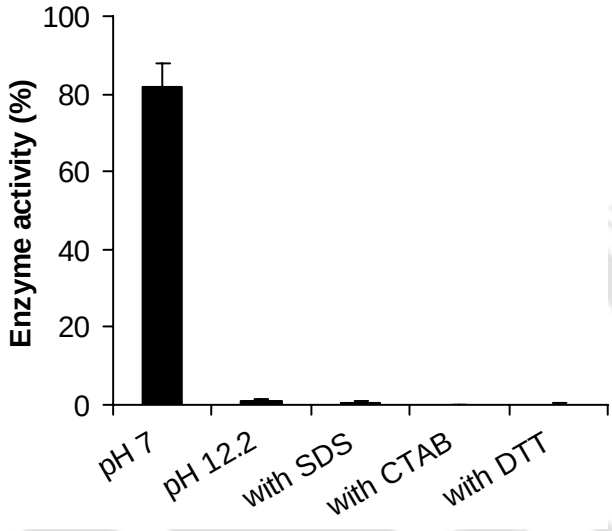

Figure 5.17 Percentage catalytic activity of HEWL in different experimental condition after 15 days of incubation at room temperature.

These findings indicate that inhibition of protein aggregation does not necessarily result in recovery of native structure and function of protein. It is likely that the surfactants are still bound to the protein after dilution, as AFM images suggest (data not shown), preventing it from attaining a native structure.

5.11 HEWL proteolysis

Condition employed by us to monitor the growth of HEWL aggregates was indeed extremely harsh. It was thus likely that prolonged incubation of protein at pH 12.2 may lead to hydrolysis of peptide bond. To monitor the degree of peptide hydrolysis at alkaline condition, 16% Tricine-Sodium dodecyl sulphate polyacrylamide gel electrophoresis (SDS-PAGE) was employed to observe the size of HEWL in *control* and in presence of additives after 16 days of incubation. Fresh HEWL at pH 7 and 38 hours old lysozyme with 20 mM DTT at pH 12.2 was also run in parallel. Figure 5.18A depicts the Tricine-SDS PAGE of HEWL in different

experimental conditions. A small fraction of bands corresponding to molecular weight less than 14.3 kDa was visible in all alkaline samples reflecting some hydrolysis in these samples. As expected for a slow hydrolysis, the fragments were relatively less prominent at 38 hours with DTT compared to 16 day old sample with DTT. The important observation obtained from this experiment was the occurrence of higher aggregates at pH 12.2 after 16 days, which was clearly absent in the presence of SDS, CTAB and DTT. In presence of additives, a significant fraction of the band equivalent to 14.3 kDa indicate that protein was mostly monomeric.

Since peptide bond displays characteristic electronic absorption at 210 nm, decrease in absorbance at this wavelength is clear indicator of peptide bond hydrolysis. We verified the extent of peptide bond hydrolysis in pH 12.2 soaked protein at different time points by diluting them 300 fold in deionised water from 120 μM sample. Figure 5.18B showing electronic absorption by peptide at 210 nm revealed no significant change in absorbance of HEWL samples after 4,5,9,20 and 31 days of incubation at pH 12.2, compared to same concentration of freshly prepared HEWL samples in water. In presence of extensive hydrolysis one would get clear decrease in absorption at 210 nm. Thus Tricine-SDS PAGE along with 210 absorbance data indicates the minimal hydrolysis of HEWL in above mentioned samples. If hydrolysis was prominent in our case, we could not obtain higher steady-state state anisotropy at long time point (Figure 5.9). However, Mishra et al. have demonstrated that partial acid hydrolysis at pH 1.6 promote lysozyme amyloidogenesis owing to formation of nicked HEWL compared to full length protein (Mishra et al., 2007).

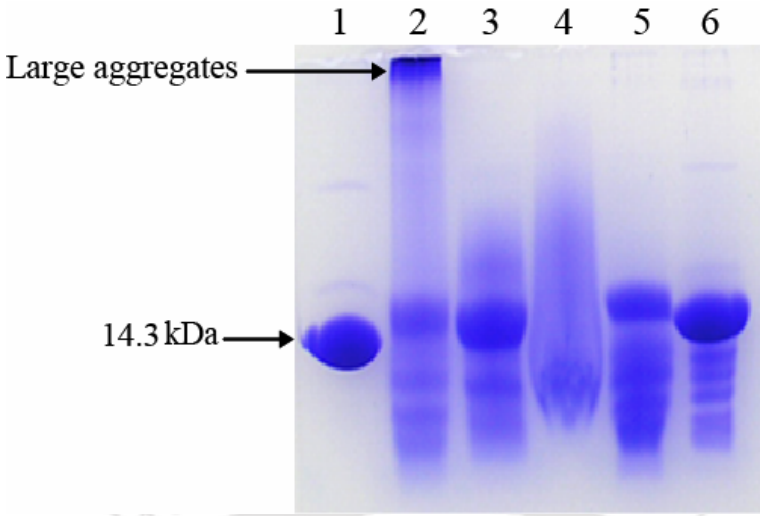

Figure 5.18A 16% Tricine-SDS PAGE to monitor the extent of proteolysis in HEWL under different experimental conditions is shown here. The description of lane depicted above is as follow, Lane 1, Freshly prepared HEWL at pH 7; lane 2, 16 days old HEWL at pH 12.2; lane 3, 16 days old HEWL at pH 12.2 with 14 mM SDS; lane 4, 16 days old HEWL at pH 12.2 with 3 mM CTAB; lane 5, 16 days old HEWL at pH 12.2 with 20 mM DTT; lane 6, 38 hrs old HEWL at pH 12.2 with 20 mM DTT. The amount of HEWL loaded in each well is 29 µg except in case of HEWL with CTAB which had 19 µg protein.

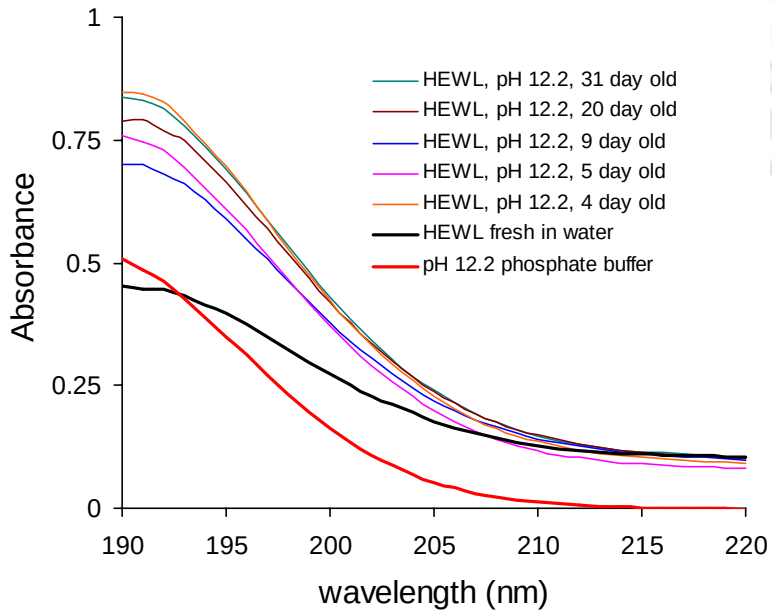

Figure 5.18B Peptide bond absorption of 120 µM HEWL samples incubated at pH 12.2 for different time periods after 1:300 dilution in deionized water is shown. Absorbance of fresh HEWL in deionized water (120 µM) and background absorption from the phosphate buffer between 190-210 nm is also depicted after 300 fold dilution.

5.12 Mechanism

On the basis of our experimental evidences, a molecular mechanism underlying the aggregation of HEWL at alkaline condition and their subsequent inhibition in presence of anionic surfactant SDS, cationic surfactant CTAB and disulphide disrupting agent DTT is proposed. Figure 5.19 depicts the proposed mechanism.

Hen egg white lysozyme begins to aggregate slowly after exposure to pH 12.2. The gradual rise in steady-state anisotropy and change in rotational correlation times coupled with decrease in enzymatic activity mirror the slow growth of HEWL aggregates over the period of 1500 minutes at alkaline condition. During the course of aggregation there was a gradual exposure of hydrophobic regions as evident from increased ANS fluorescence. Nearly 1800 minutes later, saturation in ANS fluorescence indicates the exposure of all hydrophobic regions in protein. We infer that interactions between exposed non-polar regions in HEWL are driving force in early growth of HEWL aggregates at pH 12.2. Similar observation has been reported by Felice et al. where these interactions promote oligomerization of human lysozyme at high pressure coupled with increased temperature (Felice et al., 2004). Following the hydrophobic interactions further stabilization of lysozyme aggregates occur through intermolecular disulphide bonds. Increase in free thiol groups in pH 12.2 soaked lysozyme for three days followed by decrease after five days, indicate that at least one thiol from every protein monomer participates in fresh disulphide bonds formation after three days. It is thus likely that these interactions are intermolecular in nature. Results from treatment of 120 hours old lysozyme aggregates with 20 mM DTT suggests that intermolecular disulphide bond stabilized these structures substantially in late phase of aggregation process, making them tightly packed and assembled such that DTT could not access the inner core of these aggregates. Similar findings were reported by Goto and co-workers where disulphide bonds during the process of fibrillization were found to be reactive while in mature fibrils they were resistant to reduction (Hong et al., 2002; Yamamoto et al., 2008). Hong et al. explained that disulfide bond in β_2 microglobulin, which is completely buried in the native state is exposed in immature fibrils at pH 2.5, again get buried in mature fibrils. Growth of HEWL amyloids at pH 12.2 without additives was confirmed by ThT fluorescence, where we monitored enhanced ThT signal after 48 hours of incubation followed by saturation after 120 hours onward. Comparing the extent of free thiol

with ThT fluorescence highlights the process of HEWL fibrilization at pH 12.2 where amyloid-like structures tend to form after two days of incubation and stabilize after five days. Aggregated protein are characterized by β sheet structure, nevertheless, absence of these structure in month long old lysozyme at alkaline pH indicate that population of amyloid fibrils are comparatively lesser than the globular aggregates.

In presence of additives, namely SDS, CTAB and DTT growth of lysozyme aggregates was inhibited as evident from steady-state and time-resolved anisotropy decay complimented with ANS, ThT and SDS PAGE data. The interaction between HEWL at pH 12.2 with anionic surfactant SDS and oppositely charged surfactant CTAB results in loosening the aggregates at alkaline pH. Decrease in steady-state anisotropy coupled with reasonably fast (10-14 ns) global motion observed in presence of SDS/CTAB cannot be accounted by the tumbling of the big aggregates as observed with control. A fast global motion is feasible from the tumbling of individual monomers of HEWL that are soaked up in a fluid micellar environment. Similar type of conglomeration of lysozyme in presence SDS micelles has been proposed earlier by Wennerstrom and co-workers (Stenstam et al., 2001). Lack of secondary structure of protein with CTAB but presence of helical structure with SDS shows that the anionic surfactant not only inhibit the growth of HEWL aggregates but also promote the helical conformation at extreme pH.

Significant decrease in steady-state anisotropy along with fast rotational correlation time (~7 ns) confers the emphatic inhibitory effect of DTT on HEWL aggregation in a condition employed by us. In the light of observations where disulphide bond is observed to stabilizes native structure of β_2-microglobulin and so hamper its fibrilization (Smith and Radford 2001), from our findings we propose that reduction of disulphide bond employing DTT impedes the growth of HEWL aggregates at pH 12.2, if applied from beginning. Once the ordered aggregates are formed, DTT will be no longer effective to disrupt these assemblies.

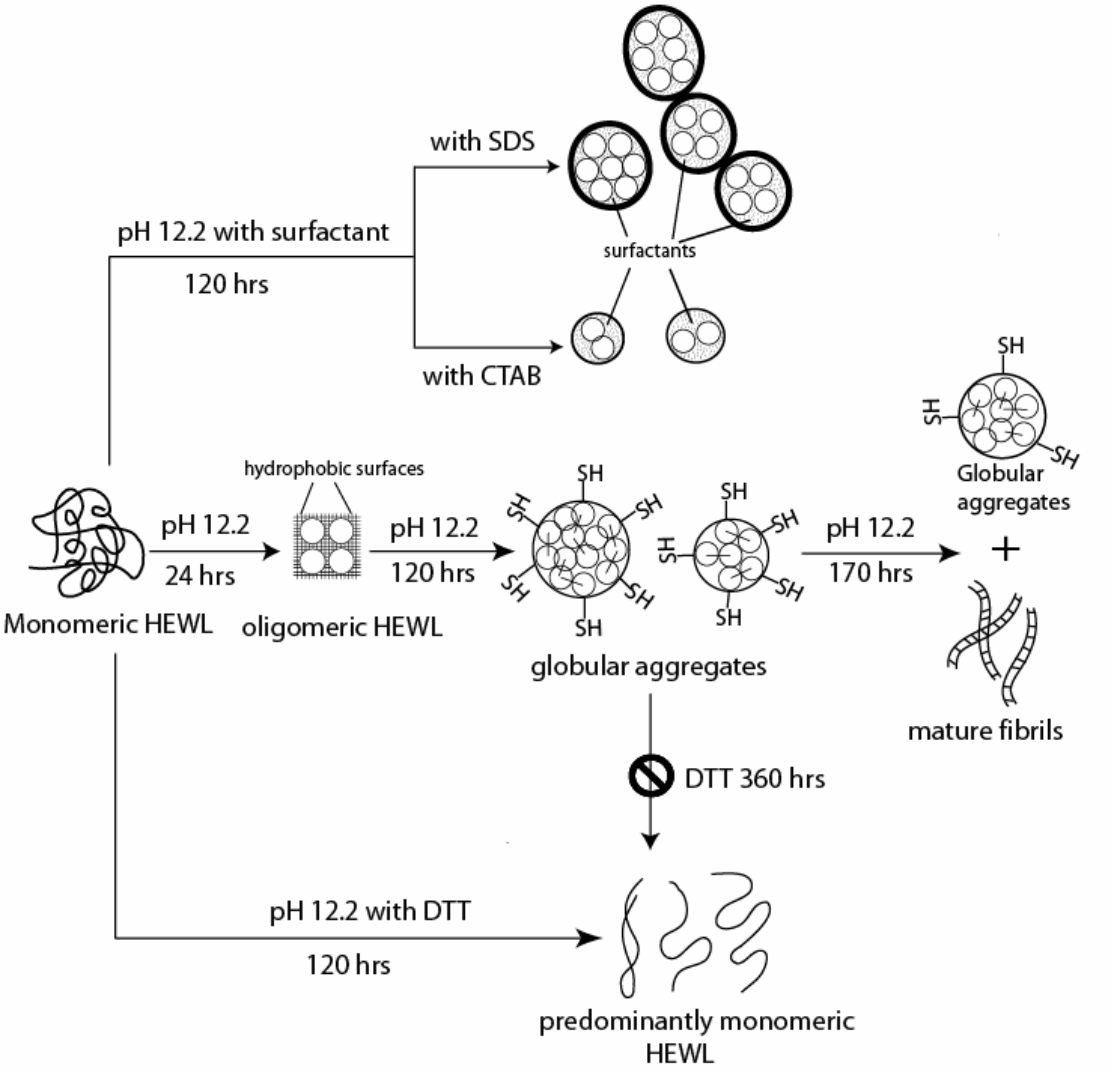

Figure 5.19 The proposed mechanism for aggregation of HEWL at pH 12.2 in presence and absence of SDS, CTAB and DTT is shown schematically.

Conclusions:

1) The rotational dynamics of the HEWL oligomers, specifically the segmental motion, is a key marker of the progress of aggregation and their inbition.

2) Anionic surfactant SDS, cationic surfactant CTAB, disulphide breaking agent DTT effectively inhibit lysozyme aggregation at alkaline condition

3) Inhibitory influence of DTT was much more prominent than SDS or CTAB.

4) DTT can impart its inhibitory property only when applied from the onset of aggregation. It is however unable to disaggregate the ordered aggregates.

5) Aggregation of lysozyme at pH 12.2 is promoted by exposed hydrophobic surfaces initially and later stabilised by intermolecular disulphide bonds.

6) Gradual decrease in HEWL enzymatic activity at pH 12.2 indicates that lysozyme aggregation is slow and abolishes activity.

7) Inhibition of aggregation not always results in recovery of native and functional protein.

8) Mild hydrolysis of HEWL at pH 12.2 does not affect its oligomerization at alkaline pH.

Chapter 6

Preincubation of chitotriose with lysozyme: An alternative approach to reduce aggregation propensity of hen egg white lysozyme

Protein aggregation is a multi-step process with several intermediates, hence varied approaches at different stages are being used to block the growth of protein oligomerization either *in vitro* or *in vivo* (Rochet 2007). One of the promising strategies to prevent protein fibrillization is to stabilize their native state by small molecules (Johnson et al., 2005). With the popular belief that native structure of protein undergoes at least partial unfolding before aggregation, stabilization of native state structure may increase the activation energy barrier and so slow the aggregation kinetics leading to amyloidogenic state (Hammarstrom et al., 2003). Although different small molecular weight compounds has been used to restrict pathogenic self-association of proteins (Ross and Poirer 2004; Bernier et al., 2004), nevertheless, hampering protein misfolding and aggregation by stabilizing their native structure has not been exploited extensively.

Different small molecules like ligand, substrate or enzyme inhibitors can selectively bind to the native protein conformer and prevent its structural fluctuation (Rochet 2007; Loo and Clarke 2007; Papp and Csermely 2006). Thyroxine (T4), the natural ligand of transthyretin (TTR) stabilizes the tetrameric structure of protein and prevents its aggregation *in vitro*. Structural analogues of thyroxine are under clinical trials that inhibit tetramer dissociation of TTR and subsequently familial amyloid polyneuropathy (Johnson et al., 2005; Miroy et al., 1996). Blocking the aggregation and amyloid formation has also been observed in acylphosphatases where specific binding of inorganic phosphate (Pi), a competitive inhibitor of acylphosphatases hinders the formation of the early oligomers and their conversion into protofibrils (Soldi et al., 2006). Disaccharide trehalose has been observed to bind and stabilize polyglutamine-containing proteins and so inhibit their aggregation (Tanaka et al., 2005).

In present work we took lysozyme-inhibitor complex to study protein self-association at alkaline condition. After overnight (~12 hours) incubation of hen egg white lysozyme with chitotriose or NAG individually in 10 mM, pH 7.3 phosphate

buffe, aggregation was induced by diluting the sample at 50 mM, pH 12.2 phosphate buffer.

6.1 Binding of chitotriose with HEWL

Before inducing aggregation, binding of chitotriose with lysozyme after nightlong incubation was ascertained by A) difference absorption spectra of HEWL complexed with chitotriose and B) comparing tryptophan emission spectra of chitotriose bound HEWL with unbound one.

Figure 6.1 shows the difference spectra of 50 µM HEWL with 850 µM chitotriose at pH 7 after overnight incubation at room temperature (298 K).

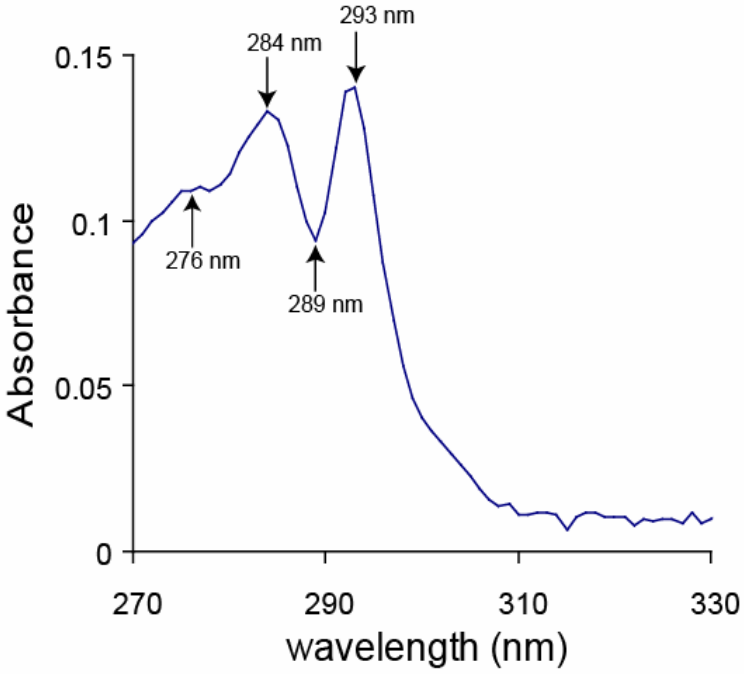

Figure 6.1 Difference absorption spectra of lysozyme-chitotriose complex after overnight incubation at 298 K is shown here in pH 7 buffer.

The binding kinetics of oligosaccharides with lysozyme has been investigated previously (Dahlquist et al., 1966; Rupley et al., 1975) where difference spectra have been widely used to monitor extent of lysozyme-saccharide association (Banerjee and Rupley 1973; Imoto et al., 1975). In Figure 6.1, the magnitude of the peak (293 nm)–trough (289 nm) difference in the different spectra confirmed the binding of chitotriose with HEWL at pH 7 which was consistent with earlier reports (Imoto et al., 1975).

Tryptophan fluorescence also supported the binding of HEWL with chitotriose. The emission maximum for uncomplexed lysozyme was observed at 348 nm at pH 7 which was blue shifted by ~8 nm with enhanced fluorescence subsequent to binding with chitotriose (Figure 6.2). The blue shift in HEWL-chitotriose complex arises due to the exclusion of Trp^{62} from the solvent exposed region to a less polar environment (Kumagai et al., 1992).

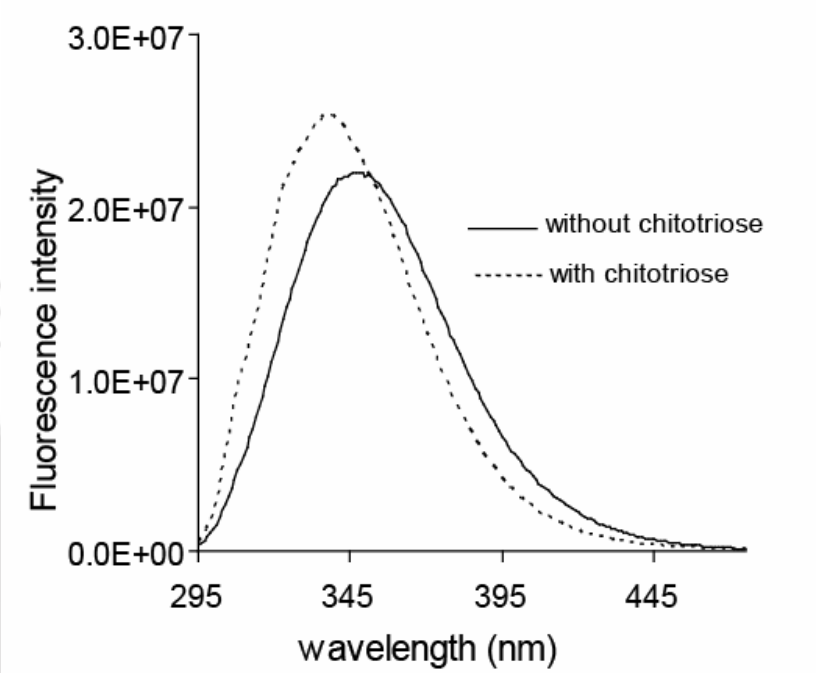

Figure 6.2 Tryptophan emission spectra of chitotriose bound HEWL after overnight incubation at 298 K is shown here in pH 7 buffer.

The above observations confirmed that chitotriose was bound to HEWL before it was transferred to pH 12.2 to induce aggregation.

6.2 ANS fluorescence

ANS fluorescence serves as a good indicator of exposed hydrophobic regions in protein and has also been used to monitor the progress of protein aggregation. Free ANS in water exhibit weak emission with λ_{max} at 514 nm which shows blue shift to 416 nm with enhanced fluorescence intensity subsequent to binding with solvent-exposed hydrophobic regions in proteins (Stryer 1968). Since exposure of non-polar regions are early events in protein oligomerization, we decided to monitor the exposure of hydrophobic regions in HEWL at pH 12.2 in control or preincubated samples either with chitotriose or NAG. Figure 6.3A and 6.3B depicts ANS

fluorescence spectrum and integrated fluorescence intensity respectively, with HEWL against incubation time for different experimental conditions.

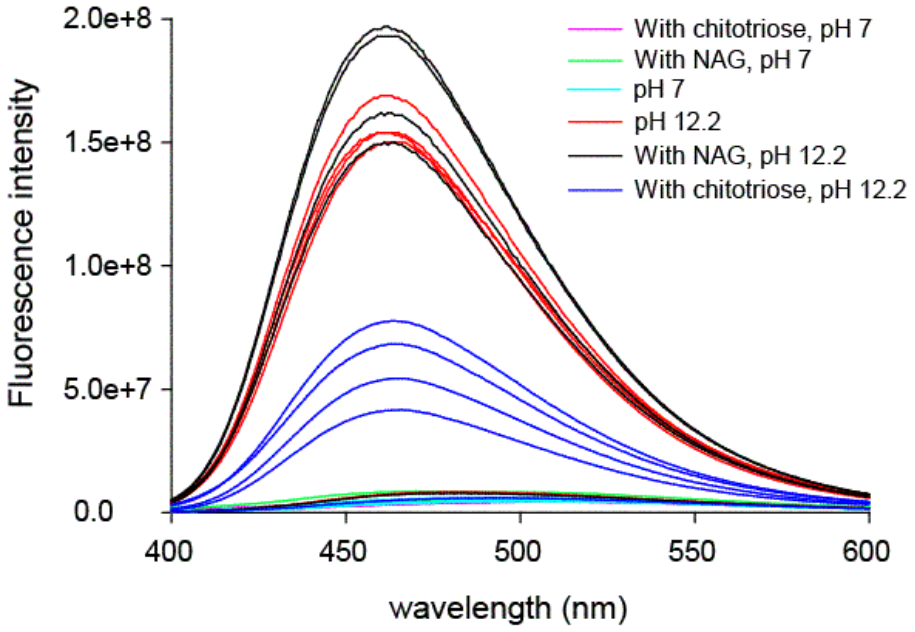

Figure 6.3A Change in fluorescence intensity of ANS with HEWL in different experimental conditions at different time intervals after incubation is shown above. Integrated fluorescence intensity of same spectra with specific time points is shown below.

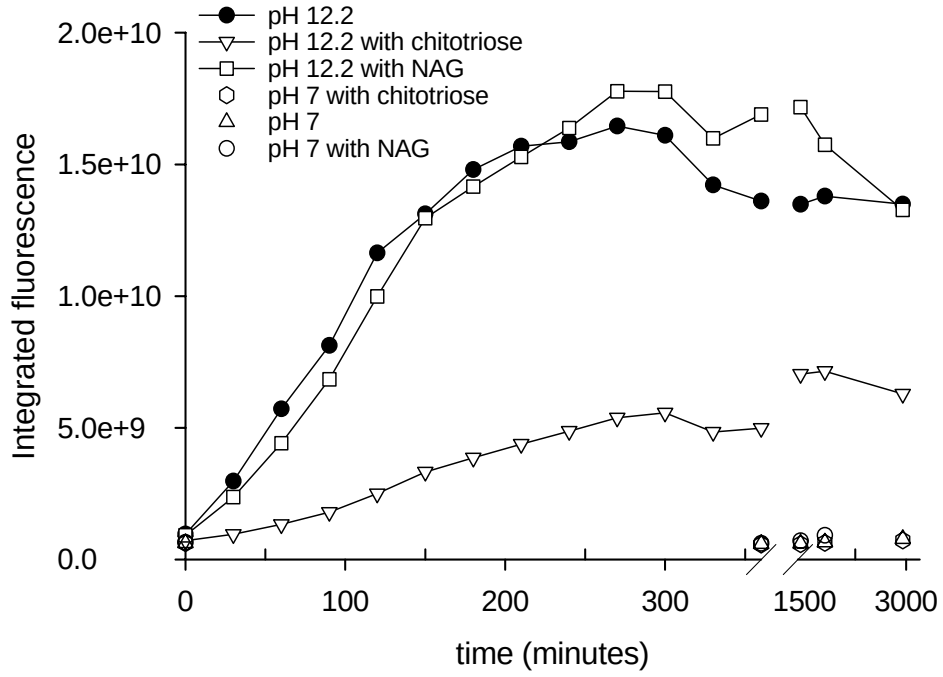

Figure 6.3B Integrated ANS fluorescence intensity in presence of HEWL at different experimental conditions at different time points is shown here.

There was a gradual increase in ANS fluorescence with HEWL at pH 12.2 both in absence (control) and presence of NAG (preincubated overnight) till ~300 minutes (Figure 6.3B) with saturation afterwards clearly indicating the exposure of hydrophobic patches in lysozyme in above mentioned experimental conditions. Additionally, blue shift in ANS emission maximum to ~464 nm in control sample and in presence of NAG also suggests that hydrophobic region are accessible during aggregation process and act as driving force in early event of HEWL oligomerization at alkaline condition (Figure 6.3A). Enhanced ANS fluorescence with HEWL at pH 12.2 was consistent with earlier observation described in chapter 5. However, ANS fluorescence was significantly reduced in HEWL sample at alkaline pH, which was preincubated overnight with chitoriose, indicating that misfolding and subsequent exposure of non-polar regions are considerably reduced after prior incubation with chitotriose. As expected, ANS fluorescence was insignificant in pH 7 soaked lysozyme either presence or absence of saccharides, indicating intact hydrophobic region of HEWL in these experimental condition.

6.3 Thioflavin T fluorescence

Thioflavin T is an extensively used probe to detect amyloid fibril formation (Vassar and Culling 1959; LeVine 1993). We employed thioflavin T fluorescence to monitor HEWL amyloid in pH 12.2 incubated protein at different experimental conditions. Figure 6.4A and 6.4B shows time dependent ThT fluorescence spectrum and integrated fluorescence intensity respectively, in presence of HEWL (both at high and low concentrations) in pH 12.2 preinubated either with NAG or chitotriose along with control having no saccharide but identical otherwise. Although ThT data prior to 50 hours could not be collected due to precipitation of HEWL after transferring to pH 8.5 buffer from pH 12.2. We observed a steady rise in ThT intensity upto 103 hours and minor change till 390 hours of observation in pH 12.2 soaked lysozyme without saccharides (Figure 6.4B). This was in agreement with our earlier observation in chapter 5. Figure 6.4B also shows that in presence of HEWL-NAG complex at pH 12.2, ThT intensity was comparatively more than control but was significantly reduced in HEWL-chitotriose complex at alkaline condition for same time span. Since ThT is an amyloid specific probe, these observations reflects a higher population of amyloid-like structure in control and HEWL-NAG complex, but a reduced amyloid population in HEWL-chitotriose complex.

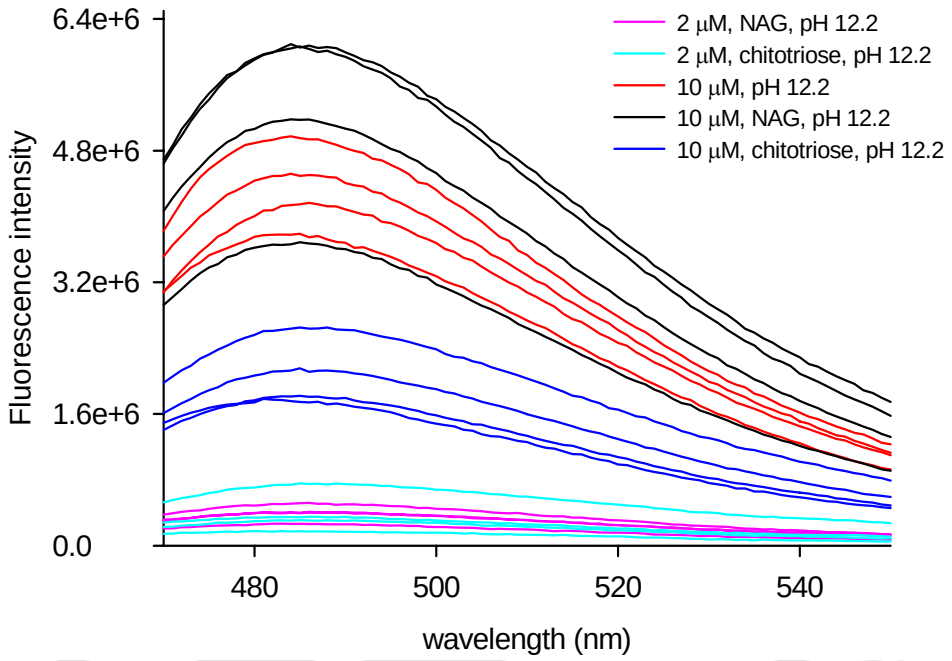

Figure 6.4A Change in fluorescence intensity of ThT with HEWL in different experimental conditions at different time intervals after incubation is shown above. Integrated fluorescence intensity of same spectra with specific time points is shown below.

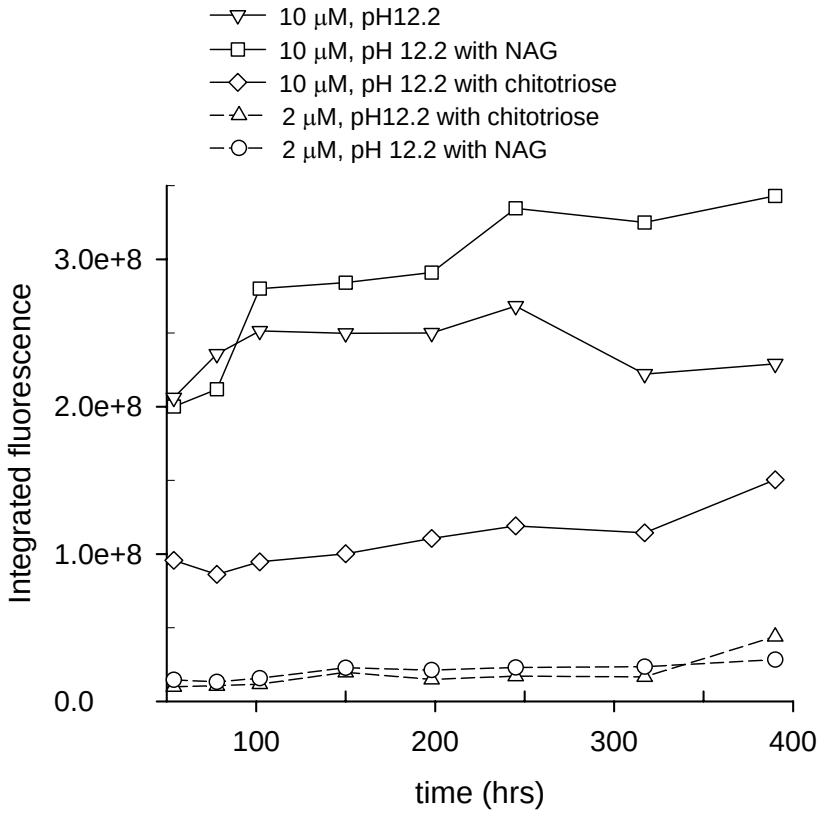

Figure 6.4B Integrated ThT fluorescence intensity with HEWL at different experimental conditions at different time points is shown here.

Figure 6.4B also reveals effect of low HEWL concentration on fibrillization of protein at alkaline condition in prior presence of chitotriose or NAG. We observed considerably low ThT fluorescence intensity in chitotriose or NAG complexed HEWL at pH 12.2 indicating the absence of amyloid at low protein concentration (20 μM) compared to higher intensity observed with higher lysozyme (100 μM) concentration under identical experimental setup. These observations suggest that a) HEWL self-association at alkaline condition is concentration dependent and b) NAG or chitotriose by themselves did not contribute to any increase in ThT fluorescence. It was thus evident that prior incubation of HEWL with trisugar, chitotriose reduces the presence of amyloid-like structure at alkaline condition while preincubation with single sugar compound, NAG did not show any inhibitory effect on lysozyme amyloid formation.

6.4 SDS PAGE

To visualize the size heterogeneity in lysozyme aggregates at different experimental conditions, 198 hours old samples of HEWL were subjected to 12% SDS PAGE. Since in chapter 5 we have shown that week old lysozyme aggregates at pH 12.2 are stabilized by intermolecular disulphide bond, it was thus unlikely that aggregates will dissociate in presence of SDS. Figure 6.5 reflects SDS PAGE of nearly 8 day old HEWL at pH 12.2 which was preincubated either with NAG or chitotriose. Control HEWL (without additives) at pH 7 and pH 12.2 for the same time period of incubation was also run in parallel along with Dalton marker VII-L and mixture of bovine serum albumin and lysozyme dissolved in deionized water. Lane 3, 5 and 8 in Figure 6.5 indicates monomeric HEWL with 14.3 kDa band in freshly prepared protein alone, in presence of NAG and in presence of chitotriose respectively, all in pH 7 buffer. A smear reflecting heterogeneous aggregates of lysozyme with high and low molecular weights were observed at pH 12.2 alone (lane 4) and sample preincubated with NAG (lane 6). However, with chitotriose incubated protein, mostly 14.3 kDa band with significantly reduced size heterogeneity was evident at pH 12.2 for same time window of incubation (lane 9). Although some oligomeric species in the range of ~24 kDa or less were observed in this sample, majority of lysozyme population in this lane appears monomeric with 14.3 kDa.

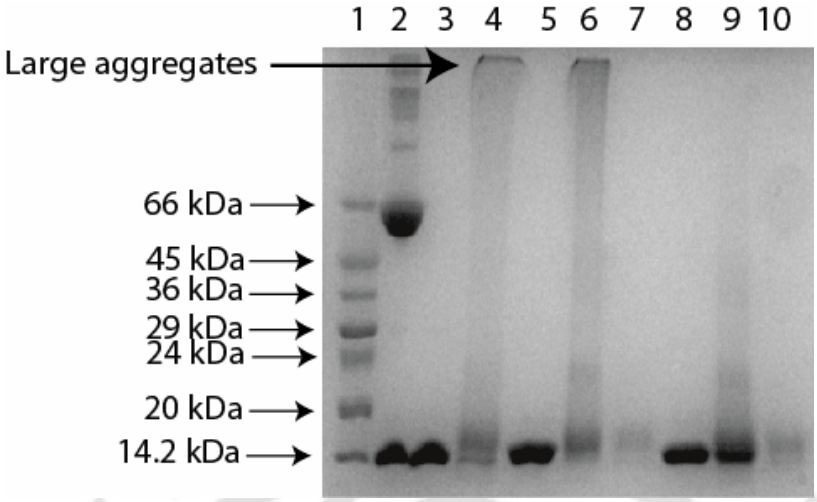

Figure 6.5 12% SDS PAGE to monitor the heterogeneity in HEWL aggregates under different experimental conditions is shown here. The description of lane depicted above is as follow: Lane 1, 14 µg Dalton marker VII-L; lane 2, mixture of bovine serum albumin (BSA) and hen egg white lysozyme (14 µg each); lane 3, 21 µg freshly prepared HEWL in pH 7; lane 4, 21 µg HEWL in pH 12.2; lane 5, 21 µg HEWL with NAG, pH 7; lane 6, 21 µg HEWL with NAG, pH 12.2; lane 7, 6 µg HEWL with NAG, pH 12.2; lane 8, 21 µg HEWL with chitotriose, pH 7; lane 9, 21 µg HEWL with chitotriose, pH 12.2 and lane 10, 6 µg HEWL with chitotriose, pH 12.2. All samples from lane 4 to 10 were 198 hours old.

All these experiments namely, ANS and ThT fluorescence and SDS PAGE data unequivocally support the effectiveness of trisugar chitotriose against self-association of HEWL at pH 12.2 compared to single sugar compound NAG. Although in earlier work Sophianopoulous reported the reduction in HEWL dimerization in presence of different size sugar molecules at pH between 7.6-8.3 (Sophianopoulous 1969), we are the first to show the inhibitory influence of chitotriose on lysozyme fibrillization at alkaline condition (pH 12.2). Similar to the observation by Sophianopoulous, where the order of effectiveness of these sugar against HEWL dimerization was trisaccharide >disaccharide >monosaccharide, we also discovered that chitotriose was much effective against lysozyme self-association at pH 12.2 compared to NAG.

6.5 HEWL activity

Enzymatic activity of HEWL incubated at pH 12.2 in presence of inhibitors is another tool to quantify the inhibition of aggregation. As enzymatic activity directly mirrors the presence of correctly folded structure of protein, we intended to measure the

activity of HEWL after incubation at pH 12.2 for different time periods either alone or in prior presence of chitotriose/NAG. Figure 6.6 reveals the percentage of activity that was recovered from alkaline samples in comparison to identical concentration of freshly prepared lysozyme at neutral pH. In control sample (with no chitotriose/NAG) there was a gradual decrease in catalytic activity of HEWL upto 360 minutes, reaching almost zero after 1500 minutes. This was consistent with our earlier work described in chapter 5. Lysozyme sample which was preincubated with NAG and then transferred to pH 12.2 buffer, showed substantial activity (70-90%) in the first 360 minutes. This value decreased to nearly 24% after 1500 minutes of incubation. The HEWL sample which was preincubated with chitotriose before transferring to pH 12.2, revealed catalytic activity that was much better compared to control or with NAG. With chitotriose one obtained nearly 80-100% lysozymal activity in first 360 minutes, while after 1500 minutes this value was >70%.

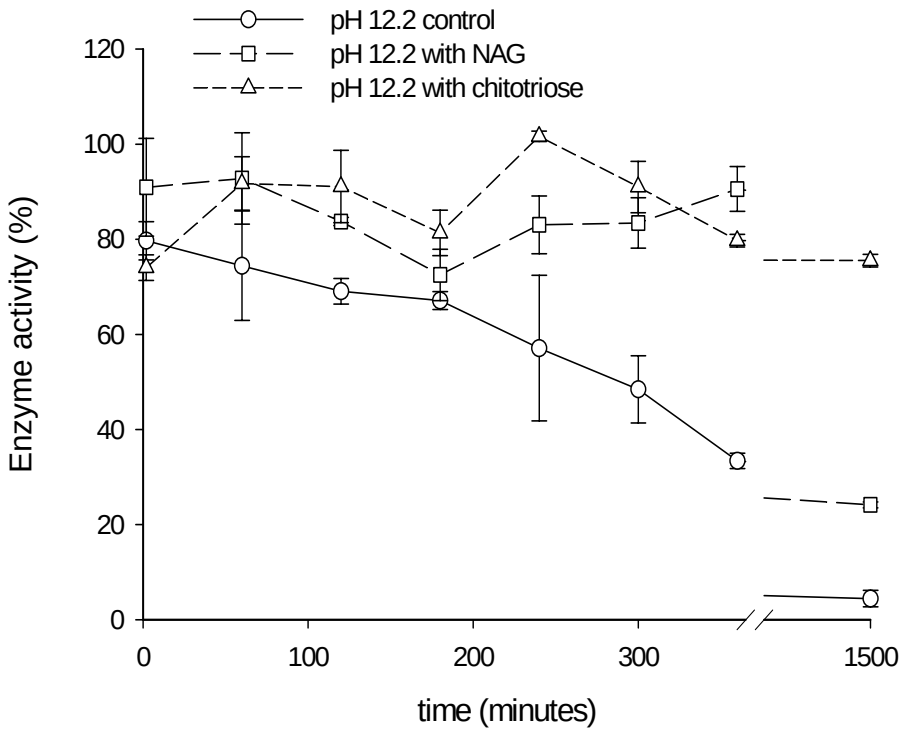

Figure 6.6 Percentage recovery of HEWL activity after incubation at different experimental conditions at different time points is shown.

When we monitored the activity of HEWL under same experimental condition after seven and sixteen days, we obtained 15% activity in chitotriose incubated sample while other samples did not show any activity after seven days (Figure 6.7).

After sixteen days of incubation at pH 12.2, all samples lost their catalytic activity as it is evident from figure 6.7.

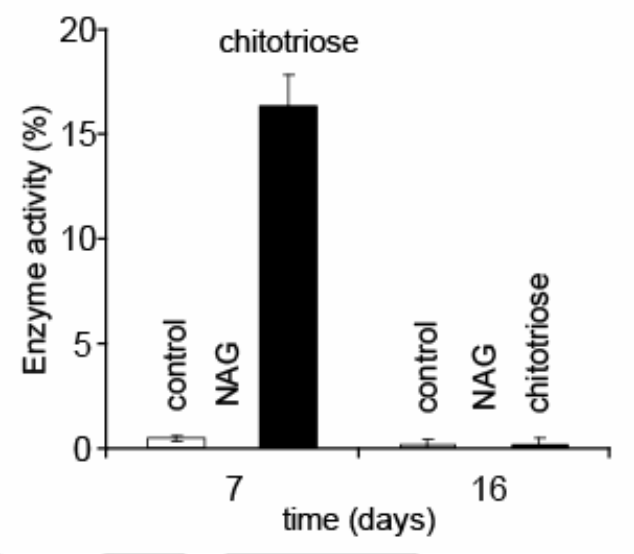

Figure 6.7 Percentage catalytic activity of pH 12.2 soaked HEWL in different experimental conditions after 7 and 16 days of incubation at room temperature.

Retaining the activity of HEWL at extremely harsh condition in presence of chitotriose is a clear indication of native from of protein in our experimental conditions. Binding of inhibitor and ligands are known to stabilize the native form of protein. Binding of trisaccharide chitotriose with HEWL has a dissociation constant ~10,000 fold smaller than NAG (Dahlquist et al., 1966), whereas $-\Delta G^0$ for the binding is ~3 fold higher for chitotriose compared to NAG (Bjurulf et al., 1970). These parameters which otherwise indicates the higher affinity of chitotriose towards HEWL indicate that preincubation of trisugar substantially stabilizes the protein such that it not only retards the structural fluctuation of protein leading to aggregation, but also helps in retaining its native structure under harsh condition for a sufficient period of time.

Conclusions:

1) Preincubation of HEWL with chitotriose stabilizes the native structure of protein, thus inhibiting aggregation whereas NAG does not exhibit such an inhibitory effect.

2) Chitotriose also helps to retain the native and functional form of HEWL at alkaline condition to a greater extent of time in comparison to NAG and control sample.

Chapter 7

Enhanced thioflavin T fluorescence selectively inside anionic micelles and mammalian cells

Thioflavin T (ThT) is a positively charged benzothiazole dye that shows enhanced fluorescence upon binding to amyloid in tissue sections. Ever since 1959, when Vassar and Culling introduced ThT, this cationic dye has been extensively used to detect amyloid fibrils in aggregated proteins (Vassar and Culling 1959; Saeed and Fine 1967; LeVine 1993). Saeed and Fine demonstrated the superiority of ThT for amyloid detection by comparing Congo red, crystal violet, van Gieson, and ThT dye for their binding with several positive and negative control tissues.

Due to the specific binding of ThT with amyloid fibrils, it has been used in many application such as diagnosis of amyloid in tissue sections (Hobbs and Morgan 1963; Vassar and Culling 1959), monitoring extracted amyloid and *in vitro* fibril formation using fluorescence microscopy (LeVine 1993) and direct observation of amyloid fibril formation using total internal reflection fluorescence microscopy (Ban et al., 2003). However, attempts are underway to detect amyloid-β *in vivo* using uncharged derivative of ThT that readily enters the brain (Klunk et al., 2001).

Upon binding to amyloid fibrils, thioflavin T shows absorbance at 450 nm and enhanced fluorescence emission at 482 nm. Despite its common use in the diagnosis of amyloid fibrils in *ex vivo*, *in vitro* and animal model, exact mechanism underlying specific binding and enhanced fluorescence emission subsequent to binding with amyloid is still elusive.

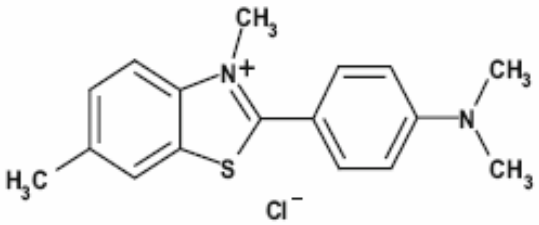

Figure 7.1 Structure of Thioflavin T

The structure of ThT shown above indicates that molecule consists of a pair of benzothiazole and benzene rings freely rotating around a shared C-C bond (Dzwolak and Pecul 2005). It has been hypothesized that enhanced ThT fluorescence may arise

from the restricted torsional relaxation between benzthiazole ring and benzene ring when ThT is bound to amyloid fibrils, which would otherwise favor the non-radiative pathway when rotation is freely possible (Voropai et al., 2003; Stsiapura et al., 2007). It has also been suggested that the thiazole nitrogen of the dye and hydroxyl group of tissue structures form hydrogen bonds leads to specific binding of ThT with amyloid and other tissue structures (Kelenyi 1967). Mandelkow and co-workers demonstrated that the quantum yield of ThT increases dramatically when the dye is located in a viscous environment (Friedhoff et al., 1998). Thus a viscous or a rigid microenvironment is likely to enhance the fluorescence of ThT. In a recent study it was shown that absorption spectrum of ThT is sensitive to the surrounding solvent polarity, where the peak in long wavelength absorption band shifts from 412 nm in water to 424 nm in chloroform (Maskevich et al., 2007)

Contrary to popular belief, binding and enhanced ThT fluorescence is not an exclusive feature of amyloid. Thioflavin T has been shown to bind with other connective tissues such as cartilage matrix, elastic fibers and mucopolysaccharide (Vassar and Culling 1959; Kelenyi 1967). Apart from protein and cellular components, ThT is also known to bind and exhibit fluorescence with DNA (Canete et al., 1987; Ilanchelian and Ramaraj 2004) and cyclodextrins (Raj and Ramaraj 1999). While detecting amyloid in different experimental conditions we serendipitously observed that ThT shows increased fluorescence in presence of anionic surfactant sodium dodecyl sulphate (SDS).

Understanding the importance of ThT as an amyloid specific probe along with several reports using SDS (near CMC) to induce amyloid formation (Rangachari et al., 2006; Movahedi et al., 2007) we questioned ourselves whether SDS micelles alone enhance ThT fluorescence? In this work we initially investigated the influence of different surfactant micelles on the absorption and fluorescence spectra of ThT. Subsequently we monitored ThT fluorescence inside the mammalian cells knowing that derivative of this cationic dye is underway to visualize amyloid fibrils *in vivo* (Klunk et al., 2001; [109]Maezawa et al., 2007).

7.1 Absorption of thioflavin T with surfactants

The interaction between ThT and surfactants was studied by measuring the electronic absorption spectrum of ThT in the presence of surfactants. Absorption spectra of 20 μM ThT was monitored in presence of different concentrations of SDS, 5 mM CTAB

and 2 mM Triton X-100 and Tween 20. Figure 7.2 shows that in absence of surfactants, ThT displays absorption maximum (λ_{max}) around 412 nm at pH 8.5 buffer, which was consistent with earlier reports (Voropai et al., 2003; Maskevich et al., 2007). Immediately after adding SDS (0.25 mM) in the medium, the peak absorbance drops by ~22% although the peak wavelength remains unchanged at 412 nm. As the SDS concentration was increased further from 0.5 mM to 2.0 mM, there was a concomitant rise in the absorbance while the absorption spectrum shifted to a longer wavelength. With the further increase in SDS concentration from 2 mM to 5 mM a degree of saturation was evident in the rising absorbance value.

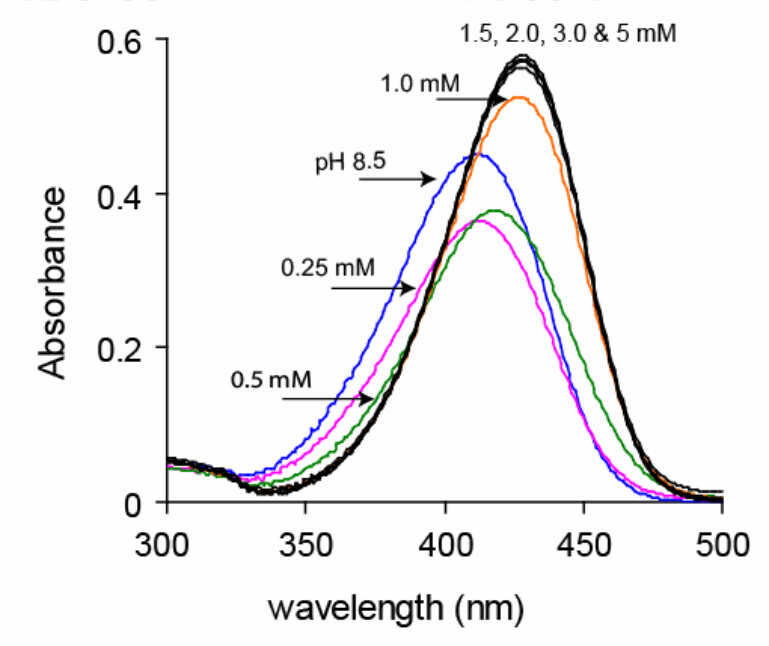

Figure 7.2 Absorption spectra of 20 µM ThT in presence of different concentrations of SDS in pH 8.5 buffer at 298 K.

As evident from figure 7.2, in presence of 5 mM SDS, ThT displays a λ_{max} ~428 nm with nearly 28% increase in peak molar absorbance comparison to that observed in pH 8.5 buffer. To monitor the change in absorbance value of ThT with other surfactants, same experiment was performed with 5 mM CTAB, 2 mM Triton X-100 and 2 mM Tween 20. It is worthwhile to mention here that calculated critical micellar concentration (CMC) of different surfactants at 20 mM pH 8.5 Gly-Gly buffer was as follow: SDS, 1.3 mM; CTAB, 0.26 mM; Triton X-100, 0.89 mM and Tween 20, 0.081 mM (see later). Thus, concentration used for CTAB, Triton X-100 and Tween 20 were well above their CMC.

Figure 7.3 compares the absorption spectrum of ThT in buffer with those in presence of 5 mM CTAB, 2 mM Triton X-100 and 2 mM Tween 20. In contrast to Figure 7.2 where dramatic change in ThT absorbance was observed with SDS, no significant change in ThT absorption spectrum was observed in presence of CTAB or Triton X-100 or Tween 20.

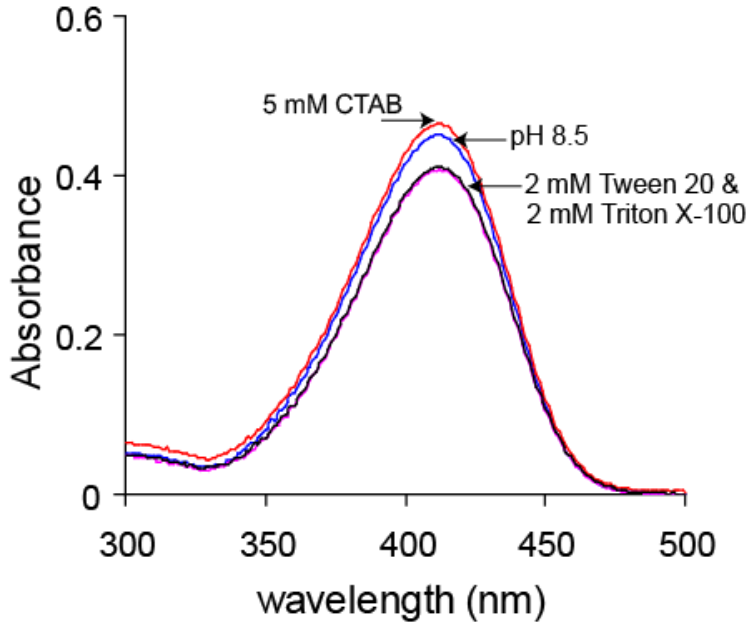

Figure 7.3 Absorption spectra of 20 μM Thioflavin T in presence of different surfactants at 298 K in pH 8.5 buffer.

As observed in Figure 7.2, the initial drop in ThT absorbance on addition of 0.25 mM SDS could arise from formation of premicellar aggregates, where negatively charged SDS monomers might cluster around positively charged ThT (Maiti et al., 1996). Further investigations with SDS in the concentration range 20 to 200 μM (Figure 7.4) revealed a gradual dip in ThT absorbance at 412 nm. Figure 7.4 indicate that at pH 8.5 buffer ThT absorbance was ~0.47 which decreased to ~ 0.35 in presence of 200 μM SDS with no observable shift in peak wavelength.

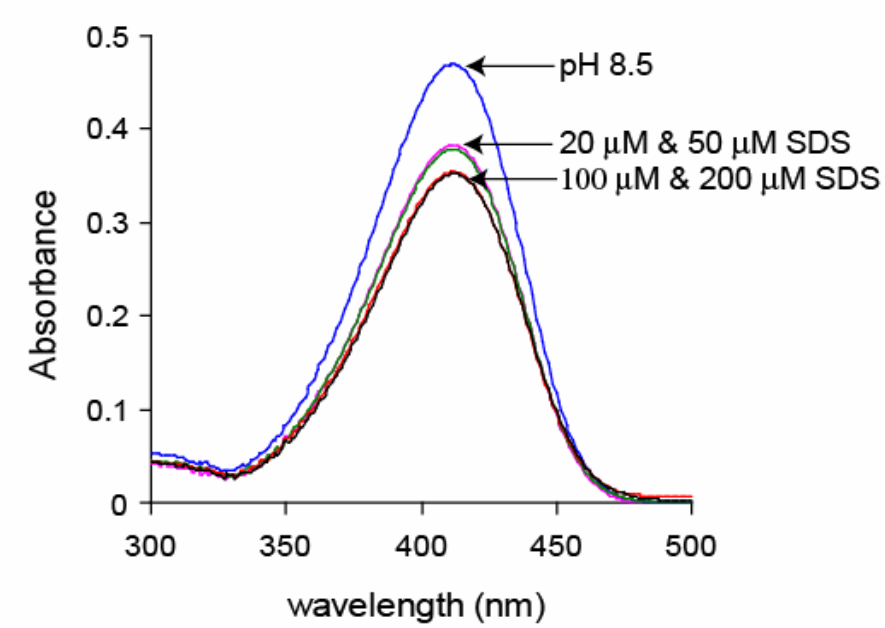

Figure 7.4 Absorption spectra of 20 µM Thioflavin T with lower concentration of SDS at 298 K in pH 8.5 buffer.

A similar dip and rise in absorbance with increasing SDS concentration in presence of cationic pyridoimidazole derivative has been observed earlier (Krishnamoorthy and Dogra 2000), however the exact mechanism behind this phenomenon has not been explained. In the absence of any clear isobestic point or shift in peak wavelength in Figure 7.2 and 7.4, it is apparent that these premicellar aggregates are likely to be disordered or nonspecific in nature. The subsequent red-shift and rise in the intensity of the spectrum from 0.5 mM SDS onwards points to increasing micellization of ThT, which appears complete at 1.5 mM SDS (Figure 7.2). Rise in ThT absorbance with increase in SDS concentration may arise from the partitioning of non-polar moieties of ThT into micellar hydrophobic interior of SDS and stabilization of positive charge by negatively charged sulphate group in the exterior surface. It is has been shown that ThT ground state is progressively less stabilized (increasing λ_{max}) as the polarity of surrounding solvent is reduced (Maskevich et al., 2007). Absorption maximum of ThT in water was 412 nm which was shifted to ~421 nm in 99% glycerol whereas at $CHCl_3$ it was ~424 nm. So, with a λ_{max} ~428 nm it is apparent that a major portion of ThT molecule resides in the interior non-polar environment of SDS micelles.

Compared to anionic surfactant SDS, absence of any shift in absorption spectrum of ThT in presence of cationic surfactant CTAB or neutral surfactant Triton X-100/Tween 20 (Figure 7.3) suggests that ThT does not enter inside these micelles. It is interesting to note that ThT clearly discriminates between SDS and other non-anionic micelles in solution on the basis of surfactant charge. Thus, Coulombic attraction, between anionic SDS and cationic ThT and Coulombic repulsion between cationic CTAB and ThT plays a major role in the events shown in Figure 7.2 and 7.3. With neutral surfactants like Tween 20 and Triton X-100, there is no Coulombic repulsion, yet no significant change is observable in the absorption spectrum. Perhaps stabilization of the positive charge in ThT is essential for the effective micellization of the probe.

7.2 Fluorescence emission of thioflavin T with surfactants

Interaction of ThT with surfactants was also monitored by measuring ThT fluorescence subsequent to excitation at 450 nm. LeVine contributed considerably in understanding the fluorescence properties of ThT and observed the new excitation peak at 450 nm subsequent to the binding with amyloid fibrils. Upon binding to amyloid fibrils, excitation of ThT at this wavelength exhibits enhanced fluorescence emission at ~482 nm (LeVine 1993; 1995). We then monitored the ThT fluorescence emission in presence of different concentration of SDS at pH 8.5 buffer.

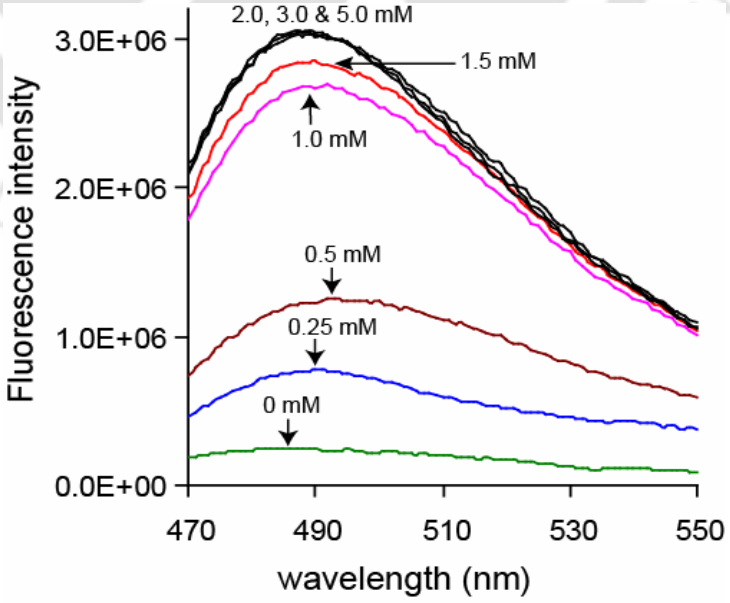

Figure 7.5 Change in the fluorescence emission spectrum of 20 µM ThT with different concentrations of SDS in pH 8.5 buffer after exciting at 450 nm.

Figure 7.5 indicate the gradual increase in ThT emission intensity as the SDS concentration rises from 0 mM SDS to 2 mM SDS. Subsequently, the emission intensity and emission maximum (λ_{max}) ~489 nm, remains unchanged from 2 mM SDS to 5 mM SDS, indicating saturation of ThT fluorescence. While monitoring emission spectra of 20 µM ThT with 5 mM SDS subsequent to excitation at different wavelength, emission maximum (λ_{max}) was observed between 484-490 nm with a single peak, when excitation wavelength was varied between 380-450 nm (Figure 7.6).

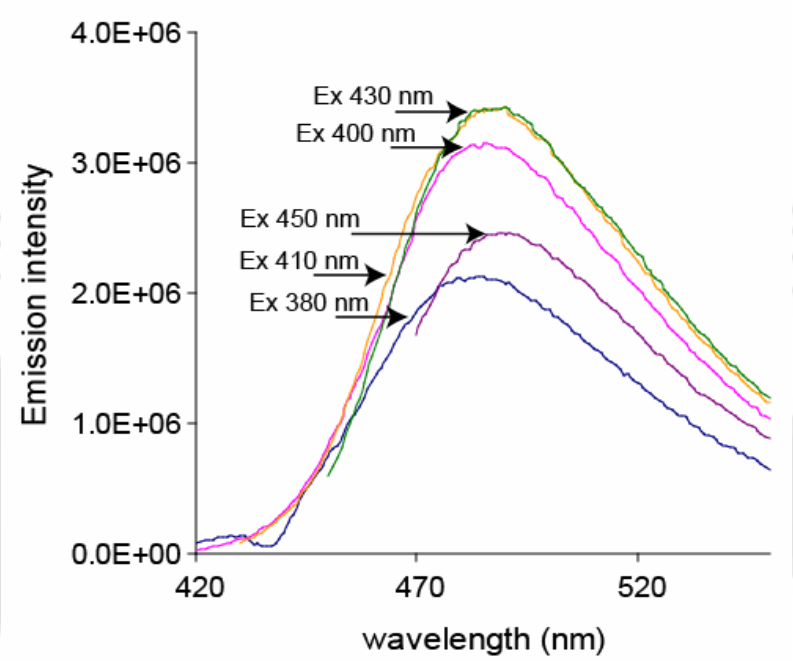

Figure 7.6 Emission spectra of 20 µM ThT with 5 mM SDS is shown at different excitation wavelength. Ex indicates different excitation wavelength.

While monitoring the excitation spectra of the same samples we observed fairly broad spectra, showing a single peak with a λ_{max} between 421-427 nm when emission wavelength was varied between 460-540 nm (Figure 7.7). Since ThT is known to show absorbance at 450 nm and enhanced fluorescence emission at 482 nm upon binding with amyloid fibrils, we selected 450 nm as excitation wavelength in SDS-ThT experiment to make our observations comparable that one can obtain with amyloid fibrils.

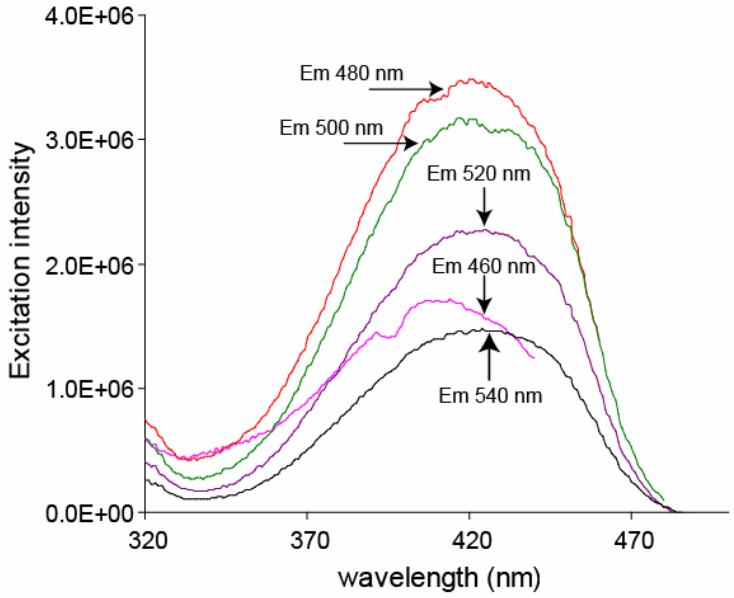

Figure 7.7 Excitation spectra of 20 µM ThT with 5 mM SDS is shown keeping fixed emission maximum at different wavelength. Em indicates different emission wavelength.

Interaction of positively charged ThT with anionic surfactant SDS as shown from absorbance and fluorescence spectroscopy can be facilitated by both hydrophobic interaction between SDS micelles and ThT, and electrostatic interaction between oppositely charged SDS head group and ThT. The increase in ThT fluorescence with SDS and subsequent saturation may be correlated to micelle formation in SDS as its concentration increases. To verify this, we monitored the micelle formation in SDS using pyrene under conditions identical to that employed in ThT experiments.

Pyrene has been employed as a fluorescence probe to monitor micelle formation. The classic dependence of vibronic band intensity ratios in pyrene monomer fluorescence towards solvent polarity has been used to study microenvironment experienced during the micelle formation. This parameter is an excellent indicator of self-association among surfactant molecules (Kalyanasundaram and Thomas 1977). We used the peak III to peak I vibronic intensity ratio (III/I ratio) in pyrene fluorescence emission to estimate critical micellar concentration of surfactant at 20 mM pH 8.5 Gly-Gly buffer. We employed 2 µM pyrene with different concentrations of surfactants. Subsequent to excitation at 310 nm, peak III to peak I vibronic intensity ratio of pyrene in all samples were measured by collecting the spectrum between 350-450 nm.

Figure 7.8 indicates the gradual increase in III/I ratio of vibronic bands as a function of SDS concentration. This value started with ~0.53 at 0 mM SDS, saturates around ~0.9 at 2.0 mM SDS and remains constant thereafter indicating the formation of SDS micelles. Here it is interesting to compare the pyrene III/I ratio with ThT integrated fluorescence intensity as a function of SDS concentration. Figure 7.8 also depicts the variation of integrated ThT fluorescence with SDS concentration. We observed that the dependence of pyrene III/I ratio and ThT integrated fluorescence intensity on SDS concentration are nearly superimposable. This finding made us to conclude that increase in ThT fluorescence is directly correlated with formation of SDS micelles. We then tried to determine the reasons behind ~13 fold increase in ThT fluorescence in presence of SDS. The enhanced fluorescence of ThT in presence of SDS micelles can originate from two factors: A) a higher quantum yield owing to a relatively rigid microenvironment in micelle interior compared to solvent and B) a higher ThT molar absorptivity at the excitation wavelength (450 nm) subsequent to micellization. Using Rhodamine 101 as a quantum yield standard, we calculated nearly three fold increase in quantum yield of ThT in presence of 5 mM SDS. We also observed three fold rise in molar absorptivity of ThT with 5 mM SDS at 450 nm. Thus a nine fold increase in the fluorescence of ThT in presence of SDS is roughly predicted, while the observed increase was about thirteen fold. This discrepancy in values may arise from possible error in determining the quantum yield, since a standard with matching emission spectrum and excitation wavelength as ThT was not available.

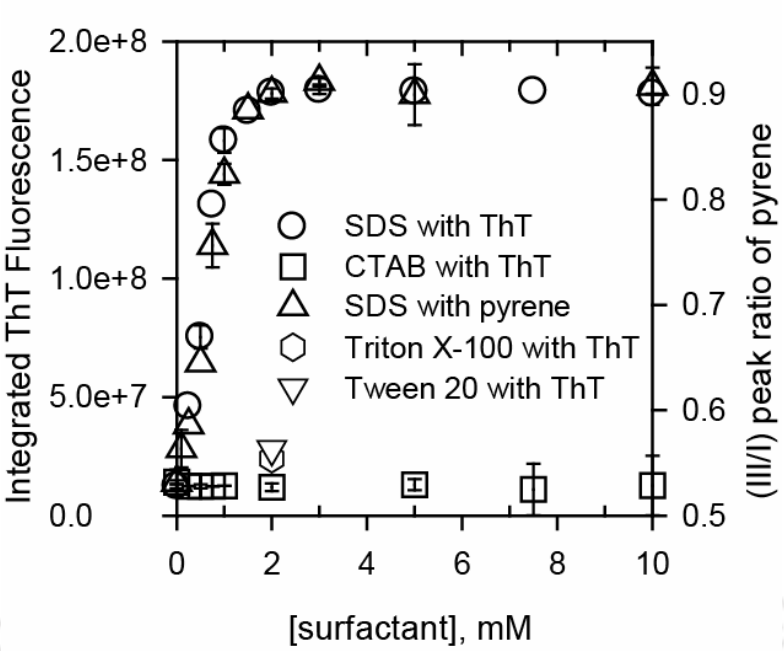

Figure 7.8 Concentration dependent changes in ThT fluorescence and III/I peak ratio of pyrene emission in presence of different surfactants**.**

Figure 7.8 also shows the change in ThT fluorescence with different concentrations of CTAB, 2 mM Triton X-100 and Tween 20. No significant change in ThT fluorescence intensity was observed with CTAB in the concentration range of 0–10 mM, Triton X-100 and Tween 20, compared to the intensity in pH 8.5 buffer. However, experiments with pyrene indicated that CTAB was indeed forming micelles as inferred by a constant III/I ratio of ~0.75 beyond 0.25 mM CTAB (Figure 7.9 B). CMC value calculated using this experiment was 1.3 mM, 0.26 mM, 0.89 mM, and 0.081 mM for SDS, CTAB, Triton X-100 and Tween 20 respectively (Figure 7.9 A, B, C and D).

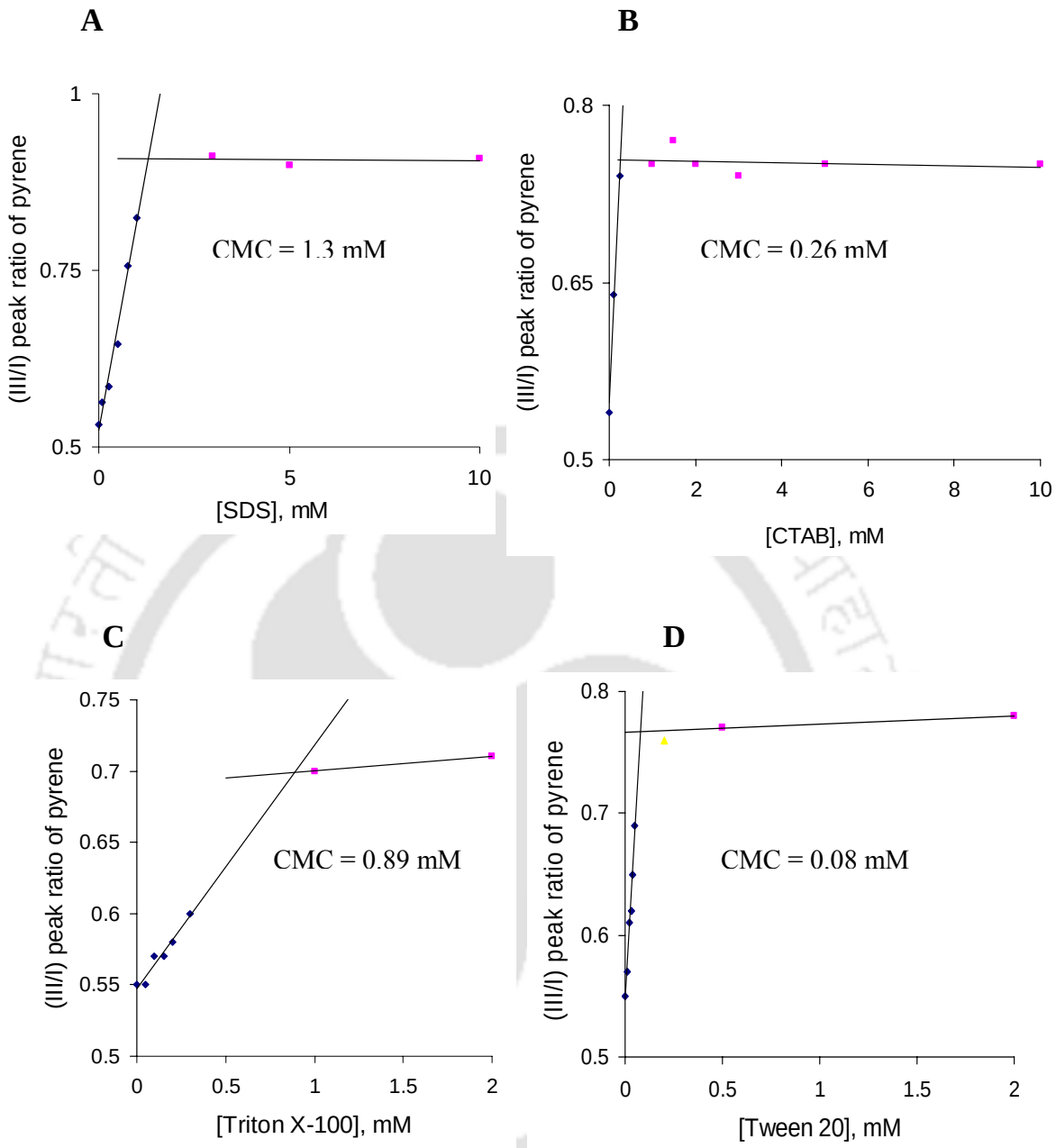

Figure 7.9 Critical micellar concentration determinations of SDS (A); CTAB, (B); Triton X-100 (C) and Tween 20, (D) using pyrene III/I intensity ratio in 20 mM pH 8.5 Gly-Gly buffer.

These observations indicates that Coulombic repulsion between positively charged CTAB head group and positively charged ThT hinders close interaction of dye with CTAB micelles. Earlier work from Khurana and co-workers have shown that electrostatic forces influence the binding of ThT to fibrils of 13 residue peptides that either contain or do not contain lysine residues (Khurana et al., 2005). Figure 7.8 also shows the ThT fluorescence intensity in presence of neutral micelles of Tween 20 and Triton X-100 indicates relatively insignificant increase in intensity in comparison to that observed with SDS.

Thioflavin T is known to display enhanced fluorescence emission at ~480 nm upon binding to amyloid fibrils. We compared the emission profile of ThT in presence of SDS with previously reported amyloid samples of HEWL at acidic pH (McAllister et al., 2005). Figure 7.10 compares the emission spectra of 20 µM ThT in 5 mM SDS, in HEWL incubated in pH 2.7 at 333 K for 13 days (HEWL sample A) and in HEWL soaked in pH 12.2 at 298 K for 8 days (HEWL sample B). HEWL concentration was 12 µM in assay medium.

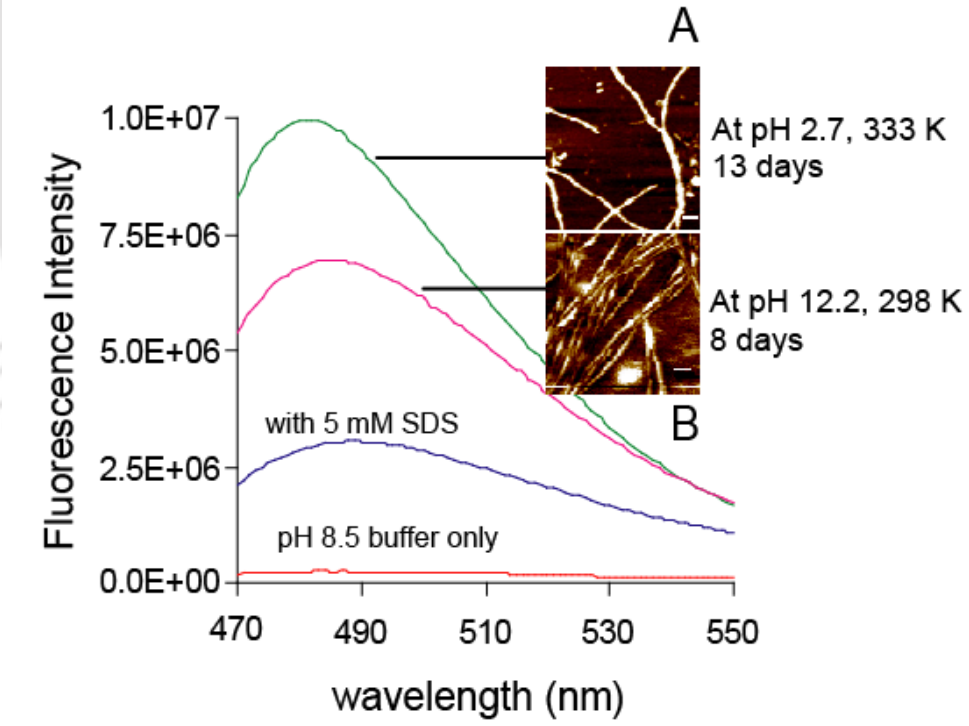

Figure 7.10 Fluorescence emission spectra of ThT (20 µM) in pH 8.5 buffer under different experimental conditions. Scale bar in AFM image is equivalent to 100 nm.

Presence of HEWL amyloid fibrils in acidic condition (sample A) was confirmed by AFM imaging (image A in Fig. 7.10). The highest ThT fluorescence intensity was observed in HEWL sample A. An intermediate level of ThT

fluorescence was detected with HEWL amyloid fibrils at alkaline condition (sample B; image B in Fig. 7.10), where amyloid fibrils were detected by AFM. But interestingly, comparatively lower but significant ThT fluorescence was observed in presence of SDS (see Table 1 for comparative intensity). The wavelength of emission maximum for ThT in HEWL sample A, B and SDS were 482, 485 and 489 nm, respectively. However, previous studies could establish no obvious correlation of ThT emission maximum with surrounding solvent properties (Friedhoff et al., 1998). The integrated fluorescence intensity of these samples is shown in Table 1.

Table 7.1: Thioflavin T fluorescence in different environments

Thioflavin T (20 μM) in presence of	Integrated fluorescence intensity λ_{ex} = 450 nm	Relative fluorescence intensity	r_{ss}* λ_{em} = 490 nm (SDS) / 484 nm (HEWL)
pH 8.5 buffer	1.35 E+07	1.0	Not determined
0.25 mM SDS	4.59 E+07	3.4	Not determined
5 mM SDS	1.79 E+08	13.2	0.359 ± 0.013
5 mM CTAB	1.30 E+07	~1.0	Not determined
2 mM Triton X-100	2.40 E+07	1.8	Not determined
2 mM Tween 20	2.81 E+07	2.1	Not determined
HEWL pH 2.7	4.87 E+08	36	0.378 ± 0.021
HEWL pH 12.2	3.81 E+08	28	0.355 ± 0.004

***** r_{ss} refers to steady-state fluorescence anisotropy. This was not determined for weakly fluorescent samples as they are prone to errors.

Table 1 reveals nearly 36 and 28 fold increase in ThT fluorescence intensity with HEWL amyloid fibrils at pH 2.7 and 12.2 respectively while with 5 mM SDS, it was increased by ~13.2 fold as compared to pH 8.5 buffer. It is thus understandable that fluorescence enhancement of ThT displays a hierarchy that is possibly related to the viscosity/rigidity in the immediate microenvironment of the probe. It is known that ThT fluorescence intensity increases by more than hundred fold when transferred from water to glycerol (Friedhoff et al., 1998). To monitor the ThT rigidity inside SDS micelles, we measured steady-state anisotropy (r_{ss}) of 20 μM ThT under the

same concentrations range as used for fluorescence emission experiment. Steady-state anisotropy of HEWL amyloid fibrils (at pH 2.7 and pH 12.2) were also measured using 12 μM of protein with 20 μM ThT. After exciting at 450 nm, emission at 490 nm was collected to measure steady-state anisotropy of ThT at different experimental conditions. Figure 7.11 shows gradual increase in r_{ss} from 0.25 mM SDS (~0.27) to 1.5 mM SDS (~0.35), which was saturated thereafter indicating restricted motion of the dye inside anionic micelles. While comparing the steady-state anisotropy with fluorescence emission of ThT with SDS, we observed that both the data were nearly superimposable in nature. These finding correlated the enhanced ThT fluorescence emission with their rigidity inside SDS micelles. This observation also confirmed that ThT fluorescence and steady-state anisotropy can be used to monitor micellization of anionic surfactant SDS.

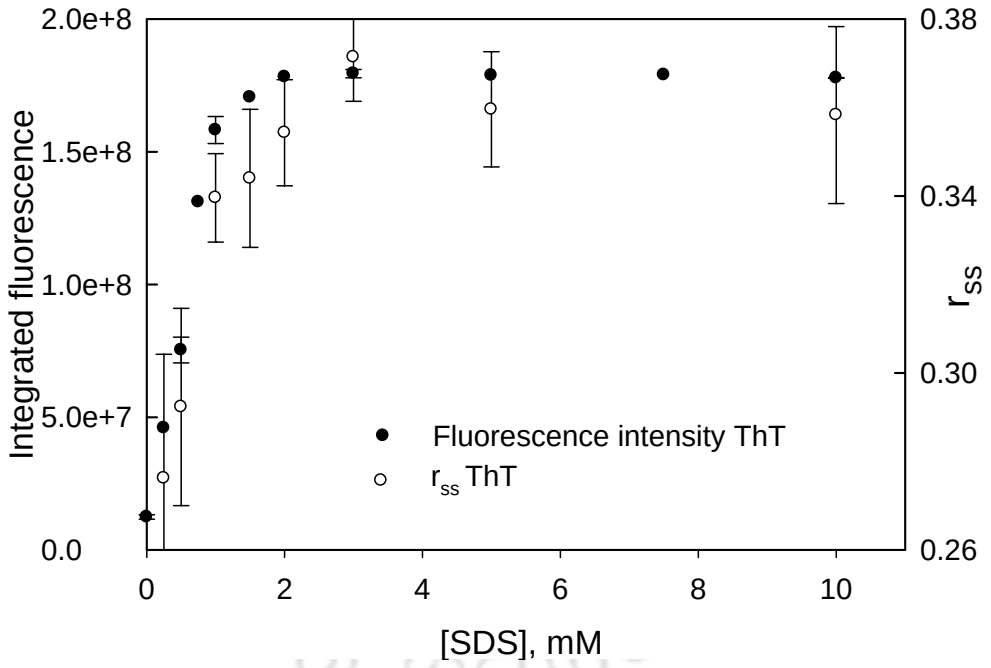

Figure 7.11 Correlation between fluorescence anisotropy and fluorescence emission of ThT in presence of SDS.

Interestingly, the r_{ss} of ThT was quite close to 0.4 in presence of HEWL fibrils and SDS (Table 7.1) suggesting that bound ThT is fairly immobile in these samples. Almost similar observation has been reported employing ThT steady-state anisotropy to monitor fibril formation in HET-s prion protein (Sabate and Saupe 2007). In a

recent report it has been observed that rigidity among different amyloid fibrils vary over nearly four orders of magnitude (Knowles et al., 2007).

7.3 Eukaryotic cells imaging

Micelles are good models of biological membranes. It is therefore possible that the fluorescence of ThT shall be enhanced by the lipid bilayer of the plasma membrane and membrane bound organelles in the cytoplasm of the living cell. To ascertain this, we proceeded to investigate the ThT fluorescence in presence of eukaryotic cells BHK-21 (baby hamster kidney cells) and HT29 (human colon adenocarcinoma cells). Both cell lines were treated with 50 μM ThT. After 15 minutes of incubation followed by washing, both cell lines were visualized employing the 458 nm Argon line for exciting ThT. Figure 7.12 and 7.13 shows the fluorescence and bright field microscopy image of BHK-21 and HT 29 mammalian cell lines respectively in presence and absence of ThT. Fluorescence images of both the cell lines in figure 7.12 and 7.13 reveals the portioning of dye inside the cells. Whereas control samples which had similarly plated cells but no ThT did not showed any trace of ThT fluorescence in fluorescence mode.

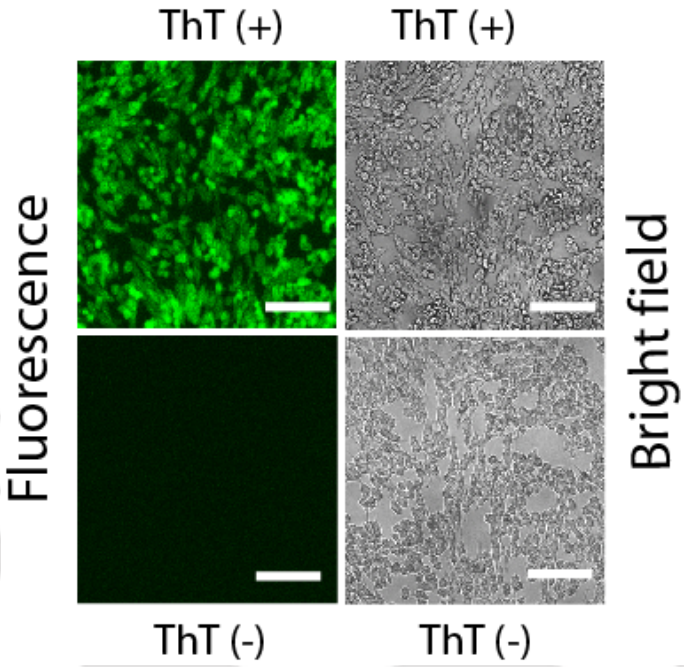

Figure 7.12 Fluorescence and bright field images of BHK-21 mammalian cell lines with and without thioflavin T. The scale bar represents 100 µm.

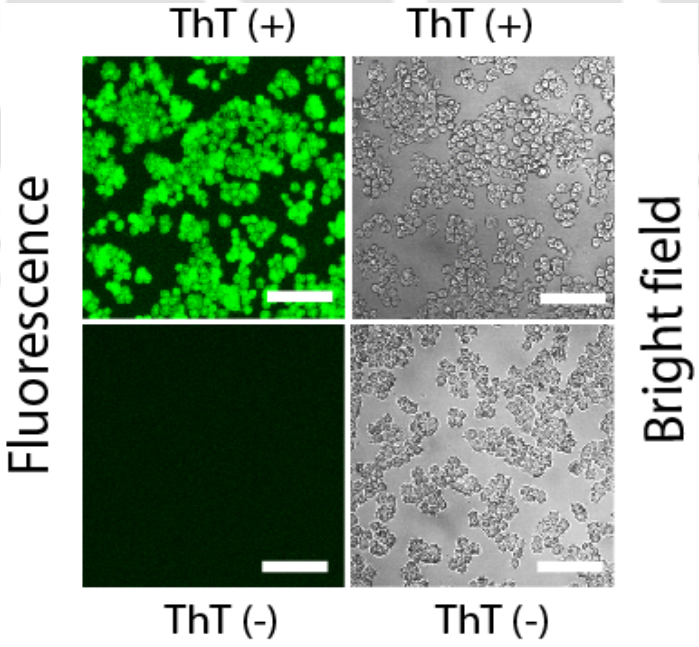

.

Figure 7.13 Fluorescence and bright field images of HT-29 mammalian cell lines with and without thioflavin T. The scale bar represents 100 µm.

Comparing the fluorescence image of same set of cells with bright field image, it is clear that ThT fluorescence originates from the cell cytoplasm and nucleus while fairly dark background was observed outside the cells. Contrary to our earlier anticipation, no characteristic membrane staining pattern was observed with ThT. Thioflavin T fluorescence originating from inside the cells was retained by both BHK-21 and HT29 even after washing away the external medium with ThT free PBS, suggesting that dye is firmly bound inside the cells.

Thioflavin T appears to behave as a membrane permeant dye that can make a facile entry into the cells. Inside the cell it is likely to encounter and bind to a host of components like nucleic acids, membranes and proteins resulting in fluorescence. The bright ThT fluorescence from mammalian cell interiors clearly emphasizes that attempts to detect amyloid-β *in vivo* using ThT (or its derivatives) will require cautious interpretation.

Thioflavin T has been earlier employed for staining human reticulocytes for flow cytometric analysis of blood samples (Sage et al., 1983) and recently with K562 leukemia cells (Darghal et al., 2006). The negative charge on the phosphate in the polar phospholipid headgroup in the membrane is likely to facilitate the entry of ThT into the cell based on our results with SDS. However, the mechanism of ThT entry into the cell is not clear at the moment. Nevertheless, ThT appears as a promising dye to label and stain biological cells chiefly due to the fact that free ThT in the extracellular medium is practically non-fluorescent rendering a sharp contrast in the cell fluorescence images while obviating the need to wash excess free dye from cell medium to improve contrast.

Conclusions:

1) Thioflavin T selectively resides inside the anionic micelles like SDS instead of cationic and neutral micelles.
2) Inside SDS micelles, the absorption peak wavelength of ThT was red shifted by 16 nm with ~28% increase in peak molar absorptivity.
3) The increase in ThT fluorescence emission inside SDS micelles arises primarily due to increases in molar absorptivity and fluorescence quantum yield.
4) Thioflavin T can prove useful as a membrane permeant dye to fluorescently label mammalian cells and selectively label anionic micelles.

Chapter 8

Concluding remarks

8.1 Summary

In the present work non-native states of proteins are explored employing different biophysical and biochemical techniques in different experimental conditions.

Residual structures in denatured proteins (studied in chapter 4) are important to understand the folding, unfolding and aggregation of proteins. Involvement of residual structures in HEWL aggregation highlights its importance. Chapter 5 and 6 describes inhibition of HEWL aggregation in presence of different additives and molecular mechanism underlying it. While monitoring HEWL aggregation in presence of SDS, I observed that thioflavin T shows enhanced fluorescence with SDS even in absence of protein. So in chapter 7, I carefully monitored the interaction of thioflavin-T (ThT), an amyloid specific probe with different surfactants. Facile entry of ThT inside the mammalian cells as observed in chapter 7 highlights (1) One has to be careful during *in-vivo* use of ThT as an amyloid specific probe (2) ThT can be used as a dye for labeling eukaryotic cells.

Bimolecular fluorescence quenching rate constant (k_q) and steady-state anisotropy (r_{ss}) were employed to locate the residual structure in the vicinity of Trp(s) in different denatured proteins. Furthermore, technique employed in chapter 4 (namely, steady-state anisotropy) was used to monitor the aggregation kinetics of dansyl tagged HEWL at alkaline pH. However fluorescence quenching experiments and emission maxima of labeled HEWL can be used to monitor the extent of exposure of fluorophore during aggregation process.

Since residual structures in HEWL containing Trp(s) are known to influence its aggregation tendency at acidic pH (Mishima et al., 2006; 2007) our observation in chapter 4 locating residual structures may influence self-association of HEWL at alkaline condition as discussed in chapter 5 and 6. However, it is difficult to directly correlate the observation form chapter 4 with chapter 5 and 6. Chapter 5 describes different biophysical and biochemical techniques to monitor the impeded growth of HEWL aggregates at pH 12.2 in presence of different additives. Whereas chapter 6 described chitotriose as a novel inhibitor of HEWL fibrillization at alkaline pH.

Binding of thioflavin T (ThT) with SDS micelles as discussed in chapter 7 is very important if one want to monitor aggregation kinetics of protein in presence of SDS. Observations from chapter 7 clearly indicate that significant ThT fluorescence with SDS micelles alone can leads the misinterpretation of results where SDS was used to induce aggregation. Furthermore facile entry of ThT inside mammalian cells and their enhanced fluorescence subsequent to binding with cellular organelles warns us for careful interpretation of observations where ThT has been used *in-vivo* as amyloid specific probe.

Specifically, the major conclusions of this thesis include:

- Tryptophan fluorescence can be used as a probe to locate residual structures in denatured proteins employing fluorescence anisotropy and quenching by external quencher.
- Anionic surfactant SDS, cationic surfactant CTAB, disulphide breaking agent DTT and competitive inhibitor chitotriose effectively inhibit lysozyme aggregation at alkaline condition.
- DTT imparts its inhibitory effect only if it applied from beginning. Once the aggregates are formed, tight molecular packing of aggregates prevents DTT or DTNP or OH^- from gaining any access to the inner core of the aggregate.
- Disulphide bonds stabilize HEWL fibril formation at alkaline condition.
- Gradual decrease in HEWL enzymatic activity at pH 12.2 indicates that lysozyme aggregation is slow and abolishes activity.
- Preincubation of HEWL with chitotriose stabilizes the native structure of protein, thus inhibiting aggregation whereas NAG does not exhibit such an inhibitory effect.
- ThT can be effectively used to monitor micellization of anionic surfactant and be used as a membrane permeant dye to fluorescently label mammalian cells.

8.2 Scope of future works

Importance of disulphide bonds during the process of aggregation and retention of enzymatic activity of HEWL in presence of chitotriose at extreme pH has given wide opportunities to explore the aggregation mechanism with greater depth. Additionally, use of ThT can be further explored to tag the different eukaryotic and prokaryotic cells.

These are the potential works which can be explored on the basis of present work.

- Observations from present thesis indicate the involvement of disulphide bonds in stabilizing the HEWL aggregates. Blocking of free thiol groups in HEWL using iodoacetamide before inducing aggregation can help in better understanding of aggregation process.
- Recent reports indicate that soluble protein oligomers behave as a toxic species. Cytotoxic effect of soluble HEWL oligomers can be studied to monitor the pathways leading to cell death. Caspase activity can be employed to monitor apoptotic cell death whereas lactate dehydrogenase assay can be employed to see the integrity of plasma membrane.
- Reactive oxygen and other free radicals are known to induce protein aggregation. Other additives like use of antioxidant or free radical scavenger can be explored to inhibit the growth of soluble aggregates employing the techniques used in this thesis.
- Facile entry of ThT inside the cells and its fluorescence offers a novel dye to label the mammalian cells. As an extension of present work, one can explore the retention of ThT inside the cells and their cytotoxic effect in different cell line over the period of times.
- As a new fluorescent dye ThT can be tried to monitor the growth kinetics of prokaryotic and eukaryotic cells.

REFERENCES

Alston, R. W.; Lasagna, M.; Grimsley, G. R.; Scholtz, J. M.; Reinhart, G. D.; Pace, C. N. Peptide sequence and conformation strong influence tryptophan fluorescence. *Biophys. J.* **2008,** 94, 2280-2287.

Anderson, W. L.; Wetlaufer, D. B. A new method for disulfide analysis of peptides. *Anal. Biochem.* **1975**, 67, 493-502.

Anfinsen, C.B. Principles that govern folding of protein chains. *Science* **1973**, 181, 223–230.

Arrasate, M.; Mitra, S. M.; Schweitzer, E. S.; Segal M. R.; Finkbeiner, S. Inclusion body formation reduces levels of mutant huntingtin and the risk of neuronal death. *Nature* **2004**, 431, 805–810.

Bahar, I.; Atilgan, A. R.; Demirel, M. C.; Erman, B. Vibrational dynamics of folded proteins: Significance of slow and fast motions in relation to function and stability. *Phys. Rev. Lett*. **1998**, 80, 2733-2736.

Bai, Y.; Sosnick, T. R.; Mayne, L.; Englander, S. W. Protein folding intermediates: native-state hydrogen exchange. *Science* **1995**, 269, 192–97.

Ban, T.; Hamada, D.; Hasegawa, K.; Naiki, H.; Goto, Y. Direct observation of amyloid fibril growth monitored by thioflavin T fluorescence. *J. Biol. Chem*. **2003**, 278, 16462–16465.

Banerjee, S. K.; Rupley, J. A. Temperature and pH dependence of the binding of oligosaccharides to lysozyme. *J. Biol. Chem*. 1973, **248**, 2117-2124.

Baynes, B. M.; Wang, D. I. C.; Trout, B. L. Role of arginine in the stabilization of protein against aggregation. *Biochemistry* **2005**, 44, 4919-4925.

Beechem J. M.; Brand L. Time-resolved fluorescence of proteins. *Ann. Rev. Biochem*. **1985**, 54, 43-71.

Belford, G. G.; Belford, R. L.; Weber, G. Dynamics of fluorescence polarization in macromolecules. *Proc. Natl. Acad. Sci. USA*. **1972**, 69, 1392-1393.

Bence, N F.; Sampat, R. M.; Kopito, R. R. Impairment of the ubiquitin-proteosome system by protein aggregation. *Science* **2001**, 292, 1552-1555.

Bennion, B. J.; Daggett, V. The molecular basis for the chemical denaturation of proteins by urea. *Proc. Natl. Acad. Sci. USA.* **2003**, 100, 5142-5147.

Bernier, V.; Lagace M.; Bichet, D. G.; Bouvier, M. Pharmacological chaperones: potential treatment for conformational diseases. *Trend. Endo. Meta.* **2004,** 15, 222-228.

Best, J. D.; Smith, D. W.; Reilly, M. A.; O'Donnell, Ruth.; Lewis, H. D.; Ellis, S.; Wilkie, N.; Rosahl, T. W.; Laroque, P. A.; Boussiquet-Leroux, C.; Churcher, I.; Atack, J. R.; Harrison, T.; Shearman, M. S. The novel gamma secretase inhibitor N-[cis-4-[(4-chlorophenyl)sulfonyl]-4-(2,5-difluorophenyl)cyclohexyl]-1,1,1 trifluoromethanesulfonamide (MRK-560) reduces amyloid plaque deposition without evidence of notch-related pathology in the Tg2576 mouse. *J. Pharmacol. Exp. Ther*. **2007**, 320, 552-558.

Bevington, P. R.; Robinson, D. K. data reduction and error analysis for the physical sciences. Second edition, McGraw-Hill, Inc., 1992.

Bhavesh, N. S.; Juneja, J.; Udgaonkar, J. B.; Hosur, R. V. Native and nonnative conformational preferences in the urea-unfolded state of barstar. *Protein Sci.* **2004**, 13, 3085-3091.

Bisaglia, M.; Trolio, A.; Bellanda, M.; Bergantino, E.; Bubacco, L.; Mammi, S. Structure and topology of the non-amyloid-β component fragment of human α-synuclein bound to micelles: Implications for the aggregation process. *Protein Sci.* **2006**, 15, 1408-1416

Bjurulf, C.; Laynez, J. and Wadso, I. Thermochemistry of lysozyme-inhibitor binding. *Eur. J. Biochem*. **1970**, 14, 47-52.

Blake, C. C.; Koenig, D. F.; Mair, G. A.; North, A. C. T.; Phillips, D. C.; Sarma, V. R. Structure of Hen Egg-White Lysozyme: A Three-dimensional Fourier Synthesis at 2 Å Resolution. *Nature* **1965,** 206, 757-761.

Blanchard, B.J.; Chen, A.; Rozeboom, L. M.; Stafford, K. A.; Weigele, P.; Ingram V. M. Efficient reversal of Alzheimer's disease fibril formation and elimination of neurotoxicity by a small molecule. *Proc. Natl. Acad. Sci. USA*. **2004**, 101, 14326-14332.

Boehm, T.; Zufal F. MHC peptides and the sensory evaluation of genotype. *Trends. Neurosci.* **2006**, 29, 100-107.

Bollag, D. M.; Rozycki, M. D.; Edelstein, S. J. Protein methods.2nd Ed., A John wiley & Sons publication, 1996.

Bucciantini, M.; Giannoni, E.; Chiti, F.; Baroni, F.; Formigli, L.; Zurdo, J.; Taddei, N.; Ramponi, G.; Dobson, C. M.; Stefani, M. Inherent toxicity of aggregates implies a common mechanism for misfolded disease. *Nature* **2002**, 416, 507-511.

Burton, D.R. Antibody the flexible adapter molecule. *Trends. Biochem sci.* **1990**, 15, 64-69.

Callender, R. H.; Dyer R. B.; Gilmanshin R.; Woodruff, W. H. Fast events in protein folding: The Time Evolution of Primary Processes *Annu. Rev. Phys. Chem*. **1998**, 49, 173–202.

Canete, M.; Villanueva, A.; Juarranz, A.; Stockert, J. C. A study of interaction of thioflavine T with DNA: evidence for intercalation. *Cell. Mol. Biol*. **1987**, 33, 191–199.

Carrio, M. M.; Villaverde, A. Construction and destruction of bacterial inclusion bodies. *J. Biotechnol*. **2002**, 96, 3-12.

Caughey, B.; Lansbury, P. T. Protofibrils, pores, fibrils, and neurodegeneration: separating the responsible protein aggregates from the innocent bystanders. *Annu. Rev. Neurosci.* **2003**, 26, 267–298.

Cavanagh, J.; Venters, R. A. Protein dynamic studies move to a new time slot. *Nature* **2001**, 8, 912-914.

Chang, B.S.; Beauvais, R.M.; Arakawa, T.; Narhi, L.O.; Dong, A.; Aparisio, D.I.; Carpenter, J.F. Formation of an active dimer during storage of interleukin-1 receptor antagonist in aqueous solution. *Biophy. J.* **1996**, 71, 3399–3406.

Chapman, M. R.; Robinson, L. S.; Pinkner, J. S.; Roth, R.; Heuser, J.; Hammar, M.; Normark, S.; Hultgren, S. J. Role of Escherichia coli curli operons in directing amyloid fiber formation. *Science*. **2002**, 295, 851 – 855.

Chatterjee, A.; Moulik, S. P.; Majhi, P. R.; Sanyal, S. K. Studies on surfactant-biopolymer interaction. I. Microcalorimetric investigation on the interaction of cetyltrimethylammonium bromide (CTAB) and sodium dodecylsulfate (SDS) with gelatin (Gn), lysozyme (Lz) and deoxyribinuclic acid (DNA). *Biophys. Chem*. **2002**, 98, 313-327.

Chen, M.; Margittai, M.; Chen, J.; Langen, R. Investigation of alpha-synuclein fibril structure by site-directed spin labeling. *J. Biol. Chem.* **2007,** 282, 24970-24979.

Chen, R.F. Dansyl labeled proteins: determination of extinction coefficient and number of bound residues with radioactive dansyl chloride. *Anal. Biochem*. **1968**, 25, 412–416.

Chen, Y.; Erickson, H. P. Rapid in vitro assembly dynamics and subunit turnover of FtsZ demonstrated by Fluorescence Resonance Energy Transfer. *J. Biol. Chem*. **2005**, 280, 22549-22554.

Chiti F.; Dobson, C. M. Protein misfolding, functional amyloid, and human disease. *Annu. Rev. Biochem*. **2006**, 75, 333–66.

Chiti, F.; Calamai, M.; Taddei, N.; Stefani, M.; Ramponi, G. &. Dobson, C. M. Studies of the aggregation of mutant proteins in vitro provide insights into the genetics of amyloid diseases. *Proc. Natl. Acad. Sci. USA*. **2002**, 99, 16419-16426.

Chothia, C.; Janin, J. Principles of protein-protein recognition. *Nature* **1975**, 256, 705-708.

Conway, K. A.; Lee, S. J.; Rochet, J. C., Ding, T. T.; Williamson, R. E.; Lansbury, P. T. Acceleration of oligomerization, not fibrillization, is a shared property of both α-synuclein mutations linked to early-onset Parkinson's disease: Implications for pathogenesis and therapy. *Proc. Natl. Acad. Sci. USA*. **2000**, 97, 571-576.

Cooper, A. A.; Gitler, A. D.; Cashikar, A.; Haynes, C. M.; Hill, K. J.; Bhullar, B.; Liu, K.; Xu, K.; Strathearn, K. E.; Liu, F.; Cao, S.; Caldwell, K. A.; Caldwell, G. A.; Marsischky, G.; Kolodner, R. D.; LaBaer, J.; Rochet, J. C.; Bonini, N. M.; Lindquist, S. alpha-Synuclein blocks ER-Golgi traffic and Rab1 rescues neuron loss in Parkinson's models. *Science* **2006**, 313, 324-328.

Creighton, T. E. Proteins structures and Molecular Properties, 2nd editon. W. H. Freeman and Company, New York, 1997.

Crowhurst, K. A.; Tollinger, M.; Forman-Kay, J. D. Cooperative interactions and a non-native buried Trp in the unfolded state of an SH3 domain. *J. Mol. Biol*. **2002**, 322, 163-178.

Dahlquist, F. W.; Jao, L.; Raftery, M. On the binding of chitin oligosaccharides to lysozyme. *Proc. Natl. Acad. Sci. USA*. **1966,** 56, 26-30.

Daniel, R.M.; Dunn, R.V.; Finney, J.L.; Smith, J.C. The role of dynamics in enzyme activity. *Annu. Rev. Biophys. Biomol. Struct*. **2003**, 32, 69–92.

Darghal, N.; Garnier-Suillerot, A.; Salerno, M. Mechanism of thioflavin T accumulation inside cells overexpressing p-glycoprotein or multidrug resistance-associated protein: role of lipophilicity and positive charge. *Biochem. Biophys. Res. Commun*. **2006**, 343, 623–629.

Davies, R. C.; Neuberger, A.; Wilson, B. M. The dependence of lysozyme activity on pH and ionic strength. *Biochim. Biophys. Acta* **1969**, 178, 294-305.

de Felice, F. G.; Vieira, M. N. N.; Meirelles, M. N. L.; Morozova-Roche, L.; Dobson, C. M.; Ferreira, S. T. Formation of amyloid aggregates from human lysozyme and its disease-associated variants using hydrostatic pressure. *FASEB J.* **2004,** 18, 1099-1101.

Di Prisco, G.; Condo. S. G.; Tamburrini, M.; Giardina, B. Oxygen transport in extreme environments. *Trends. Biochem Sci*. **1991**, 16, 471-474.

Dill K. A.; Shortle, D. Denatured states of proteins. *Annu. Rev. Biochem*. **1991**, 60, 795-825.

Dzwolak, W.; Pecul, M. Chiral bias of amyloid fibrils revealed by the twisted conformation of Thioflavin T: an induced circular dichroism/DFT study. *FEBS Lett*. **2005,** 579, 6601–6603.

Eanes, E.D.; Glenner, G.G. X-ray diffraction studies on amyloid filaments. *J. Histochem. Cytochem*. **1968**, 16, 673–677.

Eftink, M. R.; L. A. Selvidge. Fluorescence quenching of liver alcohol dehydrogenase by acrylamide. *Biochemistry* **1982,** 21, 117-125.

Eftink, M.R. Fluorescence quenching: Theory an applications, in: Topics in Fluorescence Spectroscopy, **1991**, 2, Lakowicz J.R. "Ed", NY, Plenum press, pp. 53-126.

Eichmuller, C.; Skrynnikov, N. R. Observation of μs time-scale protein dynamics in the presence of Ln^{3+} ions: application to the N-terminal domain of cardiac troponin C. *J. Biomol. NMR* **2007**, 37, 79–95.

Eisenmesser, E. Z.; Akke, M.; Bosco, D. A.; Kern, D. Enzyme dynamics during catalysis. *Science* **2002**, 295, 1520–1523.

Eisenmesser, E. Z.; Millet, O.; Labeikovsky, W.; Korzhnev, D. M.; Wolf-Watz, M.; Bosco, D. A.; Skalicky, J. J.; Kay, L. E.; Kern, D. Intrinsic dynamics of an enzyme underlies catalysis. *Nature* **2005**, 438, 117-121.

Eylesa, S. J.; Kaltashovb I. A. Methods to study protein dynamics and folding by mass spectrometry. *Methods* **2004**, 34, 88–99.

Feinstein, E.; Deikus, G.; Rusinova, E.; Rachofsky, E. L.; Ross, J. B. A.; Laws, W. R. Constrained analysis of fluorescence anisotropy decay: application to experimental protein dynamics. *Biophys. J.* **2003,** 84, 599-611.

Frare, E.; de Laureto, P. P.; Zurdo, J.; Dobson, C. M.; Fontana, A. A highly amyloidogenic region of hen lysozyme. *J. Mol. Biol.* **2004**, 340, 1153-1165.

Frederikse, P.H. Amyloid-like protein structure in mammalian ocular lenses, *Curr. Eye Res*. **2000**, 20 462– 468.

Friedhoff, P.; Schneider, A.; Mandelkow, E. M.; Mandelkow, E. Rapid assembly of Alzheimer-like paired helical filaments from microtubule-associated protein tau monitored by fluorescence in solution. *Biochemistry* **1998**, 37, 10223–10230.

Garcia, P.; Desmadril, M.; Minard, P.; Yon, J. M. Evidence for residual structures in an unfolded form of yeast phosphoglycerate kinase. *Biochemistry* **1995**, 34, 397-404.

Garcia, P.; Merola, F.; Receveur, V.; Blandin, P.; Minard, P.; Desmadril, M., Steady state and time resolved fluorescence study of residual structures in an unfolded form of yeast phosphoglycerate kinase. *Biochemistry* **1998**, 37, 7444-7455.

Gensch, T.; Hendriks, J.; Hellingwerf ,K. J. Tryptophan fluorescence monitors structural changes accompanying signalling state formation in the photocycle of photoactive yellow protein. *Photochem. Photobiol. Sci*. **2004**, 3, 531 – 536.

Giri, K.; Bhattacharyya, N. P.; Basak, S. pH dependent self-assembly of polyalanine peptides. *Biophys. J.* **2007**, 92, 293-302.

Glabe, C. G. Common mechanism of amyloid oligomer pathogenesis in degenerative disease. *Neurobiol. Aging* **2006**, 27, 570-575.

Glover, J. R.; Kowal, A. S.; Schirmer, E. C.; Patino, M. M.; Liu, J. J.; Lindquist, S. Self-seeded fibers formed by Sup35, the protein determinant of [PSI^+], a heritable prion-like factor of S.cerevisiae. *Cell* **1997**, 89, 811–819.

Goldsby, R. A.; Kindt, T. J.; Osborne, B. A.; Kuby, J. Immunology, 5th edition, W. H. Freeman and Company, New York, **2005**.

Goodman, M. F. Error-prone repair DNA polymerase in prokaryotes and eukaryotes. *Annu. Rev. Biochem*. **2002**, 71, 17–50.

Greenfield, N. J. Application of circular dichroism in protein and peptide analysis. *Trends Anal. Chem*. **1999**, 18, 236-244.

Hameed, M.; Ahmad, B.; Fazili, K. M.; Andrabi, K. and Khan, R. H. Different molten globule-like folding intermediates of hen egg white lysozyme induced by high pH and tertiary butanol. *J. Biochem*. (Tokyo) **2007,** 141, 573-583.

Hammarstrom, P.; Jiang, X.; Hurshman, A. R.; Powers, E. T.; Kelly, J. W. Sequence-dependent denaturation energetics: A major determinant in amyloid disease diversity. *Proc. Natl. Acad. Sci. USA.* **2002**, 99, 16427-16432.

Hammarstrom, P.; Wiseman, R. L.; Powers, E. T.; Kelly, J. W. Prevention of transthyretin amyloid disease by changing protein misfolding energetics. *Science* **2003**, 299, 713-716.

Hartley, D. M.; Walsh, D. M .; Ye, C. P.; Diehl, T.; Vasquez, S.; Vassilev, P. M.; Teplow, D B.; Selkoe, D. J. Protofibrillar intermediates of amyloid β-protein induce acute electrophysiological changes and progressive neurotoxicity in cortical neurons. *J. Neurosci*. **1999**, 19, 8876–8884.

Haugland, R. P. Handbook of Fluorescence Probes and Research products, 9th Edition, 2002, pp 91.

Hill, J. J.; Royer, C. A. Fluorescence approaches to study of protein-nucleic acid complexation. *Methods Enzymol*. **1997**, 278, 390–416.

Hirata, H.; Ohki, K.; Miyata, H. Mobility of integrin α5β1 measured on the isolated ventral membranes of human skin fibroblasts. *Biochimica. Biophysica. Acta* **2005**, 1723 100–105.

Hobb, J. R.; Morgan, A. D. Fluorescence microscopy with thioflavin-T in the diagnosis of amyloid. *J. Pathol. Bacteriol*. **1963**, 86, 437-442.

Hodsdon, M. E.; Frieden, C. Intestinal fatty acid binding protein: The folding mechanism as determined by NMR studies. *Biochemistry* **2001**, 40, 732–742.

Homchaudhuri, L.; Kumar, S.; Swaminathan, R. Slow aggregation of lysozyme in alkaline pH monitored in real time employing the fluorescence anisotropy of covalently labeled dansyl probe. *FEBS Lett*. **2006**, 580, 2097-2101.

Hong, D. P.; Gozu, M.; Hasegawa, K.; Naiki. H.; Goto, Y. Conformation of β_2-microglobulin amyloid fibrils analyzed by reduction of the disulfide bond. *J. Biol. Chem.* **2002**, 277, 21554–21560.

Huehns; E. R. Diseases due to abnormalities of hemoglobin structure. *Annu. Rev. Med.* **1970**, 21, 157-178.

Iconomidou, V.A.; Vriend, G.; Hamodrakas, S. J. Amyloids protect the silkmoth oocyte embryo. *FEBS Lett*. **2000**, 479, 141–145.

Ilanchelian, M.; Ramaraj, R. Emission of thioflavin T and its control in the presence of DNA. *J. Photochem. Photobiol. A* **2004**, 162,129–137.

Imoto, T.; Andrews, L. J.; Banerjee, S. K.; Shrake, A.; Forster, L. S.; Rupley, J. A. Optical properties of lysozyme. pH and saccharide binding difference spectra. *J. Biol. Chem.* **1975**, 250, 8275-8282.

Iwata, A.; Riley, B. E.; Johnston, J. A.; Kopito, R. R. HDAC6 and microtubules are required for autophagic degradation of aggregated huntingtin. *J. Biol. Chem*. **2005**, 280, 40282-40292.

Jaeger, K. E.; Eggert, T. Enantioselective biocatalysis optimized by directed evolution. *Curr. Opin. Biotechnol*. **2004,** 15, 305–313.

Jahn, T. R.; Radford, S. E. Folding versus aggregation: Polypeptide conformations on competing pathways. *Arch. Biochem. Biophys*. **2008**, 469, 100-117.

Jana, N. R.; Tanaka, M.; Wang, G.; Nukina, N. Polyglutamine length-dependent interaction of Hsp40 and Hsp70 family chaperones with truncated N-terminal huntingtin: their role in suppression of aggregation and cellular toxicity. *Hum. Mol. Genet*. **2000**, 9, 2009–2018.

Jarrett, J.T.; Lansbury, P.T. Jr. Seeding "one-dimensional crystallization" of amyloid: a pathogenic mechanism in Alzheimer's disease and scrapie? *Cell* **1993**, 73, 1055–1058.

Jean-Luc, Imler.; Hoffmann, J. A. Toll receptors in innate immunity. *Trends Cell Biol*. **2001**, 11, 304-311.

Jimenez, J. L., et al. Cryo-electron microscopy structure of an SH3 amyloid fibril and model of the molecular packing. *EMBO J*. **1999,** 18, 815–821.

Johnson, S. M.; Wiseman, R. L.; Sekijima, Y.; Green, N. S.; Adamski-Werner, S. L.; Kelly, J. W. Native state kinetic stabilization as a strategy to ameliorate protein misfolding diseases: a focus on the transthyretin amyloidoses. *Acc. Chem. Res*. **2005**, 38, 911-921.

Kalyanasundaram, K.; Thomas, J. K. Environmental effects on vibronic band intensities in pyrene monomer fluorescence and their application in study of micellar systems. *J. Am. Chem. Soc*. **1977**, 99, 2039–2044.

Kamatari, Y. O.; Kitahara. R.; Yamada. H.; Yokoyama, S.; Kazuyuki A. High-pressure NMR spectroscopy for characterizing folding intermediates and denatured states of proteins. *Methods* **2004**, 34, 133–143.

Kapp, L. D.; Lorsch, J.R. The molecular mechanics of eukaryotic translation. *Annu. Rev. Biochem.* **2004**, 73, 657–704.

Katzman, R.; Terry, R.; DeTeresa, R.; Brown, T.; Davies, P.; Fuld, P.; Renbing, X., Peck, A. Clinical, pathological, and neurochemical changes in dementia: a subgroup with preserved mental status and numerous neocortical plaques. *Ann. Neurol*. **1988**, 23, 138–144.

Kayed, R.; Head, E.; Thompson, J. L.; Mclntire, T. M.; Milton, S. C.; Cotman, C. W.; Glabe, C. G. Common structure of soluble amyloid oligomers implies common mechanism of pathogenesis. *Science* **2003**, 300, 486–489.

Kazmirski, S.L.; Wong, K.B.; Freund, S.M.V.; Tan, Y.J.; Fersht, A.R.; Daggett, V. Protein folding from a highly disordered denatured state: The folding pathway of chymotrypsin inhibitor 2 at atomic resolution. *Proc. Natl. Acad. Sci. USA*. **2001**, 98, 4349–4354.

Kelenyi, G. On the histochemistry of azo group-free thiazole dyes. *J. Histochem. Cytochem.* **1967**, 15, 172–180.

Khurana, R.; Coleman, C.; Ionescu-Zanetti, C.; Carter, S. A.; Krishna, V.; Grover, R. K.; Roy, R.; Singh, S. Mechanism of thioflavin T binding to amyloid fibrils. *J. Struct. Biol*. **2005**, 151, 229–238.

Khurana, R.; Uversky, V. N.; Nielsen, L.; Fink, A. L. Is Congo red an amyloid specific dye? *J. Biol. Chem*. **2001**, 276, 22715–21.

Kirschner, D. A.; Abraham, C.; Selkoe, D. J. X-ray diffraction from intraneuronal paired helical filaments and extaneuronal amyloid fibril in Alzheimer's disease indicates cross β conformation. *Proc. Natl. Acad. Sci. USA*. **1986**, 83, 503-507.

Kirschner, D. A.; Inouye, H.; Duffy, L. K.; Sinclair, A.; Lind, M.; Selkoe, D. J. Synthetic peptide homologous to β-protein from Alzheimer's disease from amyloid like fibrils in vitro. *Proc. Natl. Acad. Sci. USA*. **1987**, 84, 6953-6957.

Kleinschmidt, J. H. and Tamm, L. K. Folding Intermediates of a β-barrel membrane protein. Kinetic evidence for a multi-step membrane insertion mechanism. *Biochemistry* **1996**, 35, 12993-13000.

Klein-Seetharaman, J.; Oikawa, M.; Grimshaw, S.B.; Wirmer, J.; Duchardt, E.; Ueda, T.; Imoto, T.; Smith, L.J.; Dobson, C.M.; Schwalbe, H. Long-range interactions within a nonnative protein. *Science* **2002**, 295, 1719–1722.

Klucken, J.; Shin, Y.; Masliah, E.; Hyman, B. T.; McLean, P. J. Hsp70 reduces α-synuclein aggregation and toxicity. *J. Biol. Chem.* **2004**, 279, 25497–25502.

Klunk, W. E.; Wang, Y.; Huang, G. F.; Debnath, M. L.; Holt, D. P.; Mathis, C. A. Uncharged thioflavin-T derivatives bind to amyloid-beta protein with high affinity and readily enter the brain. *Life Sci*. **2001**, 69, 1471–1484.

Knowles, T. P.; Fitzpatric, A. W.; Meehan, S.; Mott, H. R.; Vendruscolo, M.; Dobson, C. M.; Welland, M. E. Role of intermolecular forces in defining material properties of protein nanofibrils. *Science* **2007**, 318, 1900–1903.

Kobayashi, Y.; Sobue, G. Protective effect of chaperones on polyglutamine diseases. *Brain Res. Bull*. **2001**, 56, 165–168.

Kohn, J.E.; Millett, I.S.; Jacob, J.; Zagrovic, B.; Dillon, T.M.; Cingel, N.; Dothager, R.S.; Seifert, S.; Thiyagarajan, P.; Sosnick, T.R.; Hasan M. Z.; Pande V. S.; Ruczinski I.; Doniach S.; Plaxco K. W. Random-coil behavior and the dimensions of chemically unfolded proteins. *Proc. Natl. Acad. Sci. USA*. **2004**, 101, 12491–12496.

Koshland D. E. Application of a theory of enzyme specificity to protein synthesis. *Proc. Natl. Acad. Sci. USA*. **1958**, 44, 98–104.

Krebs, M. R. H., Wilkins, D. K., Chung, E. W., Pitkeathly, M. C., Chamberlain, A. K., Zurdo, J., Robinson, C. V.; Dobson, C. M. Formation and seeding of amyloid fibril from wild type hen lysozyme and a peptide fragment from the β-domain. *J. Mol. Biol.* **2000**, 300, 541-549.

Krishnamoorthy, G.; Dogra, S. K. Effect of micelles on the prototropic equilibrium of 2-(4'-N,N-dimethylaminophenyl) pyrido [3,4-d] imidazole. *Phys Chem Chem Phys*. **2000,** 2, 2521–2528.

Kumagai, I.; Sunada, F.; Takeda, S.; Miura, Kin-ichiro. Redesign of the substrate-binding site of hen egg white lysozyme based on the molecular evolution of C-type lysozymes. *J. Biol. Chem*. **1992**, 267, 4608-4612.

Kumar, A.; Srivastava, S.; Mishra, R. K.; Mittal, R.; Hosur, R. V. Local structural preferences and dynamics restrictions in the urea-uenatured state of SUMO-1: NMR characterization. *Biophys. J.* **2006**, 90, 2498–2509.

Kungl, A. J.; Visser, N. V.; van Hoek, A.; Visser, A. J. W. G.; Billich, A.; Schilk, A.; Gstach, H.; Auer M. Time-Resolved Fluorescence Anisotropy of HIV-1 protease inhibitor complexes correlates with inhibitory activity. *Biochemistry* **1998**, 37, 2778-2786.

Laemmli, U. K. Cleavage of structural proteins during the assembly of the head of bacteriophage T4. *Nature* **1970**, 227, 680-685.

Lakowicz, J. R. Principles of Fluorescence Spectroscopy, 2nd Ed., 1999, Kluwer Academic/Plenum Publisher, New York.

Lakowicz, J. R. Principles of Fluorescence Spectroscopy, 3rd Ed., 2006, Springer, New York.

Lakshmikanth, G. S.; Krishnamoorthy, G. Solvent-exposed tryptophans probe the dynamics at protein surface. *Biophys. J*. **1999,** 77, 1100-1106.

Laurent, M. Prion diseases and the 'protein only' hypothesis: a theoretical dynamic study. *Biochem. J*. **1996**, 318, 35–39.

Le Corre, S.; Klafki, H. W.; Plesnila, N.; Hubinger, G.; Obermeier, A.; Sahagun H.; Monse, B.; Seneci, P.; Lewis, J.; Eriksen, J.; Zehr, C.; Yue, M.; McGowan, E.; Dickson, D. W.; Hutton, M.; Roder, H. M. An inhibitor of tau hyperphosphorylation prevents severe motor impairments in tau transgenic mice. *Proc. Natl. Acad. Sci. USA.* **2006**, 103, 9673-9678.

Levi, V.; Flecha, F. L. G. Labeling of proteins with fluorescent probes. Photophysical characterization of dansylated bovine serum albumin. *Biochem. Mol. Biol. Educ*. **2003**, 31, 333–336.

LeVine III, H. Thioflavine T interaction with amyloid β-sheet structures. *Amyloid Int. J. Exp. Clin. Invest*. **1995**, 2, 1–6.

LeVine III, H. Thioflavine T interaction with synthetic Alzheimer's disease β-amyloid peptides: detection of amyloid aggregation in solution. *Protein Sci*. **1993**, 2, 404–410.

Li, E.; Hristova, K. Role of receptor tyrosine kinase transmembrane domains in cell signaling and human pathologies. *Biochemistry* **2006,** 45, 6241-51.

Loo, T. W.; Clarke D. M. Chemical and pharmacological chaperones as new therapeutic agents. *Exp. Rev. Mol. Med*. **2007**, 9, 1-18.

Louhivuori, M.; Paakkonen, K.; Fredriksson, K.; Permi, P.; Lounila, J.; Annila, A. On the origin of residual dipolar couplings from denatured proteins. *J. Am. Chem. Soc.* **2003,** 125, 15647–15650.

Lundstrom, K. Structural genomics for membrane proteins. *Cell. Mol. Life. Sci.* **2006**, 63, 2597-2607.

Maeda, R.; Ado, K.; Takeda N.; Taniguchi, Y. Promotion of insulin aggregation by protein disulfide isomerase. *Biochimica et Biophysica Acta* **2007**, 1774, 1619–1627

Maezawa, I.; Hong, H. S.; Liu, R.; Wu, C.Y.; Cheng, R. H.; Kung, M. P.; Kung, H. F.; Lam, K. S.; Oddo, S.; LaFerla, F. M.; Jin, L.W. Congo red and thioflavin-T analogs detect Aβ oligomers. *J. Neurochem.* **2007**, 104, 457-468.

Maiti, N. C.; Mazumdar, S.; Periasamy, N. Controlled J aggregation of porphyrins by cationic surfactants. *Curr. Sci*. **1996**, 70, 997–999.

Maity, H.; Jarori, G. K. Fluorescence quenching of dimeric and monomeric forms of yeast hexokinase (PII): effect of substrate binding. *Physiol. Chem. Phys. Med. NMR* **2002**, 34, 43-60.

Makin, O. S.; Atkins, E.; Sikorski, P.; Johansson, J.; Serpell, L. C. Molecular basis for amyloid fibril formation and stability. *Proc. Natl. Acad. Sci USA.* **2005**, 102, 315–320.

Maskevich, A. A.; Stsiapura, V. I.; Kuzmitsky, V. A.; Kuznetsova, I. M.; Povarova, O. I.; Uversky, V. N.; Turoverov, K. K. Spectral properties of thioflavin T in solvents with different dielectric properties and in a fibril-incorporated form. *J. Proteome. Res*. **2007**, 6, 1392–1401.

Masuda, M.; Suzuki, N.; Taniguchi, S.; Oikawa, T.; Nonaka, T.; Iwatsubo, T.; Hisanaga, S.; Goedert, M.; Hasegawaet, M. Small molecule inhibitors of alpha-synuclein filament assembly. *Biochemistry* **2006**, 45, 6085-6094.

Matsuura, H.; Shimotakahara, S.; Sakuma, C.; Tashiro, M.; Shindo, H.; Mochizuki, K.; Yamagishi, A.; Kojima, M.; Takahashi, K. Thermal unfolding of ribonuclease T1 studied by multidimensional NMR spectroscopy. *Biol. Chem*. **2004**, 385, 1157-1164.

May, B. C. H., C. Govaerts.; F. E. Cohen. Developing therapeutics for diseases of protein misfolding. *Neurology* **2006,** 66(suppl 1):S118-S122.

McAllister, C.; Karymov, M. A.; Kawano, Y.; Lushnikov, A. Y.; Mikheikin, A.; Uversky, V.; Lyubchenko, Y. L. Protein interactions and misfolding analyzed by AFM force spectroscopy. *J. Mol. Biol*. **2005**, 354, 1028-1042.

McCarney, E. R.; Kohn, J. E.; Plaxco, K.W. Is there or isn't there? The case for (and against) residual structure in chemically denatured proteins. *Crit. Rev. Biochem. Mol Biol*. **2005**, 40, 181 – 189.

McDermott, A. E. Structural and dynamic studies of proteins by solid-state NMR spectroscopy: rapid movement forward. *Curr. Opin. Struct. Biol*. **2004**, 14, 554–561.

MHC Sequencing Consortium. Complete sequence and gene map of a human major histocompatibility complex. *Nature* **1999**, 401, 921–923.

Miranker, A. D.; Dobson C. M. Collapse and cooperativity in protein folding. *Curr. Opin. Struct. Biol*. **1996**, 6, 31-42.

Miroy, G. J.; Lai, Z.; Lashuel, H. A.; Peterson, S. A.; Strang, C.; Kelly, J. W. Inhibiting transthyretin amyloid fibril formation via protein stabilization. *Proc. Natl. Acad. Sci. USA*. **1996**, 93, 15051–15056.

Mirsky, A. E.; Pauling, L. On the structure of native, denatured and coagulated proteins. *Proc. Natl. Acad. Sci. USA*. **1936**, 22, 439-447.

Mishima, T.; Ohkuri, T.; Monji, A.; Imoto, T.; Ueda, T. Amyloid formation in denatured single-mutant lysozymes where residual structures are modulated. *Protein Sci.* **2006**, 15, 2448–2452.

Mishima, T.; Ohkuri, T.; Monji, Akira.; Imoto T.; Ueda, T. A particular hydrophobic cluster in the residual structure of reduced lysozyme drastically affects the amyloid fibrils formation. *Biochem. Biophys. Res. Commun*. **2007**, 356, 769–772.

Mishra, R.; Sorgjerd, K.; Nystrom, S.; Nordigarden, A.; Yu, Y. C.; Hammarstrom, P. Lysozyme amyloidogenesis is accelerated by specific nicking and fragmentation but decelerated by intact protein binding and conversion. *J. Mol. Biol.* **2007**, 366, 1029-1044.

Mittag, T.; Forman-Kay, J. D. Atomic-level characterization of disordered protein ensembles. *Curr. Opin. Struct. Biol*. **2007**, 17, 3–14.

Modler, A.J.; Gast, K.; Lutsch, G.; Damaschun, G. Assembly of amyloid protofibrils via oritical Oligomers-a novel pathway of amyloid formation *J. Mol. Biol*. **2003**, 325 135–148.

Mohana-Borges, R.; Goto, N. K.; Kroon, G. J. A.; Dyson, H. J.; Wright P. E. Structural characterization of unfolded states apomyoglobin using residual dipolar couplings. *J. Mol. Biol.* **2004**, 340, 1131–1142.

Monsonego, A.; Weiner, H. L. Immunotherapeutic approaches to Alzheimer's disease. *Science* **2003**, 302, 834-838.

Movahedi, A. A. M.; Pirzadeh, P.; Hashemnia S.; Ahmadian, S.; Hemmateenejad, B.; Amani, M.; Saboury, A. A.; Ahmad, F.; Shamsipur, M.; Hakimelahi, G. H.; Tsai, F. Y.; Alijanvand, H. H.; Yousefi, R. Fibril formation of lysozyme upon interaction with sodium dodecyl sulfate at pH 9.2. *Colloid Surface B* **2007**, 60, 55-61.

Muchowski, P. J.; Wacker, J. L. Modulation of neurodegeration by molecular chaperones. *Nature Review Neurosci*. **2005**, 6, 11-22.

Neri, D.; Billeter, M.;Wider, G.; Wuthrich K. NMR determination of residual structure in a urea-denatured protein, the 434-Repressor. *Science* **1992**, 257, 1559–1563.

Nilsson M. R. Techniques to study amyloid fibril in vitro. *Methods* **2004**, 34, 151–60.

Noble, W.; Planel E.; Zehr C.; Olm V.; Meyerson J.; Suleman F.; Gaynor, K.; Wang, L.; LaFrancois, J.; Feinstein B.; Burns, M.; Krishnamurthy, P.; Wen, Y.; Bhat, R.; Lewis, J.; Dickson, D.; Duff, K. Inhibition of glycogen synthase kinase-3 by lithium correlates with reduced tauopathy and degeneration in vivo. *Proc. Natl. Acad. Sci. USA.* **2005**, 102, 6990-6995.

Ohnishi, S.; Lee, A.L.; Edgell, M. H.; Shortle, D. Direct demonstration of structural similarity between native and denatured Eglin C. *Biochemistry* **2004**, 43, 4064–4070.

Ono, K.; Yamada, M. Antioxidant compounds have potent anti-fibrillogenic and fibril-destabilizing effects for alpha-synuclein fibrils in vitro. *J. Neurochem.* **2006**, 97, 105-115.

Onuchic J.; Wolynes P. G. Theory of protein folding. *Curr. Opin. Struct.Biol.* **2004**, 14, 70–75.

Otzen, D. E.; Kristensen, O.; Oliveberg, M. Designed protein tetramer zipped together with a hydrophobic Alzheimer homology: A structural clue to amyloid assembly. *Proc. Natl. Acad. Sci. USA*. **2000**, 97, 9907–9912.

Papp, E.; Csermely, P. Chemical chaperones: mechanisms of action and potential use. *Handb Exp Pharmacol.* **2006**, 172, 405-416.

Parihar, M. S.; Hemnani, T. Alzheimer's disease pathogenesis and therapeutic intervention. *J. Clini. Neurosci*. **2004**, 11, 456-467.

Parker, W.; Song, P. S. Protein structures in SDS micelle-protein complexes. *Biophys. J.* **1992**, 61, 1435-1439.

Pearce, M. C.; Cabrita, L. D; Rubin, H; Gore, M. G.; Bottomley, S. P. Identification of residual structure within denatured antichymotrypsin: implications for serpin folding and misfolding. *Biochem. Biophys. Res. Commun.* **2004,** 324, 729-735.

Pepys, M. B.; Hawkins, P. N.; Booth, D. R.; Vigushin, D. M.; Tennent, G. A.; Soutar, A. K.; Totty, N.; Nguyen, O.; Blake, C. C. F.; Terry, C. J.; Feest, T. G.; Zalin, A. M.; Hsuan, J. J. Human lysozyme gene mutations cause hereditary systemic amyloidosis. *Nature* **1993**, 362, 553-557.

Perutz, M. F. Glutamine repeats and neurodegenerative diseases: molecular aspects. *Trends Biochem. Sci*. **1999**, 24, 58-63.

Pitcher, J. A.; Freedman, N. J.; Lefkowitz, R. J. G Protein–coupled receptor kinases. *Annu. Rev. Biochem*. **1998**, 67, 653–692.

Raj, C. R.; Ramaraj, R. Influence of cyclodextrin complexation on the emission of thioflavin T and its off-on control. *J. Photochem. Photobiol. A* **1999**, 122, 39–46.

Rangachari, V.; Reed, D. K.; Moore, B. D; Rosenberry, T. L. Secondary structure and interfacial aggregation of amyloid-β 1(–40) on sodium dodecylsulfate micelles. *Biochemistry* **2006**, 45, 8639–8648.

Robertson, A. D.; Baldwin, R. L. Hydrogen exchange in thermally denatured ribonuclease-A. *Biochemistry* **1991**, 30, 9907-9914.

Robillard G.T.; Swaving-Dukstra D.; Broos J. Tryptophan fluorescence spectroscopy, fluorescent impurities [amp] membrane-bound proteins. *Prog. Biophys. Mol. Biol*, **1996**, 65, 135-135.

Rochet, J. C. Novel therapeutic strategies for the treatment of protein-misfolding diseases. *Exp. Rev. Mol. Med*. **2007**, 9, 1-34.

Roder, H.; Shastry, M. C. R. Methods for exploring early events in protein folding. *Curr. Opin. Struct. Biol*. **1999**, 9, 620–626.

Ross, C. A.; Poirier, M. A. Protein aggregation and neurodegenerative disease. *Nature Med*. **2004**, 10, S10-S17.

Royant,A.; Nollert, P.; Edman, K.; Neutze, R.; Landau, E. M.; Pebay-Peyroula, E.; Navarro, J. X-ray structure of sensory rhodopsin II at 2.1-Å resolution. *Proc. Natl. Acad. Sci. USA*. **2001**, 98, 10131–10136.

Rupley, J. A.; Butler, L.; Gerring, M.; Hartdegen, F. J.; Pecoraro, R. Studies on the enzymic activity of lysozyme, III. The binding of saccharides. *Proc. Natl. Acad. Sci. USA*. **1967**, 57, 496-510.

Rusinova, E.; Tretyachenko-Ladokhina, V.; E. Vele, O.; Senear, D. F.; Alexander, J. B. R. Alexa and Oregon green dyes as fluorescence anisotropy probes for measuring protein–protein and protein–nucleic acid interactions. *Anal. Biochem*. **2002,** 308, 18–25.

Saab-Rincon, G.; Gualfetti, P. J.; Matthews, C. R. Mutagenic and thermodynamic analyses of residual structure in the subunit of tryptophan synthase. *Biochemistry* **1996**, 35, 1988–1994.

Sabate, R.; Saupe, S. J. Thioflavin T fluorescence anisotropy: An alternative technique for the study of amyloid aggregation. *Biochem. Biophys. Res. Commun*. **2007**, 360135–138.

Saeed S. M.; Fine, G. Thioflavin-T for amyloid detection. *J. Clin. Pathol.* **1967**, 47, 588–593.

Sage, B. H. Jr.; O'Connell, J. P.; Mercolino, T. J. A rapid, vital staining procedure for flow cytometric analysis of human reticulocytes. *Cytometry* **1983**, 4, 222–227.

Saibil, H. R.; Orlova, E. V. Challenges at the frontier of structural biology. *Nat. Stru. Biol*. **2002**, 9, 414-415.

Saito, Y.; Yokota, T.; Mitani, T.; Ito, K.; Anzai, M.; Miyagishi, M.; Taira, K.; Mizusawa, H. Transgenic small interfering RNA halts amyotrophic lateral sclerosis in a mouse model. *J. Biol. Chem.* **2005**, 280, 42826-42830.

Sasahara K.; Nitta K. Effect of ethanol on folding of hen egg-white lysozyme under acidic condition. *Proteins Stru. Funct Bioinfo*. **2006**, 63, 127-35.

Saxena, A. M.; Udagaonkar, J. B.; Krishnamoorthy, G. Characterization of Intra-molecular distances and site-specific dynamics in chemically unfolded barstar: evidence for denaturant-dependent non-random structure. *J. Mol. Biol.* **2006**, 359, 174-189.

Scapin, G. Structural biology and drug discovery. *Curr. Pharm. Des*. **2006**, 12, 2087-2097.

Schagger, H. Tricine-SDS-PAGE. *Nat. Protocols*. **2006,** 1, 16-22.

Schwarzinger, S.; Wright, P.E.; Dyson, H.J. Molecular hinges in protein folding: the urea-denatured state of apomyoglobin. *Biochemistry* **2002**, 41, 12681–12686.

Sciarretta, K. L.; Boire, A.; Gordon, D. J.; Meredith, S. C. Spatial separation of β-sheet domains of β-amyloid: disruption of each β-sheet by N-methyl amino acids. *Biochemistry* **2006**, 45, 9485-9495.

Shevelev, I. V.; Hubscher, U. The 3' 5' exonucleases. *Nat. Rev. Mol. Cell. Biol*. **2002**, 3, 364–376.

Shortle, D. Denatured states of proteins and their role in folding and stability. *Curr. Opi. Struct. Biol*. **1993**, 3, 66-74.

Shortle, D.; Ackerman, M. S. Persistence of native-like topology in a denatured protein in 8 M Urea. *Science* **2001**, 293, 487–489.

Shweitzer, B.; Zanette, D.; Itri, R. Bovine serum albumin (BSA) plays a role in the size of SDS micelle-like aggregates at the saturation binding: the ionic strength effect. *J. Colloid. Inter. Sci*. **2004**, 277, 285-91.

Silveira, J. R.; Raymond, G. J.; Hughson, A. G.; Race, R. E.; Sim, V. L.; Hayes, S. F.; Caughey, B. The most infectious prion protein particles. *Nature* **2005**, 437, 257-261.

Silverton, E. W.; Navia, M. A.; Davies D. R. Three-Dimensional Structure of an Intact Human Immunoglobulin. *Proc. Natl. Acad. Sci. USA*. **1977**, 74, 5140-5144.

Sirangelo, I.; Malmo, C.; Iannuzzi, C.; Mezzogiorno, A.; Bianco, M. R.; Papa, M.; Irace, G. Fibrillogenesis and Cytotoxic Activity of the Amyloid-forming Apomyoglobin Mutant W7FW14F. *J. Biol. Chem*. **2004**, 279, 13183–13189.

Small, E. W.; Isenberg, I. Hydrodynamics properties of a rigid molecule: Rotational and linear diffusion and fluorescence anisotropy. *Biopolymers* **1977**, 16, 1907-1928.

Smith, A. W.; Chung, H. S.; Ganim, Z.; Tokmakoff, A. Residual native structure in thermally denatured β-hairpin. *J. Phys. Chem. B* **2005**, 109, 17025-17027.

Smith, D. P.; Radford, S. E. Role of single disulphide bond of β2-microglobulin in amyloidosis in vitro. *Protein Sci*. **2001,** 10, 1775-1784.

Soldi, G.; Plakoutsi, G.; Taddei, N.; Chiti, F. Stabilization of a native protein mediated by ligand binding inhibits amyloid formation independently of the aggregation pathway. *J. Med. Chem*. **2006**, 49, 6057–6064.

Sophianopoulos, A. J. Association sites of lysozyme in solution. The active site. *J. Biol. Chem*. **1969**, 244, 3188-3193.

Sophianopoulos, A. J.; Van Holde, K. E. Evidence for dimerization of lysozyme in alkaline solution. *J. Biol. Chem*. **1961**, 236, PC82-PC83.

Sophianopoulos, A. J.; Van Holde, K. E. Physical studies of muramidase (Lysozyme). *J. Biol. Chem*. **1964,** 239, 2516-2524.

Soto C.; Castilla, J. The controversial protein only hypothesis of protein propagation. *Nature Med*. **2004**, S63-S67.

Souillac, P. O.; Uversky, V. N.; Millett I. S.; Khurana, R.; Doniach, S.; Fink, A. L. Effect of association state and conformational stability on the kinetics of immunoglobulin light chain amyloid fibril formation at physiological pH. *J. Biol. Chem.* **2002**, 277, 12657-12665.

Stefani M. Protein misfolding and aggregation: new examples in medicine and biology of the dark side of the protein world. *Biochim. Biophys. Acta*. **2004**, 1739, 5-25.

Steiner, R.F. Fluorescence anisotropy: Theory and application, in: Topics of Fluorescence Spectroscopy, **1991**, 2, Lakowicz, J.R. "Ed", New York, Plenum press, pp. 1-52.

Stenstam, A.; Khan, A. and Wennerstrom, K. The lysozyme-dodecyl sulfate system. An example of protein-surfactant aggregation. *Langmuir* **2001**, 17, 7513-7520.

Stryer, L. Fluorescence spectroscopy of proteins. *Science* **1968**, 162, 526-533.

Stsiapura, V. I.; Maskevich, A. A.; Kuzmitsky, V. A.; Turoverov, K.; Kuznetsova, I. M. Computational study of thioflavin T torsional relaxation in the excited state. *J. Phys. Chem. A* **2007**, 111, 4829–4835.

Swaminathan R, Ph.D. Thesis. 1995, Time-resolved fluorescence studies in biological macromolecules. University of Bombay, Mumbai.

Swaminathan, R.; Krishnamoorthy, G.; Periasamy N. Similarities of fluorescence lifetime distributions of single tryptophan proteins in the random coil state. *Biophys. J.* **1994,** 67, 2013-2023.

Swaminathan, R.; Nath, U.; Udgaonkar, J B.; Periasamy, N.; Krishnamoorthy, G. Motional dynamics of a buried tryptophan reveals the presence of partially structured form during denaturation of barstar. *Biochemistry* **1996**, 35, 9150-9157.

Swaminathan, R.; Periasamy, N.; Udgaonkar, J. B.; Krishnamoorthy, G. Molten globule-like conformation of barstar: A study by fluorescence dynamics. *J. Phys. Chem*. **1994**, 98, 9270-9278.

Tafer, H.; Hiller, S.; Hilty, C.; Fernandez, C.; Wuthrich, K. Nonrandom structure in the urea-unfolded Escherichia coli outer membrane protein X (OmpX). *Biochemistry* **2004**, 43, 860–869.

Tanaka, F.; Forster, L. S.; Pal, P. K.; Rupley, J. A. The circular dichroism of lysozyme. *J. Biol. Chem.* **1975,** 250, 6977-6982.

Tanaka, M.; Machida, Y.; Nukina, N. A novel therapeutic strategy for polyglutamine diseases by stabilizing aggregation-prone proteins with small molecules. *J. Mol. Med*. **2005**, 83, 343-352.

Tanford, C.; Kawahare, K.; Lapanje, S. Proteins in 6 M Guanidine hydrochloride demonstration of random coil behavior. *J. Biol. Chem*. **1996**, 241, 1921-1923.

Tcherkasskaya, O.; Uversky, V.N. Denatured collapsed states in protein folding: Example of apomyoglobin. *Proteins Struct. Funct. Genet.* **2001**, 44, 244–254.

Terry, R. D.; Peck, A.; DeTeresa, R.; Schechter, R.; Horoupian, D. S. Some morphometric aspects of the brain in senile dementia of the Alzheimer type. *Ann. Neurol*. **1981**, 10, 184–192.

Thirumalai, D.; Klimov, D. K.; Dima, R. I. Emerging ideas on the molecular basis of protein and peptide aggregation. *Curr. Opin. Struct. Biol*. **2003**, 13, 146-159.

Thomas, G. J. Jr. Raman spectroscopy of protein and nucleic acid assemblies. *Annu. Rev. Biophys. Biomol. Struct*. **1999**, 28, 1–27.

Tompkins, M. M.; Hill, W. D. Contribution of somal Lewy bodies to neuronal death. *Brain Res*. **1997**, 775, 24–29.

Trexler, A. J.; Nilsson, M. R. The formation of amyloid fibrils from proteins in the lysozyme family. *Curr. Protein Pept. Sci.* **2007**, 6, 537-557.

Truong, K.; Ikura, M. The use of FRET imaging microscopy to detect protein–protein interactions and protein conformational changes in vivo. *Curr. Opin. Struct. Biol*. **2001**, 11, 573–578.

Tycko, R. Solid-state NMR as a probe of amyloid fibril structure. *Curr. Opin. Chem. Biol*. **2000**, 4, 500-506.

Uversky, V. N. Natively unfolded proteins: A point where biology waits for physics. *Protein Sci.* **2002**, 11, 739–56.

Vassar, P. S.; Culling, C. F. A. Fluorescent stains with special reference to amyloid and connective tissues. *Arch. Pathol*. **1959,** 68, 487-49.

Voropai, E. S.; Samtsov, M. P.; Kaplevskii, K. N.; Maskevich, A. A.; Stepuro, V. I.; Povarova, O. I.; Kuznetsova, I. M.; Turoverov, K. K.; Fink, A. L.; Uverskii, V. N. Spectral properties of thioflavin T and it's complexes with amyloid fibrils. *J. Appl. Spectrosc*. **2003**, 70, 868–874.

Vos, K.; van Hoek, A.; Visser, A. J. Application of a reference convolution to tryptophan fluorescence in proteins. A refined description of rotational dynamics. *Eur. J. Biochem*. **1987**, 165, 55-63.

Wall, J.; Murphy, C. L.; Solomon, A. In Vitro immunoglobulin light chain fibrillogenesis. *Methods Enzymol*. **1999**, 309, 204-217.

Wallrabe, H.; Periasamy, A. Imaging protein molecules using FRET and FLIM microscopy. *Curr. Opin. Biotechnol.* **2005**, 16, 19–27.

Walsh, D. M., Klyubin, I.; Fadeeva, J. V.; Cullen, W. K.; Anwyl, R.; Wolfe, M. S.; Rowan, M. J.; Selkoe, D. J. Naturally secreted oligomers of amyloid beta protein potently inhibit hippocampal long term potentiation in vivo. *Nature* **2002**, 416, 535-539.

Wang, X.; de Vocht, M. L.; de Jonge, J.; Poolman, B.; Robillard, G. T. Structural changes and molecular interactions of hydrophobin SC3 in solution and on a hydrophobic surface. *Protein Sci.* **2002,** 11, 1172-1181.

Wang, X.;Graveland-Bikker, J. F.; de Kruif, C. G.; Robillard, G. T. Oligomerization of hydrophobin SC3 in solution: from soluble state to self assembly. *Protein Sci.* **2004,** 13, 810-821.

Wang; W. Instability, stabilization, and formulation of liquid protein pharmaceuticals. *Int. J. Pharm*. **1999,** 185, 129–188.

Waxman, E.; Laws, W. R.; Laue, T. M.; Nemerson, Y.; Ross, J. B. A. Human factor VIIa and its complex with soluble tissue factor: evaluation of asymmetry and conformational dynamics by ultracentrifugation and fluorescence anisotropy decay methods? *Biochemistry* **1993**, 32, 3005-3012.

Weber, G.; Young, L. B. Fragmentation of bovine serum albumin by pepsin. I. the origin of the acid expansion of the albumin molecule. *J. Biol. Chem*. **1964,** 239, 1415–1423.

Weber, K.; Osborn, M. The reliability of molecular weight determinations by dodecyl sulfate-polyacrylamide gel electrophoresis *J. Biol. Chem.* **1969**, 244, 4406-4412.

Wetter, L. R.; Deutsch, H. F. Immunological studies on egg white proteins IV. Immunochemical and physical studies of lysozyme. *J. Biol. Chem.* **1951**, 192, 237-242.

Weyden, L.V. D.; Adams, D.J. The Ras-association domain family (RASSF) members and their role in human tumourigenesis. *Biochem Biophys Acta*, **2007**, 1776, 58-85.

Wilkins, D. K.; Grimshaw, S. B.; Receveur, V.; Dobson, C. M.; Jones, J. A., Smith, L. J. Hydrodynamic radii of native and denatured proteins measured by pulse field gradient NMR techniques. *Biochemistry* **1999**, 38, 16424–16431.

Williamson, M.P; Havel, T.F.; Wuthrich, K. Solution Conformation of proteinase inhibitor IIA from bull seminal plasma by ^{1}H Nuclear Magnetic Resonance and distance geometry. *J. Mol. Biol*. **1985**, 182, 295–315.

Wittmann, C.W.; Wszolek, M. F.; Shulman, J. M.; Salvaterra, P. M.; 2 Lewis, J.; Hutton, M.; Feany, M. B. Tauopathy in Drosophila: neurodegeneration without neurofibrillary tangles. *Science* **2001**, 293, 711-714.

Wong, K. B.; Freund, S. M. V.; Fersht, A. R. Cold denaturation of barstar: ^{1}H, ^{15}N and ^{13}C NMR assignment and charaterisation of residual structure. *J. Mol. Biol*. **1996**, 259, 805-818.

www.rcsb.org

Yamamoto, K.; Yagi, H.; Ozawa, D.; Sasahara, K.; Naiki, H.; Goto, Y. Thiol compounds inhibit the formation of amyloid fibrils by β_2-microglobulin at neutral pH. *J. Mol. Biol*. **2008**, 376, 258–268.

Yan, L. M.; Nossol, M. T.; Velkova, A.; Kazantzis, A.; Kapurniotu, A. Design of a mimic of nonamyloidogenic and bioactive human islet amyloid polypeptide (IAPP) as nanomolar affinity inhibitor of IAPP cytotoxic fibrillogenesis. *Proc. Natl. Acad. Sci. USA*, **2005**, 103, 2046-2051.

Yang, F.; Giselle, P. L.; Begum, A. N.; Ubeda, O. J.; Simmons, M. R.; Ambegaokar, S. S.; Chen, P.; Kayed, R.; Glabe, C. G.;. Frautschy, S. A.; Cole, G. M. Curcumin inhibits formation of amyloid beta oligomers and fibrils, binds plaques, and reduces amyloid in vivo. *J. Biol. Chem*. **2005**, 280, 5892-5901.

Yang, Y.; Turner, R. S.; Gaut, J. R. The chaperone BiP/GRP78 binds to amyloid precursor protein and decreases Aβ40 and Aβ42 secretion. *J. Biol. Chem*. **1998**, 273, 25552–25555.

Yguerabide, J.; Epstein, H. F.; Stryer, L. Segmental flexibility in an antibody molecule. *J. Mol. Biol*. **1970**, 51, 573-590.

Zhang, X.; Smith, D. L.; Meriin, A. B.; Engemann, S.; Russel, D. E.; Roark, M.; Washington, S. L.; Maxwell, M. M.; Marsh, L.; Thompson, L. M.; Wanker, E. E.; Young, A. B.; Housman, D. E.; Bates, G. P.; Sherman, M. Y.; Kazantsev, A. G. A potent small molecule inhibits polyglutamine aggregation in Huntington's disease neurons and suppresses neurodegeneration in vivo. *Proc. Natl. Acad. Sci. USA*. **2005**, 102, 892-897.

Zhou, H.; Li, S. H.; Li, X. J. Chaperone suppression of cellular toxicity of huntingtin is independent of polyglutamine aggregation. *J. Biol. Chem*. **2001**, 276, 48417–48424.

Zhu, M.; Rajamani, S.; Kaylor, J.; Han, S.; Zhou, F.; Fink A. L. The flavonoid baicalein inhibits fibrillation of α-synuclein and disaggregates existing fibrils. *J. Biol. Chem*. **2004**, 279, 26846-26857.

Si, K.; Lindquist, S.; Kandel, E. R. The neuronal isoform of the *Aplysia* CPEB has prion-like properties. Cell. **2003**, 115, 879-891. **(Reference added to page 18)**

List of publications

In journals

1) Satish Kumar, Vijay Kumar Ravi and Rajaram Swaminathan. How do surfactants and DTT affect the size, dynamics activity and growth of soluble lysozyme aggregates? *Biochem. J.* (in press) doi: 10.1042/BJ20071499
2) Satish Kumar, Atul Kumar Singh, G. Krisnamoorthy and Rajaram Swaminathan. Thioflavin T displays enhanced fluorescence selectivity inside anionic micelles and mammalian cells. *J. Fluoresc.* (in press) doi: 10.1007/s10895-008-0378-2
3) Satish Kumar and Rajaram Swaminathan**.** Employing the fluorescence anisotropy and quenching kinetics of tryptophan to hunt for residual structures in denatured proteins. *J. Chem. Sci.* **2007**, 119, 141-145.
4) Homchaudhuri, L.; Kumar, S.; Swaminathan, R. Slow aggregation of lysozyme in alkaline pH monitored in real time employing the fluorescence anisotropy of covalently labeled dansyl probe. *FEBS Lett*. 2006, 580, 2097-2101.
5) Satish Kumar, Vijay Kumar Ravi, and Rajaram Swaminathan. Prior incubation with N,N′,N′′-Triacetylchitotriose but not N-Acetyl-D-glucosamine confers resistance towards aggregation in lysozyme at alkaline pH. (*To be submitted*)

Conference papers

1) **Satish Kumar,** Vijay Kumar Ravi and R. Swaminathan. How Does SDS, CTAB and DTT Affect the Size, Rotational Dynamics and Growth Kinetics of Soluble Lysozyme Aggregates? Abstract accepted for 52nd Annual meeting of Biophysical Society, during 2-6 February 2008, Long Beach, California, USA.
2) L. Homchaudhuri, **Satish Kumar**, R. Swaminathan. Slow aggregation of lysozyme in alkaline pH monitored in real time employing the fluorescence anisotropy of covalently labeled probe. Abstract accepted for 50th Annual meeting of Biophysical Society, during 18-22 February 2006, Salt Lake city, Utah, USA.